The thermodynamic behavior of thorium and the rare earth elements (REE) in hydrothermal solutions

by Haylea Nisbet

April 2022

A thesis submitted to McGill University in partial fulfillment of the requirements of the degree of Doctor of Philosophy

---

The Department of Earth and Planetary Sciences
McGill University
Montreal, Quebec
Canada

Abstract

The ability to accurately predict the mobility of elements in natural and industrial settings hinges on accurate thermodynamic data for aqueous species and minerals at relevant conditions. Thermodynamic data for thorium (Th) and the rare earth elements (REE) remain largely restricted to ambient conditions, precluding representative modeling of hydrothermal systems, of which they are commonly present together in high concentrations.

In this thesis, I experimentally explore the solubility and speciation of Th in chloride, sulfate, and carbonate-bearing hydrothermal fluids, ligands that are important to natural REE- and Th-bearing hydrothermal fluids due to their abundance and demonstrated ability to form stable complexes at ambient conditions. Autoclave solubility experiments were carried out at 175, 200, 225, and 250 °C in titanium autoclaves with crystalline thorium oxide (ThO_2) as a reference phase. The predominant aqueous complexes were identified for each set of experiments, and thermodynamic formation constants were derived. Our results indicate that chloride does not form stable aqueous complexes with Th in acidic solutions (pH_T 1.68−4.03) and, instead, Th hydroxyl species, $Th(OH)_4^0$ and $Th(OH)_2^{2+}$, predominate. These complexes do not promote the significant dissolution of ThO_2, and likely represent a minimum concentration of Th in natural systems. In contrast to chloride, sulfate-bearing solutions permitted the formation of the $Th(SO_4)_2^0$ species, which increased the solubility of Th by orders of magnitude in acidic hydrothermal fluids (pH_T 3.69−4.6). Moreover, it was demonstrated by thermodynamic modeling that the presence of moderate sulfate concentrations can promote the fractionation of Th from the REE in ore-forming solutions, which is an effective, natural mechanism that can remove radioactivity from REE ore. Our experiments with carbonate-bearing hydrothermal fluids did not detect Th-carbonate

complexes under alkaline conditions (pH_T 7.84–9.82), in contrast to ambient conditions for which they are reportedly highly stable. Rather, $Th(OH)_4^0$ and $Th(OH)_5^-$ predominated under the conditions investigated. Carbonate-bearing solutions are thus deemed unlikely to transport significant concentrations of Th in hydrothermal systems.

The solubility and speciation of Nd in carbonate-bearing hydrothermal fluids is also explored in this thesis. Carbonate is one of the least studied potential REE ligands, despite it being one of the most important species from a geochemical perspective due to its ubiquitous presence in REE ore-forming systems. Similar autoclave solubility experiments were carried out at 175, 200, 225, and 250 °C in acidic and alkaline experimental solutions. The reference phase, Nd-hydroxylbastnäsite ($NdCO_3OH$), was synthesized hydrothermally before the experiments. From the experimental data, it was determined that the predominant aqueous species are $NdCO_3^+$ and $NdCO_3OH^0$ under acidic and alkaline conditions, respectively. The results suggest that Nd mobilization could be promoted by carbonate-complexation in natural hydrothermal systems.

Résumé

La capacité de prédire avec précision la mobilité des éléments dans les milieux naturels et industriels repose sur des données thermodynamiques précises et des conditions spécifiques pour les espèces aqueuses et les minéraux . Les données thermodynamiques pour le thorium (Th) et les éléments de terres rares (REE) sont encore largement limitées aux conditions ambiantes, empêchant une modélisation représentative des systèmes hydrothermaux, où ils sont couramment présents à des concentrations élevées.

Dans cette thèse, j'explore expérimentalement la solubilité et la spéciation du Th dans les fluides hydrothermaux contenant des chlorures, des sulfates et des carbonates, ligands qui sont importants pour les fluides hydrothermaux naturels contenant des REE et du Th en raison de leur abondance et de leur capacité à former des complexes stables aux conditions ambiantes. Des expériences de solubilité ont été réalisées à 175, 200, 225 et 250 °C dans des autoclaves en titane avec de l'oxyde de thorium cristallin (ThO_2) comme phase de référence. Les complexes aqueux prédominants ont été identifiés pour chaque série d'expériences, et les constantes de formation thermodynamique ont été dérivées. Nos résultats indiquent que les chlorures ne forment pas de complexes aqueux stables avec Th dans des solutions acides (pH_T 1,68−4,03) mais, à la place, les espèces Th hydroxyle, $Th(OH)_4^0$ et $Th(OH)_2^{2+}$, prédominent. Ces complexes ne favorisent pas la dissolution significative de ThO_2 et représentent probablement une concentration minimale de Th dans les systèmes naturels. Contrairement aux chlorures, les solutions contenant des sulfates ont permis la formation de l'espèce $Th(SO_4)_2$, qui a augmenté la solubilité de Th de plusieurs ordres de grandeur dans les fluides hydrothermaux acides (pH_T 3,69−4,6). De plus, il a été démontré par modélisation thermodynamique que la présence de concentrations modérées de sulfates peut

favoriser le fractionnement de Th des terres rares dans les solutions de formation de minerai, un mécanisme naturel efficace qui peut éliminer la radioactivité du minerai de terres rares. Nos expériences avec des fluides hydrothermaux carbonatés n'ont pas détecté de complexes Th-carbonates dans des conditions alcalines (pH_T 7,84−9,82), contrairement aux conditions ambiantes pour lesquelles ils seraient très stables. Plutôt, $Th(OH)_4^0$ et $Th(OH)_5^-$ prédominent dans les conditions étudiées. Les solutions contenant des carbonates sont donc considérées comme peu susceptibles de transporter des concentrations importantes de Th dans les systèmes hydrothermaux.

La solubilité et la spéciation du Nd dans les fluides hydrothermaux carbonatés sont également explorées dans cette thèse. Les carbonates sont l'un des ligands potentiels des terres rares les moins étudiés, bien qu'ils soient l'une des espèces les plus importantes d'un point de vue géochimique en raison de son omniprésence dans les systèmes de formation de minerai de terres rares. Des expériences similaires de solubilité en autoclave ont été réalisées à 175, 200, 225 et 250 °C dans des solutions expérimentales acides et alcalines. La phase de référence, Nd-hydroxylbastnäsite ($NdCO_3OH$), a été synthétisée hydrothermiquement avant les expériences. À partir des données expérimentales, il a été déterminé que les espèces aqueuses prédominantes sont $NdCO_3^+$ et $NdCO_3OH^0$ dans des conditions acides et alcalines, respectivement. Les résultats suggèrent que la mobilisation du Nd pourrait être favorisée par la complexation des carbonates dans les systèmes hydrothermaux naturels.

i

Acknowledgments

First and foremost, I would like to thank Artas Migdisov for his unwavering support throughout this Ph.D. His continuous encouragement allowed me to realize my full potential, and I will forever be grateful for his lessons, both in research and in life. I am pretty certain that I could not have completed this degree without his recurrent humble reminders that “we are so damn good”.

I would like to sincerely thank Vincent van Hinsberg for believing that I could be successful in the world of thermodynamics and for encouraging me to take on this project. His steadfast enthusiasm and seemingly endless repertoire of knowledge have aided me tremendously throughout my time at McGill.

I am incredibly grateful for A.E. “Willy” Williams-Jones and his helpful insight in seeing the “bigger picture” of my research. He has taught me a great deal during my degrees at McGill, and his unrivaled enthusiasm and passion are some of the main reasons why I fell in love with geology.

I am indebted to the Radiogeochemistry team at Los Alamos National Laboratory for embracing me and helping me grow over the past 5 years. I would like to thank Doug Ware, Marley Rock, Kirsten Sauer, Rose Harris, George Perkins, Chelsea Neil, and Oana Marina for their assistance in experimental and laboratory tasks, Hongwu Xu for his invaluable insight, Florie Caporuscio for our lunchtime chats, and Andrew Strzelecki for his encouragement and friendship. Being a member of such an incredibly brilliant group of minds has been an honor and encourages me to continually strive to be a better researcher.

The Earth and Planetary Science department at McGill has been my family over the past 10 years as I progressed from an undergraduate to a graduate student. My memories of this chapter in my life will forever be encapsulated as some of my happiest and most cherished times. I would not be where I am today without the numerous professors and fellow students that have influenced me along the way, for which there are too many to name. During my Ph.D., I was fortunate to be a member of the Willy group and the FlexPet group; two incredible research groups that helped guide me through scientific problems and aided me in presenting my research to its fullest potential. I would also like to give a special thanks to Anne, Kristy, and Angela for making the administrative stuff easy, and for feeding me an unhealthy number of cookies. A special shout out to Catherine Crotty for going through this Ph.D. journey alongside me with friendship and humor. I imagine these past few months leading up to submitting would have been exceedingly more dispiriting if it hadn't been for your encouragement and mutual stress.

To my wonderful friends Sandy, Nick, Sophie, Georgina, Nina, Derek and Allie, thank you for ensuring my life outside of research was as adventurous and fulfilling as possible.

The financial support of the Seaborg Institute Summer Research Fellowship, the Center for Space and Earth Sciences Student Fellowship, and the Laboratory Directed Research and Development program from Los Alamos National Laboratory provided me with the means to carry out this research, for which I am thankful.

Last, but certainly not least, I would like to thank my family and Ryan for their continued encouragement throughout this Ph.D. and their needed reassurance when setbacks and failed experiments occurred. I am sincere in that I could not have reached this point without you.

ii

Table of Contents

---

iii

List of Figures

iv

List of Tables

V

Preface and contribution of authors

This thesis contains four manuscripts, three of which have been published in peer-reviewed journals. The first manuscript, investigating the solubility and speciation of thorium in chloride-bearing hydrothermal solutions, was published in Geochimica et Cosmochimica Acta, the second, on the solubility and speciation of thorium in sulfate-bearing hydrothermal fluids, was published in Scientific Reports, the third, on the solubility and speciation of thorium in carbonate-bearing fluids was published in Geochimica et Cosmochimica Acta (Special Issue: Metals-Fluids-Minerals) (In press), and the fourth, on the solubility and speciation of neodymium in carbonate-bearing hydrothermal fluids, has been submitted to a Chemical Geology.

The first manuscript, presented in Chapter 2, was conceived by Haylea Nisbet and Artas Migdisov and carried out at the radiogeochemistry laboratories of EES-14 at Los Alamos National Laboratory (LANL). The experimental method used, the autoclave solubility technique, was developed by Migdisov. Nisbet carried out all solubility experiments. Analyses of the experimental solutions via ICP-MS at the Geochemical and Geomaterials Research Laboratories were conducted by Haylea Nisbet under the supervision of Oana Marina and George Perkins. Derivation of thermodynamic data was completed by Nisbet with guidance from Migdisov. The manuscript was prepared by Haylea Nisbet, and edited by Artas Migdisov, A.E. Williams-Jones, Vincent van Hinsberg, and Hongwu Xu. Valuable comments for the final draft of the paper were provided by Xiaofeng Guo, Hakim Boukhalfa, and Robert Roback.

The study presented in Chapter 3 was conceived by Haylea Nisbet and Artas Migdisov and carried out at the same facilities and using the same experimental technique, as in Chapter 2.

Derivation of standard thermodynamics was carried out by Nisbet. The manuscript was written by Haylea Nisbet with invaluable insight from Artas Migdisov, A.E. Williams-Jones, and Vincent van Hinsberg. Hongwu Xu and Robert Roback provided helpful suggestions on the final draft of the paper.

The experimental research of Chapter 4 was conducted by Haylea Nisbet in collaboration with Artas Migdisov at the radiogeochemistry laboratories of EES-14 at Los Alamos National Laboratory (LANL). All experiments were conducted by Haylea using the autoclave solubility technique. Analyses of the experimental solutions via ICP-MS were conducted by Oana Marina. The manuscript was written by Nisbet. Migdisov, Williams-Jones, Xu, van Hinsberg and Roback assisted in editing and refining the manuscript prior to its submission.

The final study, presented in Chapter 5, describes an experimental study carried out by Haylea Nisbet. Synthesis of the reference phase and characterization via X-Ray Diffraction (XRD) were carried out at Los Alamos National Laboratory by Haylea Nisbet, and Haylea Nisbet and Marley Rock, respectively. Autoclave solubility experiments were carried out by Nisbet. Analyses of the experimental solutions via ICP-MS were conducted by Oana Marina. The manuscript was prepared by Nisbet with constructive feedback from Artas Migdisov, Vincent van Hinsberg, and A.E. Williams-Jones.

Chapter 1

Introduction

1.1 Metal solubility and speciation

The solubility of a given metal is controlled by the thermodynamic properties of its aqueous species, the physicochemical properties of the aqueous solution, and the stability of the metal's mineral phases (Brugger et al., 2016). The thermodynamic stability of a given aqueous complex is a measure of the tendency of a metal ion to form a metal complex and is directly associated with the metal-ligand bond energy (Muthaiah et al., 2020). It represents the tendency for a specific complex to exist under equilibrium conditions and is defined by a stability constant or formation constant (β). The thermodynamic formation constant can be represented by the following reactions:

$$iM + jL \leftrightarrow M_iL_j$$

$$\beta_{i,j} = \frac{a(M_iL_j)}{a(M)^i a(L)^j}$$

where M is the metal, L is the ligand, and a is the activity of the species. The higher the β value, the greater the stability of the complex.

If formation constants are not available, the relative stability of a metal with different ligands can be predicted using Pearson's principle of Hard and Soft Acids and Bases (HSAB) (Pearson, 1963), where acids and bases are cations and anions, respectively. In this theory, hard acids and bases are characterized by small ionic radii, high positive charge, and weak polarizability, whereas soft acids and bases have larger ionic radii and low charge (Pearson, 1963). Hard acids preferentially bond with hard bases, whereas soft acids prefer to form complexes with soft bases. Both thorium (Th) and the rare earth elements (REE) are considered hard acids, and thus tend to bond with hard bases. In hydrothermal solutions, the most abundant hard bases are fluoride, carbonate, hydroxyl, and sulfate (Seward et al., 2014). Although considered “borderline” between hard and soft, chloride is also an important ligand in these systems due to its high concentration in most hydrothermal fluids. Indeed, in addition to the stability of a given complex, the availability of the ligand to form a complex is important. For example, although REE-fluoride complexes are predicted to be among the most stable at hydrothermal conditions, the ability of fluoride to transport the REE in significant quantities at moderate pH (> 2) is suppressed by the formation of the insoluble phases such as $REEF_3$, or more commonly in nature, CaF_2, which will buffer the fluoride content in the solution, inhibiting REE transport (Migdisov et al., 2016). Thus, at any given condition, the dissolved concentration of a metal is controlled by the stability of the least soluble mineral (Seward et al., 2013). Therefore, predicting the solubility of a phase requires an extensive evaluation of all its geochemical properties at relevant conditions.

1.2 The link between thorium and the rare earth elements

Thorium and the REE are both classified as high field strength elements (HFSE) that are characterized by high charge, small ionic radii, and thus a high electric field strength (Ault et al., 2015). As a result, Th and the REE do not readily substitute into common rock-forming minerals and tend to concentrate in the residual melt during fractional crystallization. Consequently, the co-occurrence of these elements is ubiquitous− it is rare to find a REE deposit that is free of Th (and U). For example, the Mountain Pass and Bear Lodge deposits have an average of 0.025 and 0.1−0.12 elemental weight percent Th, respectively (Ault et al., 2015). Thorium commonly substitutes into the REE-phosphate minerals, monazite, and xenotime. Indeed, concentrations of thorium oxide in monazite can reach 20 wt.% thorium oxide (Long et al., 2010). If not incorporated into the structure of REE minerals, geochemical correlations are evident as Th will be hosted in other host rock minerals such as thorite (Ault et al., 2015). Owing to its intrinsic radioactivity, from a mining perspective, the presence or absence of significant Th can dictate the economic viability of an ore deposit, making some impossible to mine. Thus, owing to the common coexistence of the REE and Th, in modeling the formation of REE ore systems, an additional requirement is understanding the physicochemical behavior and complexes of thorium. Such information considered in the context of the well-known fractionation of the REE can be used to develop predictive thermodynamic models which could then guide exploration for new REE ore deposits that are depleted in Th.

Predicting the formation of a REE ore body relies on accurate thermodynamic data of the REE and Th at the modeled conditions. Although recently there has been a consistent effort to study the stability of solid and aqueous REE species at hydrothermal conditions in various systems (see below), there remains a critical gap in our understanding of their behavior in carbonate-bearing systems with which they are intimately associated. In contrast, there have been no studies of Th solubility and speciation at hydrothermal conditions. Deriving the fundamental thermodynamic data needed to fill this knowledge gap is the primary motivation of this thesis.

1.3 Thorium

1.3.1 Thorium geochemistry

Thorium belongs to a group of radioactive elements called the actinides, of which it is the most abundant in the Earth’s crust, comparable in concentrations to those of Pb and Mo (Morss et al., 2006). Despite its abundance, our understanding of the physicochemical behavior of Th in aqueous fluids remains incomplete, especially at elevated temperatures. The bulk of studies on Th solubility and speciation are reported and reviewed in an extensive review by the Nuclear Energy Agency (NEA) entitled “Chemical Thermodynamics of Thorium” (Rand et al., 2008). These studies evaluate the speciation of Th with various ligands that are abundant in natural systems including chloride, sulfate, and carbonate.

The majority of reported studies on Th complexation at ambient conditions have focused on the hydrolysis of Th. It is well established that at ambient temperature, Th, a tetravalent actinide ion with a high charge, has a strong tendency to hydrolyze. Only at a $pH_{25°C} < 3$ does the Th^{4+} ion predominate in aqueous solutions (Langmuir and Herman, 1980). A large number of hydroxyl complexes have been reported in the literature, including monomeric, dimeric, trimeric, tetrameric, and hexameric species (Zanonato et al., 2016). Polynuclear species, complexes containing two or more metals, have also been proposed in some studies (Grenthe and Lagerman, 1991; Neck and Kim, 2001), but the extent of their contribution to Th solubility in these fluids remains a topic of debate. Owing to a wide disparity of experimental methods and ionic media, a consensus on the Th-hydroxyl species expected to predominate has not been reached. In chloride-bearing solutions, experimental measurements at ambient conditions using large angle X-ray scattering methods in perchlorate and chloride solutions showed that while no complexation was detected in perchlorate, there is very weak complexation between Th and chloride ions (Johansson et al., 1991). However, the stoichiometry of these species was not identified, nor were thermodynamic data derived. Studies investigating the speciation of Th in sulfate solutions have been carried out by numerous researchers (Zebroski et al., 1951; Maiorova and Fomin, 1958; Zielen, 1959; Patil and Ramakrishna, 1972) who proposed the predominant species to be $Th(SO_4)_2^{\circ}$ and $ThSO_4^{2+}$. Thermodynamic formation constants were derived for each species at ambient conditions. In carbonate solutions, results of 19 sets of experiments have been reported for ambient conditions, all of which show that Th has a strong affinity for carbonate ions. However, there are considerable inconsistencies in the identification of the dominant Th-carbonate species. Altmaier et al. (2005) identified the ternary complexes $Th(OH)(CO_3)_4^{5-}$ and $Th(OH)_2(CO_3)_2^{2-}$ as the dominant species with minor contributions from $Th(OH)_2(CO_3)_{aq}$, $Th(OH)_3(CO_3)^-$ and $Th(OH)_4(CO_3)^{2-}$ in solutions with an ionic strength of 0.5 M. In contrast, Osthols et al. (1994), Felmy et al. (1997), and Felmy and Rai (1999) proposed that $Th(CO_3)_5^{6-}$ is the dominant complex in solutions containing 0.1−2.0 M CO_3^{2-} and $Th(OH)_3(CO_3)^-$ dominates at lower carbonate concentrations and near-neutral pH.

Studies of the solubility of thorium oxides at elevated temperatures are limited, with most restricted to ambient conditions (Baes Jr. et al., 1965; Moon, 1989; Grenthe and Lagerman, 1991; Moriyama et al., 1999; Ekberg et al., 2000; Neck and Kim, 2001), save for those conducted at temperatures between 85 and 95 °C by Baes Jr. et al. (1965), Rai et al. (2000), and Zanonato et al. (2016). Unfortunately, thermodynamic formation constants were not reported for the experiments conducted by Zanonato et al. (2016). The experiments primarily approached equilibrium from undersaturation (i.e., dissolution of ThO_2), with the majority using an amorphous ThO_2 phase as a reference solid. Very few studies have assessed the solubility of crystalline ThO_2, and those that have were compromised by the slow dissolution kinetics of $ThO_{2(cr)}$ at ambient temperature, and difficulty in attaining a steady-state or equilibrium in the system (Rai et al., 2000; Hubert et al., 2001; Neck et al., 2003). It was concluded in the NEA review (Rand et al., 2008) that none of the low-temperature undersaturation experiments with $ThO_{2(cr)}$ (Moon, 1989; Rai et al., 2000; Neck et al., 2003) reached equilibrium, rendering their thermodynamic data unreliable. As highlighted by Kobayashi et al. (2016), it is essential when comparing thermodynamic data that the nature of the phase remains consistent due to orders of magnitude discrepancies that arise between thermodynamic formation constants of amorphous versus crystalline phases; amorphous being more soluble. However, a few researchers have been successful in performing solubility experiments with crystalline ThO_2 from the direction of oversaturation (Baes Jr. et al., 1965; Rai et al., 2000; Neck et al., 2003). These authors derived solubility products for the dissolution of $ThO_{2(cr)}$ that were consistent when particle size was factored in. Baes Jr. et al. (1965) and Rai et al. (2000) also derived solubility products at 90 and 95 °C, respectively.

1.4 The rare earth elements

1.4.1 Rare earth element geochemistry

The rare earth elements (REE), which comprise the lanthanides (La-Lu), Y, and Sc, are a group of 17 elements linked by their striking similarity in physical and chemical properties. Their common behavior emerges from their electronic configuration; all of the REE occur naturally in the trivalent (3+) state, except for Eu and Ce which can also have 2+ and 4+ oxidation states, respectively (Voncken, 2016a). The lanthanides each have two electrons in their 6s outermost shell, varying only in the number of electrons added to the *f*-subshells. Because these electrons are added deep within the 4f orbital, they are strongly shielded and thus are not generally involved in chemical reactions (Clark, 1984), leading to the similarity in the chemical behavior of the REE. As a result, REE-bearing minerals invariably incorporate multiple REEs into their mineral structure, as solid solutions. The addition of electrons, however, contributes to a systematic decrease in effective ionic radii with an increasing atomic number (Å=1.061-0.848; Moeller, 1973), referred to as the “lanthanide contraction”. Although small, these differences in ionic radii can effectively fractionate the light REE (those with a smaller atomic number (La-Sm), LREE), from the heavy REE (those with larger atomic numbers (Eu-Lu), HREE). This explains why the LREE, which have larger radii, will preferentially occupy mineral sites with a higher coordination number (8−10), whereas the HREE prefer sites with lower coordination numbers, closer to 8

(Clark, 1984). Although they belong to the transition group metals, where electrons are added to the 3 and 4*d*-subshells, Y and Sc are frequently grouped with the REE due to their more similar physicochemical properties to the lanthanides than the transition metals. Both elements prefer a 3^+ oxidation state like the lanthanides. Yttrium's ionic radius is almost identical to holmium, and it is therefore frequently associated with the HREE (Williams-Jones and Vasyukova, 2018). Scandium, however, has a much smaller radius which allows it to substitute easily into major rock-forming minerals as a compatible element (Williams-Jones and Vasyukova, 2018). For this reason, many geologists do not consider Sc as a REE.

1.4.2 REE aqueous transport and ore formation

Despite their name, the rare earth elements are rather plentiful in nature. However, their tendency to become concentrated into exploitable and economic quantities, thus achieving "ore" status, is rare. Owing to their incompatible nature, REE ore deposits are typically hosted in carbonatites, highly evolved nepheline syenite intrusions, and highly differentiated peralkaline A-type granitic bodies (i.e., NYF pegmatites) (Voncken, 2016a; Vasyukova and Williams-Jones, 2020). Other important sources of the REE include ion-adsorption clays and placer deposits (Verplanck and Hitzman, 2016; Li et al., 2019). Although there are cases where REE ore deposits are proposed to have originated from minerals precipitating directly from a magma (e.g. the Sulphide Queen ore body at Mountain Pass, California; Castor, 2008), growing evidence suggests that hydrothermal fluids are responsible for mobilizing REE from a magmatic source, and subsequently, concentrating them to economic grades. Evidence of REE hydrothermal mobilization and concentration is found in fluid inclusion, mineralogical, and petrological studies of deposits such as the giant Bayan Obo ore deposit (Smith and Henderson, 2000), Browns Range (Cook et al., 2013), and the unexploited Gallinas Mountains deposit (Williams-Jones et al., 2000).

Based on fluid inclusion studies, the fluids generally range in temperatures from 250−500 °C and are typically dominated by chloride (anywhere from 5−45 wt.% NaCl have been recorded; Migdisov et al. (2016)), sulfate (up to 2.4 wt.%), fluoride (up to 0.5 wt.%) (Banks et al., 1994), as well as appreciable concentrations of carbonate (0.1-1 m) (Vasyukova and Williams-Jones, 2018). As a result, research on REE aqueous complexation at hydrothermal conditions has centered primarily on these ligands. Thermodynamic data on REE speciation at hydrothermal conditions remains incomplete, however, significant progress has been made in the past few decades (summarized in Migdisov et al. (2016)). Because hydrothermal fluids are typically highly saline, with recorded values reaching 25 wt.% NaCl (Vasyukova and Williams-Jones, 2018), REE-chloride speciation has been the focus of numerous high-temperature studies. Solubility experiments performed with solutions containing up to 5 M NaCl at temperatures up to 250 °C have identified $REECl^{2+}$ and $REECl_2^{+}$, as the predominant REE-chloride complexes (Gammons and Wood, 2002; Migdisov et al., 2009). Interestingly, it has been determined that the stability of these REE-chloride species increases with temperature, and the magnitude of this increase differs from the LREE to the HREE, with the LREE forming more stable complexes as temperature increases (Migdisov et al., 2016). Based on these data, it has been proposed that the differences in stability between the LREE and HREE complexes in chloride-bearing hydrothermal solutions can lead to the natural fractionation of these elements. In comparison to chloride, the REE form much more stable complexes with fluoride. At hydrothermal conditions, reliable experimental data for REE-fluoride speciation are limited to the studies of Migdisov and Williams-Jones (2007) and Migdisov et al. (2009) for temperatures up to 250 °C and saturated vapor pressure. Under the experimental conditions, the $REEF^{2+}$ species was identified as the sole contributor to the budget of dissolved REE, in contrast to studies performed at ambient conditions which proposed $REEF_2^{+}$

to be the dominant species (Luo and Millero, 2004). In addition, it was found that the stability of the $REEF^{2+}$ species decreased with increasing REE atomic number, similar to the chloride complexes, and that this effect increases with increasing temperature. However, as previously mentioned, the $REEF^{2+}$ complexes are unlikely to play a role in the transport of the REE in low to intermediate pH hydrothermal fluids due to the low solubility of $REEF_3$ and CaF_2 solids. The speciation of the REE with sulfate at hydrothermal conditions is limited to spectroscopic studies of Nd, Sm, and Er for temperatures up to 250 °C (Migdisov and Williams-Jones, 2008) and theoretical extrapolations from low-temperature data (Wood, 1990b; Haas et al., 1995). In the high-temperature experiments, the mono- and bi-sulfate complexes, $REESO_4^+$ and $REE(SO_4)_2^-$, were identified as the dominant species in solution, with the bi-sulfate complex becoming increasingly more important with increasing temperature. In contrast to REE-chloride and fluoride speciation, there is no apparent variation with atomic number in the stability of the REE-sulfate complexes with temperature, although this conclusion has been based on just three REE complexes with sulfate. Using the values derived from Migdisov and Williams-Jones (2008), it was shown that REE-sulfate complexes are likely to play a significant role in the transport of the REE, particularly at higher temperatures (300−400 °C) in weakly acidic solutions, resulting in substantial concentrations of REE in solution (A. A. Migdisov and Williams-Jones, 2014). Thermodynamic data on the hydrolysis of the REE and formation of REE-hydroxyl complexes are very sparse, and at elevated temperatures are limited to the study of Wood et al. (2002) who performed experiments with Nd up to 290 °C. Unfortunately, this study was only able to determine the stability of the $Nd(OH)_3^\circ$ complex over the entire experimental temperature range, with stability constants derived for $Nd(OH)^{2+}$ and $Nd(OH)_2^+$ restricted to lower temperatures. However, based on the existing data, REE-hydroxyl aqueous complexes are not expected to predominate at low to moderate pH conditions, and at more alkaline conditions, the precipitation of the $Nd(OH)_3$ solid is promoted (Migdisov et al., 2016). Finally, it is the behavior of the REE in carbonate-bearing systems that is the most unexplored. There are no experimental data on REE-carbonate speciation at elevated temperatures. However, at ambient temperature, the CO_3^{2-} ion is known to form among the strongest REE complexes (Jones et al., 1996). Currently, our understanding of REE-carbonate speciation in hydrothermal solutions is restricted to theoretical extrapolations of formation constants that are inconsistent (Wood, 1990a; Haas et al., 1995). As many hydrothermal fluids can contain considerable concentrations of carbonate and bicarbonate ions (Vasyukova and Williams-Jones, 2018), REE-carbonate complexes can potentially play an important role in the transport of the REE.

1.4.3 REE ore minerals

Although more than 70 minerals are known to host major contents of the REE (Clark, 1984), it is the REE-fluorocarbonates, bastnäsite [$(Ce,La,Y)CO_3F$)], and REE phosphates, monazite [$(Ce,La,Nd,Th)PO_4$], and xenotime [$(Y,Dy,Er,Tb,Yb,U,Th)PO_4$] that are the primary minerals exploited for commercial production. Monazite solid solutions, that adopt a monoclinic structure, are dominated by the LREE due to the large nine-fold coordinated site (Cuney and Friedrich, 1987). Xenotime solid solutions, having a tetragonal structure like zircon, are typically dominated by Y and the HREE because they prefer the smaller eight-fold coordinated site. Since they have similar ionic radii to the REE, the actinides, U and Th, are also commonly incorporated into monazite and xenotime via charge-coupled substitutions (Vance et al., 2011), with Th preferentially incorporated into monazite owing to its larger ionic radius, and U showing a preference for xenotime. Bastnäsite solid solutions, that adopt a hexagonal structure, mainly host the LREE (i.e., Ce and La) but are also known to incorporate Y (Jones et al., 1996). Up to 2 wt. %

ThO_2 has also been reported in bastnäsite (Smith et al., 2000; Beland and Williams-Jones, 2021), although this is less common.

The thermodynamic properties of REE-bearing solids are essential to model and predict the behavior of the REE in hydrothermal solutions. These properties are determined mainly through calorimetric and solubility approaches. Of the three primary ore minerals, monazite has been the most extensively investigated by calorimetry, with data derived for synthetic monazite end-members from $LaPO_4$ to $GdPO_4$ (summarized in Navrotsky et al. (2015)). At ambient conditions, the solubility of monazite has been determined by deriving the solubility products of all REE end-members (Liu and Byrne, 1997). At high-temperature (150−800 °C) data for Nd end-members were derived by Poitrasson et al. (2004), Cetiner et al. (2005), and Pourtier et al. (2010), and recently, solubility products were reported by Van Hoozen et al. (2020) for $LaPO_4$, $PrPO_4$, $NdPO_4$, and $EuPO_4$ endmembers from 100−250°C. Xenotime calorimetric functions have been derived for Y-, Tb-, Dy- Er-, Yb-, and $LuPO_4$ end-members (Gavrichev et al., 2006; Gysi et al., 2016). As is the case for monazite, xenotime solubility products are mostly limited to ambient conditions (Liu and Byrne, 1997), except for the studies conducted by Gysi et al. (2015, 2021), in which solubility products were determined for YPO_4, $ErPO_4$, $DyPO_4$,$YbPO_4$, $TbPO_4$, $HoPO_4$, $TmPO_4$, and $LuPO_4$ mineral end-members, and a natural xenotime-(Y) crystal up to 250 °C. There are very few thermodynamic data for bastnäsite, with high-temperature calorimetric studies limited to that of a natural sample (Gysi and Williams-Jones, 2015). The solubility data are restricted to the low-temperature values reported for the Nd- and La-bastnäsite-(OH) end-members (Voigt et al., 2016). There have been no direct measurements of the solubility of the fluorocarbonate endmembers at hydrothermal conditions.

1.5 Objectives

The objective of this thesis centers on the urgent need to extend the available thermodynamic data for actinide and lanthanide elements beyond ambient conditions. Thorium and the REE are frequently concentrated by hydrothermal solutions, for which their physicochemical behavior is expected to differ considerably to their behavior in low-temperature fluids. Extrapolating data from ambient conditions is simply unreliable, and therefore, to fill this knowledge gap, thermodynamic data on the solubility and speciation of Th and the REE at elevated temperatures are required.

Although Th is the most abundant actinide, there are essentially no data on its solubility and speciation at elevated temperatures. For this reason, solubility experiments via the autoclave solubility technique were carried out with some of the most common ligands found in natural hydrothermal systems, chloride, sulfate, and carbonate; for which results are reported in Chapters 2, 3, and 4, respectively. The main goal of these experiments was to identify the predominant aqueous species and to derive thermodynamic formation constants for these species from the collected experimental data.

Of the REE, Nd is among the most highly sought after, and consequently, its aqueous speciation and solubility in REE-bearing phases have been among the most studied (Migdisov and Williams-Jones, 2002, 2008; Migdisov et al., 2006, 2009; Migdissov and Williams-Jones, 2007). A major gap that hinders our ability to predict the mobility of Nd in hydrothermal systems is its physicochemical behavior in carbonate-bearing systems: Does Nd form stable complexes with carbonate at elevated temperatures? Is carbonate an effective ligand at transporting and concentrating Nd to ore-forming quantities? Therefore, the aim of the experimental research presented in Chapter 5 was to identify the predominant Nd aqueous species in high-temperature carbonate solutions of varying concentrations.

The thermodynamic data obtained from these studies are presented in a form that can be readily incorporated into modeling software and permits, for the first time, the accurate modeling of Th and the REE at hydrothermal conditions for the full suite of common ligands in the Earth's crust.

1.6 Organization of thesis

This thesis is organized into six chapters. The first chapter introduces the objectives of the research and presents a brief literature review of information pertinent to the subsequent chapters. The second to the fifth chapters are written in the form of manuscripts. The second chapter, published in Geochimica et Cosmochimica Acta, presents an experimental study on the solubility and speciation of Th in chloride-bearing solutions at hydrothermal conditions; the third chapter, published in Scientific Reports, discusses the results of experiments investigating the solubility of Th in sulfate-bearing solutions at hydrothermal conditions; the fourth chapter, published in Geochimica et Cosmochimica Acta Special Issue: Metals, Fluids Minerals (In press), reports the results of an experimental investigation of the behavior of Th in carbonate-bearing hydrothermal solutions; and the fifth chapter, to be submitted, presents the findings of an experimental study on the speciation of Nd in carbonate-bearing hydrothermal solutions. The final chapter summarizes the major conclusions and contributions of this thesis and proposes future avenues of research.

1.7 References

Altmaier M., Neck V., Müller R. and Fanghänel T. (2005) Solubility of $ThO_2 \cdot xH_2O_{(am)}$ in carbonate solution and the formation of ternary Th(IV) hydroxide-carbonate complexes. Radiochim. Acta 93.

Ault T., Van Gosen B., Krahn S. and Croff A. (2015) Natural thorium resources and recovery: options and impacts. Nucl. Technol. 194, 136–151.

Baes Jr. C. F., Meyer N. J. and Roberts C. E. (1965) The Hydrolysis of Thorium(1V) at 0 and 95°C. Inorg. Chem. 4, 518–527.

Banks D. A., Yardley B. W. D., Campbell A. R. and Jarvis K. E. (1994) REE composition of an aqueous magmatic fluid: A fluid inclusion study from the Capitan Pluton, New Mexico, U.S.A. Chem. Geol. 113, 259–272.

Beland C. M. J. and Williams-Jones A. E. (2021) The genesis of the Ashram REE deposit, Quebec: Insights from bulk-rock geochemistry, apatite-monazite-bastnäsite replacement reactions and mineral chemistry. Chem. Geol. 578, 120298.

Brugger J., Liu W., Etschmann B., Mei Y., Sherman D. M. and Testemale D. (2016) A review of the coordination chemistry of hydrothermal systems, or do coordination changes make ore deposits? Chem. Geol. 447, 219–253.

Castor S. B. (2008) The Mountain Pass rare-earth carbonatite and associated ultrapotassic rocks, California. Can. Mineral. 46, 779–806.

Cetiner Z. S., Wood S. A. and Gammons C. H. (2005) The aqueous geochemistry of the rare earth elements. Part XIV. The solubility of rare earth element phosphates from 23 to 150 °C. Chem. Geol. 217, 147–169.

Clark A. M. (1984) Mineralogy of the Rare Earth Elements. In Developments in Geochemistry Elsevier. pp. 33–61.

Cook N. J., Ciobanu C. L., O'Rielly D., Wilson R., Das K. and Wade B. (2013) Mineral chemistry of Rare Earth Element (REE) mineralization, Browns Ranges, Western Australia. Lithos 172–173, 192–213.

Cuney M. and Friedrich M. (1987) Physicochemical and crystal-chemical controls on accessory mineral paragenesis in granitoids: implications for uranium metallogenesis. Bull. Mineral. 110, 235–247.

Ekberg C., Albinsson Y., Comarmond M. J. and Brown P. L. (2000) Study on the complexation behavior of thorium(IV).1. Hydrolysis equilibria. J. Solut. Chem. 29, 63–86.

Felmy A. R. and Rai D. (1999) Application of Pitzer's Equations for Modeling the Aqueous Thermodynamics of Actinide Species in Natural Waters: A Review. J. Solut. Chem. 28, 533–553.

Felmy A. R., Rai D., Sterner S. M., Mason M. J., Hess N. J. and Conradson S. D. (1997) Thermodynamic models for highly charged aqueous species: Solubility of Th(IV) hydrous oxide in concentrated $NaHCO_3$ and Na_2CO_3 solutions. J. Solut. Chem. 26, 233–248.

Gammons C. H. and Wood S. A. (2002) Complexation of the rare earth elements with aqueous chloride at 200°C and 300 °C and saturated water vapor pressure. Geochem. Soc. Spec. Publ. 7, 191–207.

Gavrichev K. S., Smirnova N. N., Gurevich V. M., Danilov V. P., Tyurin A. V., Ryumin M. A. and Komissarova L. N. (2006) Heat capacity and thermodynamic functions of $LuPO_4$ in the range 0–320K. Thermochim. Acta 448, 63–65.

Grenthe I. and Lagerman B. (1991) Studies on metal carbonate equilibria: 23. Complex formation in the Th(IV)-H_2O-CO_2(g) system. Acta Chem. Scand. 45, 231–238.

Gysi A. P., Harlov D., Filho D. C. and Williams-Jones A. E. (2016) Experimental determination of the high temperature heat capacity of a natural xenotime-(Y) solid solution and synthetic $DyPO_4$ and $ErPO_4$ endmembers. Thermochim. Acta 627–629, 61–67.

Gysi A. P. and Williams-Jones A. E. (2015) The thermodynamic properties of bastnäsite-(Ce) and parisite-(Ce). Chem. Geol. 392, 87–101.

Gysi A. P., Williams-Jones A. E. and Harlov D. (2015) The solubility of xenotime-(Y) and other HREE phosphates (DyPO 4 , ErPO4 and YbPO 4) in aqueous solutions from 100 to 250 °C and p sat. Chem. Geol. 401, 83–95.

Gysi A. P. and Harlov D. (2021) Hydrothermal solubility of $TbPO_4$, $HoPO_4$, $TmPO_4$, and $LuPO_4$ xenotime endmembers at pH of 2 and temperatures between 100 and 250 °C. Chemical Geology 567, 120072.

Haas J. R., Shock E. L. and Sassani D. C. (1995) Rare earth elements in hydrothermal systems: Estimates of standard partial molal thermodynamic properties of aqueous complexes of the rare earth elements at high pressures and temperatures. Geochim. Cosmochim. Acta 59, 4329–4350.

Hubert S., Barthelet K., Fourest B., Lagarde G., Dacheux N. and Baglan N. (2001) Influence of the precursor and the calcination temperature on the dissolution of thorium dioxide. J. Nucl. Mater. 297, 206–213.

Johansson G., Magini M. and Ohtaki H. (1991) Coordination around thorium (IV) in aqueous perchlorate, chloride and nitrate solutions. J. Solut. Chem. 20, 775–792.

Jones A. P., Wall F. and Williams C. T. (1996) Rare earth minerals. Chemistry, origin and ore deposits.,

Kobayashi T., Sasaki T., Takagi I. and Moriyama H. (2016) Effect of solid phase transformation on the solubility product of thorium hydrous oxide at 363 K. J. Nucl. Sci. Technol. 53, 1787–1793.

Langmuir D. and Herman J. S. (1980) The mobility of thorium in natural waters at low temperatures. Geochim. Cosmochim. Acta 44, 1753–1766.

Li M. Y. H., Zhou M.-F. and Williams-Jones A. E. (2019) The Genesis of Regolith-Hosted Heavy Rare Earth Element Deposits: Insights from the World-Class Zudong Deposit in Jiangxi Province, South China. Econ. Geol. 114, 541–568.

Liu X. and Byrne R. H. (1997) Rare earth and yttrium phosphate solubilities in aqueous solution. Geochim. Cosmochim. Acta 61, 1625–1633.

Long K. R., Van Gosen B. S., Foley N. K. and Cordier D. (2010) The Principal Rare Earth Elements Deposits of the United States- A Summary of Domestic Deposits and a Global Perspective., U.S. Geological Survey.

Luo Y. and Millero F. J. (2004) Effects of temperature and ionic strength on the stabilities of the first and second fluoride complexes of yttrium and the rare earth elements. Geochim. Cosmochim. Acta 68, 4301–4308.

Maiorova E. P. and Fomin V. V. (1958) Extraction of thorium with tributyl phosphate. III. Effect of sulfate ions on the distribution of thorium. Russ. J. Inorg. Chem. 3, 295–316.

Migdisov A. A. and Williams-Jones A. E. (2002) A spectrophotometric study of neodymium(III) complexation in chloride solutions. Geochim. Cosmochim. Acta 66, 4311–4323.

Migdisov A. A. and Williams-Jones A. E. (2014) Hydrothermal transport and deposition of the rare earth elements by fluorine-bearing aqueous liquids. Miner. Deposita 49, 987–997.

Migdisov A. and Williams-Jones A. E. (2008) A spectrophotometric study of Nd(III), Sm(III) and Er(III) complexation in sulfate-bearing solutions at elevated temperatures. Geochim. Cosmochim. Acta 72, 5291–5303.

Migdisov A., Williams-Jones A. E., Brugger J. and Caporuscio F. A. (2016) Hydrothermal transport, deposition, and fractionation of the REE: experimental data and thermodynamic calculations. Chem. Geol. 439, 13–42.

Migdisov Art. A., Reukov V. V. and Williams-Jones A. E. (2006) A spectrophotometric study of neodymium(III) complexation in sulfate solutions at elevated temperatures. Geochim. Cosmochim. Acta 70, 983–992.

Migdisov Art. A., Williams-Jones A. E. and Wagner T. (2009) An experimental study of the solubility and speciation of the Rare Earth Elements (III) in fluoride- and chloride-bearing aqueous solutions at temperatures up to 300°C. Geochim. Cosmochim. Acta 73, 7087–7109.

Migdissov A. A. and Williams-Jones A. E. (2007) An experimental study of the solubility and speciation of neodymium (III) fluoride in F-bearing aqueous solutions. Geochim. Cosmochim. Acta 71, 3056–3069.

Moeller T. (1973) The Lanthanides. In The Chemistry of the Lanthanides Elsevier. pp. 1–101.

Moon H. (1989) Equilibrium ultrafiltration of hydrolyzed thorium(IV) solutions. Bull. Korean Chem. Soc. 10, 270–272.

Moriyama H., Kitamura A., Fujiwara K. and Yamana H. (1999) Analysis of mononuclear hydrolysis constants of actinide ions by hard sphere model. Radiochim. Acta 87, 97–104.

Morss L. R., Edelstein N. M. and Fuger J. (2006) Thorium. In The Chemistry of the Actinide and Transactinide Elements pp. 52–160.

Muthaiah S., Bhatia A. and Kannan M. (2020) Stability of Metal Complexes. In Stability and Applications of Coordination Compounds

Navrotsky A., Lee W., Mielewczyk-Gryn A., Ushakov S. V., Anderko A., Wu H. and Riman R. E. (2015) Thermodynamics of solid phases containing rare earth oxides. J. Chem. Thermodyn. 88, 126–141.

Neck V., Altmaier M., Muller R., Bauer A., Fanghanel Th. and Kim J. I. (2003) Solubility of crystalline thorium dioxide. Radiochim. Acta 91, 253–262.

Neck V. and Kim J. I. (2001) Solubility and hydrolysis of tetravalent actinides. Radiochim. Acta 89, 1–16.

Nisbet H., Migdisov A., Xu H., Guo X., van Hinsberg V., Williams-Jones A. E., Boukhalfa H. and Roback R. (2018) An experimental study of the solubility and speciation of thorium in chloride-bearing aqueous solutions at temperatures up to 250 °C. Geochim. Cosmochim. Acta 239, 363–373.

Osthols E., Bruno J. and Grenthe I. (1994) On the influence of carbonate on mineral dissolution: III. The solubility of microcrystalline ThO_2 in CO_2-H_2O media. Geochim. Cosmochim. Acta 58, 613–623.

Patil S. K. and Ramakrishna V. V. (1972) Study of the sulphate complexing of Th(IV) by solvent extraction with dinonyl naphthalene sulphonic acid. Radiochim. Acta 18, 190–192.

Pearson R. G. (1963) Hard and soft acids and bases. J. Am. Chem. Soc. 85, 3533–3539.

Poitrasson F., Oelkers E., Schott J. and Montel J.-M. (2004) Experimental determination of synthetic $NdPO_4$ monazite end-member solubility in water from 21°C to 300°C: implications for rare earth element mobility in crustal fluids. Geochim. Cosmochim. Acta 68, 2207–2221.

Pourtier E., Devidal J.-L. and Gibert F. (2010) Solubility measurements of synthetic neodymium monazite as a function of temperature at 2kbars, and aqueous neodymium speciation in equilibrium with monazite. Geochim. Cosmochim. Acta 74, 1872–1891.

Rai D., Moore D. A., Oakes C. S. and Yui M. (2000) Thermodynamic model for the solubility of thorium dioxide in the Na+-Cl–-OH–-H_2O system at 23 °C and 90°C. Radiochim. Acta 88, 297–306.

Rand M. H., Mompean F. J., Perrone J. and Illemassene M. (2008) Chemical Thermodynamics of Thorium., OECD, NEA.

Seward T. M., Williams-Jones A. E. and Migdisov A. A. (2014) The Chemistry of Metal Transport and Deposition by Ore-Forming Hydrothermal Fluids. In Treatise on Geochemistry Elsevier. pp. 29–57.

Seward T. M., Williams-Jones A. E. and Migdissov A. A. (2013) The Chemistry of Metal Transport and Deposition by Ore-Forming Hydrothermal Fluids. Treatise Geochem. 10, 29–57.

Smith M. P. and Henderson P. (2000) Preliminary Fluid Inclusion Constraints on Fluid Evolution in the Bayan Obo Fe-REE-Nb Deposit, Inner Mongolia, China. Econ. Geol. 95, 1371–1388.

Smith M. P., Henderson P. and Campbell L. S. (2000) Fractionation of the REE during hydrothermal processes: constraints from the Bayan Obo Fe-REE-Nb deposit, Inner Mongolia, China. Geochim. Cosmochim. Acta 64, 3141–3160.

Van Hoozen C. J., Gysi A. P. and Harlov D. E. (2020) The solubility of monazite (LaPO4, PrPO4, NdPO4, and EuPO4) endmembers in aqueous solutions from 100 to 250 °C. Geochimica et Cosmochimica Acta 280, 302–316.

Vance E. R., Zhang Y., McLeod T. and Davis J. (2011) Actinide valences in xenotime and monazite. J. Nucl. Mater. 409, 221–224.

Vasyukova O. V. and Williams-Jones A. E. (2018) Direct measurement of metal concentrations in fluid inclusions, a tale of hydrothermal alteration and REE ore formation from Strange Lake, Canada. Chem. Geol. 483, 385–396.

Vasyukova O. and Williams-Jones A. (2020) Partial melting, fractional crystallisation, liquid immiscibility and hydrothermal mobilisation – A ‘recipe’ for the formation of economic A-type granite-hosted HFSE deposits. Lithos 356–357, 105300.

Verplanck P. L. and Hitzman M. W. (2016) Rare earth and critical elements in ore deposits., Voigt M., Rodriguez-Blanco J. D., Vallina B., Benning L. G. and Oelkers E. H. (2016) An experimental study of hydroxylbastnasite solubility in aqueous solutions at 25 °C. Chem. Geol. 430, 70–77.

Voncken (2016) The Ore Minerals and Major Ore Deposits of the Rare Earths. In The Rare Earth Elements Springer International Publishing, Cham. pp. 15–52.

Williams-Jones A. E., Samson I. M. and Olivo G. R. (2000) The genesis of hydrothermal fluorite-REE deposits in the Gallinas Mountains, New Mexico. Econ. Geol. 95, 327–341.

Williams-Jones A. E. and Vasyukova O. V. (2018) The Economic Geology of Scandium, the Runt of the Rare Earth Element Litter. Econ. Geol. 113, 973–988.

Wood S. A. (1990a) The aqueous geochemistry of the rare-earth elements and yttrium. Chem. Geol. 82, 159–186.

Wood S. A. (1990b) The aqueous geochemistry of the rare-earth elements and yttrium 2. Theoretical predictions of speciation in hydrothermal solutions to 350°C at saturation water vapor pressure. Chem. Geol. 88, 99–125.

Wood S. A., Palmer D. A., Wesolowski D. J. and Bénézeth P. (2002) The aqueous geochemistry of the rare earth elements and yttrium. Part XI. The solubility of $Nd(OH)_3$ and hydrolysis of Nd^{3+} from 30 to 290 °C at saturated water vapor pressure with in-situ pHm measurement. Water-Rock Interact. Ore Depos. Environ. Geochem. Tribute David Crerar Geochem. Soc. Spec. Publ., 229–256.

Zanonato P. L., Bernardo P. D., Zhang Z., Gong Y., Tian G., Gibson J. K. and Rao L. (2016) Hydrolysis of thorium(IV) at variable temperatures. Dalton Trans. 45, 12763–12771.

Zebroski E. L., Alter H. W. and Heumann F. K. (1951) Thorium Complexes with Chloride, Fluoride, Nitrate, Phosphate and Sulfate. J. Am. Chem. Soc. 73, 5646–5650.

Zielen A. J. (1959) Thermodynamics of the sulfate complexes of thorium. J. Am. Chem. Soc. 81, 5022–5028.

Preface to Chapter 2

The mobility of thorium in hydrothermal fluids depends on the solubility of a Th-bearing mineral, the availability of ligands to form aqueous complexes with Th ions, and the stability of those complexes. To date, high-temperature data on the solubility and speciation of Th are absent from the literature, thus calling for a comprehensive study to assess the complexation of Th with ligands that are abundant in natural hydrothermal fluids.

Chloride is one of the dominant ligands in hydrothermal fluids, and this ligand has been shown to form stable complexes with the REE, with which Th is intimately associated in natural hydrothermal systems. In the following chapter, we explore the speciation of Th in chloride-bearing hydrothermal solutions. Through a series of autoclave solubility experiments, we determine that Th-chloride complexes are not stable under the experimental conditions investigated, in contrast to the REE, and rather, Th-hydroxyl complexes predominate. Using the experimental data collected in this study, we derive thermodynamic formation constants for the predominant Th-hydroxyl species and discuss the potential for chloride-bearing hydrothermal solutions to transport Th in natural settings.

Chapter 2

An experimental study of the solubility and speciation of thorium in chloride-bearing aqueous solutions at temperatures up to 250 °C

Haylea Nisbet[1,2*], Artas Migdisov[1], Hongwu Xu[1], Xiaofeng Guo[3], Vincent van Hinsberg[2], Anthony Williams-Jones[2], Hakim Boukhalfa[1], Robert Roback[1]

[1] Earth and Environmental Sciences Division, Los Alamos National Laboratory, P.O. Box 1663, M.S. J535, Los Alamos, NM 87545, USA

[2] Department of Earth and Planetary Sciences, McGill University, 3450 University Street, Montreal H3A 0E8, Canada

[3] Department of Chemistry and Alexandra Navrotsky Institute for Experimental Thermodynamics, Washington State University, Pullman, Washington 99164, USA

*haylea.nisbet@mail.mcgill.ca

Published in Geochmica et Cosmochimica Acta, August 2018.

DOI: https://doi.org/10.1016/j.gca.2018.08.001

Abstract

The solubility and speciation of Th in Cl-bearing solutions saturated in ThO_2 were investigated experimentally at 150, 175, 200, 225, and 250 °C, and saturated water vapor pressure. At these experimental conditions ($pH_{25°C} < 3.8$, $mNaCl < 2.5$), Th-chloride complexation is insignificant, and the solubility of Th is controlled by hydrolysis. The two main species in solution were identified as $Th(OH)_2^{2+}$ and $Th(OH)_4^0$ and formed via the reactions $Th^{4+} + 2OH^- \leftrightarrow Th(OH)_2^{2+}$ and $Th^{4+} + 4OH^- \leftrightarrow Th(OH)_4^0$. The logarithms of the formation constants determined for the first reaction are 23.91 ± 0.05, 24.79 ± 0.07, 25.78 ± 0.05, and 25.85 ± 0.05 for 175, 200, 225 and 250 °C, respectively, and 42.18 ± 0.06, 43.50 ± 0.07, 43.17 ± 0.08, and 43.74 ± 0.11 for the second reaction at the same temperatures. Formation constants could not be determined reliably for 150 °C. Extrapolations of our formation constants to 25 °C are in excellent agreement with the values determined at 25 °C by Neck and Kim (2001) and Ekberg et al. (2000). For natural systems buffered by thorianite (ThO_2), the solubility determined in our study likely reflects a minimum, as the presence of additional ligands would lead to higher solubility.

2.1 Introduction

The presence of Th and its intrinsic radioactivity is a critical issue in ore deposits, particularly with the extraction of rare earth elements (REE). The REE have attracted considerable attention because of the emergence of new technologies with energy and environmental applications. Indeed, several of these elements are considered to be critical elements because of concerns about their supply (U.S. Department of Energy, 2011), which has made exploration for new REE deposits a priority. A major issue associated with the recovery of REE from these deposits is that two of the primary REE ore minerals, monazite and xenotime, commonly have high Th contents, and this has led to significant increases in REE recovery costs and the production of undesirable radioactive waste (Findeib and Schaffer, 2017). For example, monazite can contain up to 20 wt.% ThO_2, causing the radioactivity of monazite ores to reach 6 pCi/g (Seydoux-Guillaume et al., 2002). In addition to being a liability, the presence of Th can also provide a benefit, as shown by the fact that Steenkampskraal (South Africa), the richest monazite deposit in the World with REE_2O_3 (TREO) and ThO_2 reserves of 86,900 tons and 11,700 tons, respectively (http://steenkampskraalrareearths.co.za), is currently being considered for exploitation of both Th (nuclear energy) and the REE; the monazite contains ~60 wt.% TREO and ~8 wt.% Th (Andreoli et al., 1994). Modern exploration is based on genetic models and, thus, in the case of REE deposits, this requires an understanding of the factors controlling the transport and deposition of both Th and the REE. This understanding will promote the discovery of Th depleted ores, required for REE mining, or Th-enriched ores, which would be of interest in the nuclear energy industry.

There is now general agreement that hydrothermal fluids play a significant and, in some cases, dominant role in the formation of REE ore deposits. An important example of this is the Bayan Obo REE deposit in China, which is responsible for ~45% of world REE production, and for which there is compelling evidence of a major role for hydrothermal fluids in its genesis (e.g. (Chao et al., 1992; Smith et al., 2000, 2015). The mobilization of REE by hydrothermal fluids is controlled mainly by the availability of suitable ligands (e.g., CO_3^{2-}, Cl^-, SO_4^{2-}) in significant concentrations and the stability of REE complexes involving these ligands. Migdisov and Williams-Jones (2002, 2008) have provided experimental evidence that chloride and sulfate form very stable aqueous complexes with the REE at elevated temperatures, and Migdisov and Williams-Jones (2014) that these are the main ligands for REE transport in natural hydrothermal systems. This behavior of the REE suggests that similar complexation may be responsible for the mobilization of Th in these systems, due to their common association in minerals such as monazite. Unfortunately, whereas there is now a reasonably good understanding of the complexation of the REE in hydrothermal fluids (Migdisov et al., 2016), this is not the case for Th. There are no relevant experimental data for Th complexation at elevated temperatures and consequently, its mobilization in hydrothermal systems cannot be evaluated.

The experimental studies of Th solubility and speciation in aqueous solutions have been restricted to ambient temperature (Baes Jr. et al., 1965; Moon, 1989; Grenthe and Lagerman, 1991; Moriyama et al., 1999; Ekberg et al., 2000; Neck and Kim, 2001) except for a few at 85–95 °C (Baes Jr. et al., 1965; Rai et al., 2000; Zanonato et al., 2016). It is well established that at ambient temperature, Th, a tetravalent actinide ion with a high electric charge, has a strong tendency to hydrolyze in aqueous solutions (Neck and Kim, 2001). This strong affinity for hydroxyl ligands results in highly polymerized hydroxy complexes. Only under extremely acidic conditions ($pH_{25°C}$ < 3) does the Th^{4+} ion predominate (Langmuir and Herman, 1980). Experimental studies of the coordination around the Th^{4+} ion in aqueous chloride and perchlorate solutions via large angle X-ray scattering measurements have shown that, whereas no complexation is detectable with perchlorate, Th forms weak complexes with chloride ions (Johansson et al., 1991). In comparison to other actinides, aqueous Th-chloride complexes are weaker than aqueous uranium (IV), neptunium, and plutonium(IV) chloride complexes (Grenthe et al., 1992; Lemire et al., 2001; Guillaumont et al., 2003). Aqueous REE chloride complexes are also weak at ambient temperature, but their stability increases with increasing temperature. It is, therefore, reasonable to predict that the same would also be true for Th-chloride complexes.

The observation that Th is commonly present in appreciable concentrations in monazite and xenotime provides strong evidence that the REE and Th can be transported by the same hydrothermal fluids. This and the findings that the REE and Th form detectable chloride complexes at ambient temperature, and that the REE form relatively strong chloride complexes at elevated temperature, suggest that chloride complexes may also be important for the transport of Th in ore-forming hydrothermal systems. The main objective of our study, therefore, was to experimentally investigate the speciation of Th in NaCl-bearing aqueous solutions at hydrothermal conditions and determine stability constants for the main Th complexes.

2.2 Experimental method

The experiments involved determining the solubility of Th in aqueous solutions of variable pH and NaCl concentration at 150, 175, 200, 225, and 250 °C, and the pressure of saturated water vapor. Teflon reactors (50 mL PFA test tubes) were used to contain the experimental solutions and were placed inside titanium autoclaves that had been treated with nitric acid to create a dense layer of TiO_2 for the purpose of ensuring the chemical inertness of the internal surfaces. At the beginning of each experiment, small quartz tubes containing crystalline ThO_2 (IBI Labs, Technical Grade 99.8%), capped with silica wool were added to the Teflon reactors and submerged in their respective chloride solutions (between 10 and 12 mL). The titanium autoclaves were sealed with a Teflon O-ring, and heated for 1–2 weeks in a Muffle Furnace inside an aluminum box with 1.5 cm thick walls to reduce temperature gradients. After the conclusion of each experiment, the autoclaves were quenched in a stream of cold air, the ThO_2 was removed from the reactors, and the pH of the solutions was measured using a calibrated glass electrode at ambient conditions. The electrode was calibrated using a series of NaCl/HCl solutions ($pH_{25°C}$ = 1.14, 1.43, 1.98, 2.43, 2.63) with NaCl concentrations identical to those used in the experimental solutions. After measuring pH, 1 mL of H_2SO_4 (TraceMetal Grade) was added to the solutions and left for 24h in order to ensure the dissolution of any possible Th that may have precipitated on the walls of the reactors during quenching. Concentrations of Th were measured using inductively coupled plasma mass spectrometry (ICP-MS) at the Geochemical and Geomaterials Research Laboratories of the Los Alamos National Laboratory. A sketch of the experimental setup is shown in Fig.2.1.

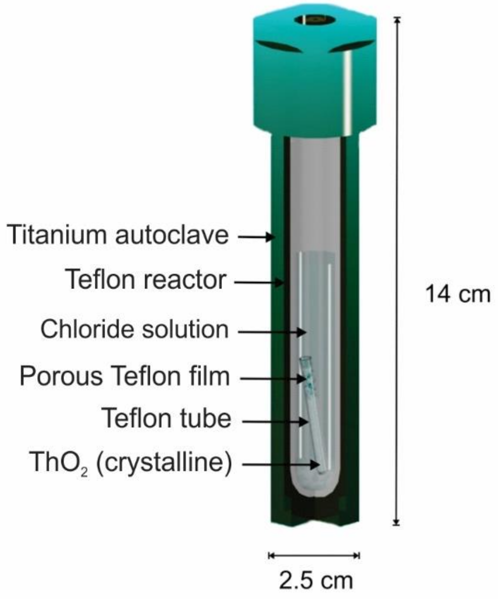

Figure 2.1 A sketch of the experimental setup used in this study.

Two series of solutions were prepared and used in the experiments: (1) NaCl-HCl solutions with 0.25–2.5 m [mol/kg] NaCl and $pH_{25°C}$ 1.55–1.97 to investigate the solubility of Th as a function of Cl concentration, and (2) NaCl-HCl solutions with 1.0 m NaCl and $pH_{25°C}$ 1.45–3.81, to determine the effect of pH. The solutions were prepared with distilled water acidified with hydrochloric acid (TraceMetal Grade), and predetermined amounts of NaCl (A.C.S. Grade) were added to set the chloride concentration in each solution.

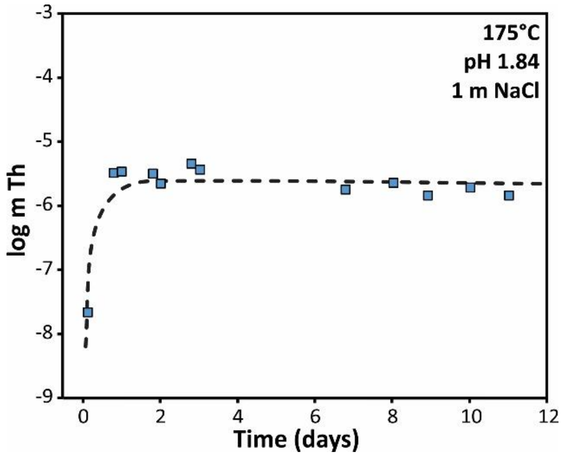

Figure 2.2 Results of time series experiments performed at 175 °C. As illustrated in the graph, equilibrium was attained after less than 1 day.

To ensure there was no contamination between experiments, the Teflon reactors and titanium autoclaves were cleaned repeatedly with nitric acid (TraceMetal Grade) and distilled water. A series of washing solutions were analyzed alongside the experimental solutions to verify that there was no residual Th in the vessels. The time required to attain equilibrium in the solutions was determined by a set of independent time-series experiments having durations from 1−12 days. An example of these experiments for 175 °C and a solution having 1 m NaCl and a $pH_{25°C}$ of 1.84 is shown in Fig. 2.2. From the Figure, it can be seen that equilibrium was attained in less than 24 h; the time would have been even less at a higher temperature. All of our experiments, which were performed for durations longer than a week, thus represent equilibrium/steady-state conditions. The constancy of Th concentration observed in these time series suggests that contamination by additional ligands (e.g. F attributed to the slow release from Teflon tubes) is insignificant in the experimental solutions. In order to confirm the reference phase (ThO_2) was not modified during the experiments and that the solubility values obtained correspond to saturation with respect to crystalline ThO_2, phase characterization of the post-experimental solids was performed using scanning electron microscopy (SEM). This showed that the only solid present was crystalline ThO_2.

Table 2.1 The composition of the experimental solutions including pH values measured after quenching (25 °C) and extrapolated to the temperatures of the experiments.

T (°C)	NaCl, m (mol/Kg)	$pH_{25°C}$	pH_T	Log m Th
150	0.25	1.55	1.70	-5.727
150	0.5	1.65	1.80	-8.084
150	0.75	1.67	1.83	-8.076
150	1.0	1.71	1.87	-7.220
150	1.25	1.74	1.91	-7.513
150	1.5	1.70	1.87	-7.234
150	2.0	1.77	1.94	-8.028
150	2.5	1.95	2.12	-8.374
150	1.0	2.84	2.92	-5.454
150	1.0	3.01	3.09	-5.812
150	1.0	2.35	2.43	-6.234
150	1.0	2.36	2.43	-5.987
150	1.0	1.84	1.90	-5.265
150	1.0	1.89	1.95	-5.661
150	1.0	1.90	1.96	-5.098
150	1.0	1.95	2.01	-5.519
150	1.0	2.17	2.23	-6.305
150	1.0	2.16	2.22	-5.704
150	1.0	2.41	2.48	-5.701
150	1.0	2.44	2.51	-6.257
150	1.0	2.91	3.00	-6.002
150	1.0	2.96	3.05	-6.187
175	0.25	1.58	1.80	-5.648
175	0.5	1.63	1.85	-5.855
175	0.75	1.66	1.87	-5.718
175	1.0	1.71	1.92	-5.832
175	1.5	1.81	2.02	-5.391
175	2.0	1.84	2.06	-5.501
175	2.5	1.97	2.19	-5.832
175	1.0	1.47	1.69	-4.952
175	1.0	1.45	1.67	-5.031
175	1.0	1.91	2.13	-6.454
175	1.0	1.91	2.12	-6.448

175	1.0	2.46	2.67	-7.601
175	1.0	2.47	2.68	-8.084
175	1.0	3.06	3.27	-8.920
175	1.0	3.08	3.29	-8.489
175	1.0	3.77	3.99	-7.293
200	0.25	1.58	1.68	-5.634
200	0.5	1.67	1.80	-8.083
200	0.75	1.65	1.79	-7.614
200	1.0	1.71	1.86	-7.738
200	1.25	1.76	1.92	-7.036
200	1.5	1.73	1.90	-8.234
200	2.0	1.74	1.92	-7.877
200	2.5	1.97	2.16	-8.087
200	1.0	1.92	2.07	-5.855
200	1.0	1.96	2.11	-6.230
200	1.0	2.36	2.51	-6.663
200	1.0	2.37	2.52	-6.541
200	1.0	2.81	2.96	-7.307
200	1.0	2.80	2.95	-7.336
200	1.0	3.69	3.84	-6.587
225	0.25	1.58	1.72	-6.731
225	0.5	1.65	1.83	-6.323
225	0.75	1.66	1.86	-6.443
225	1.0	1.73	1.94	-7.051
225	1.25	1.78	2.02	-6.369
225	1.5	1.75	2.00	-7.585
225	2.0	1.77	2.04	-6.553
225	2.5	1.81	2.10	-6.560
225	1.0	1.91	2.12	-5.710
225	1.0	2.17	2.39	-5.848
225	1.0	2.17	2.38	-6.087
225	1.0	2.71	2.93	-6.961
225	1.0	2.75	2.96	-7.042
225	1.0	3.06	3.27	-7.632
225	1.0	3.25	3.46	-7.812
225	1.0	3.81	4.03	-7.500
250	0.5	1.61	1.86	-6.505
250	0.75	1.63	1.91	-6.522
250	1.0	1.72	2.03	-6.371
250	1.5	1.67	2.01	-6.155
250	2.0	1.70	2.07	-6.174
250	2.5	1.86	2.26	-6.450
250	1.0	1.93	2.23	-5.845
250	1.0	1.95	2.25	-5.975
250	1.0	2.20	2.50	-6.973

250	1.0	2.15	2.45	-6.553
250	1.0	2.45	2.75	-7.145
250	1.0	2.47	2.77	-7.527
250	1.0	3.10	3.40	-7.464

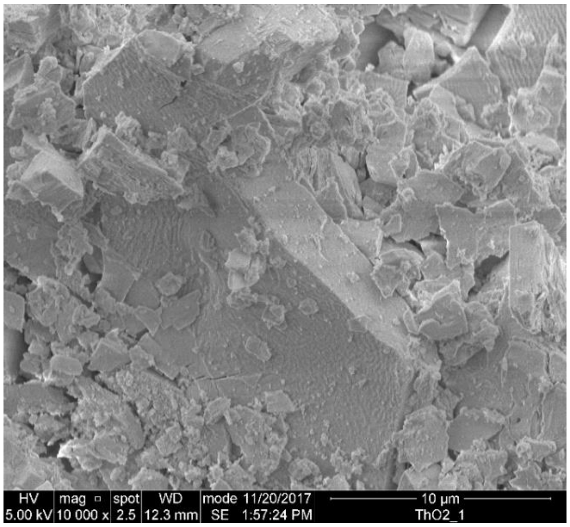

Figure 2.3 A representative micrograph from an SEM analysis of the reference phase. Micron-sized crystalline particles were observed, confirming that the experimental solutions only equilibrated with crystalline ThO_2.

2.3 Results and data treatment

A representative SEM micrograph of the ThO_2 solid after an experiment is displayed in Fig. 2.3. The SEM image shows aggregates of micron-sized crystals with scattered crystallites ~10 µm in length. Although most of the crystals have irregular shapes, cube-like crystals are present, and no amorphous coating was detected, indicating that the ThO_2 was entirely crystalline. The results of the solubility experiments are given in Table 2.1. The table lists the values of pH determined in the experimental solutions after quenching ($pH_{25°C}$), and the values of pH extrapolated to the experimental temperatures (pH_T). This pH adjustment was performed using the extended Debye Hückel model modified by Helgeson et al. (1981), and Oelkers and Helgeson (1990, 1991) for NaCl-dominated solutions (recommended for up to I = 6 and temperatures up to 600 °C):

$$\log \gamma_i = -\frac{A Z_i^2 \sqrt{I}}{1 + B \dot{a} \sqrt{I}} + b_\gamma I + \Gamma \tag{1}$$

where A and B are the Debye–Hückel solvent parameters, γ_i, $Z_{i,}$ and $\dot{a}_i$ are the individual molal activity coefficient, the charge, and the distance of closest approach of an ion *i*, respectively. The effective ionic strength calculated using the molal scale is I, Γ is a molarity to molality conversion factor, and b_γ is the extended-term parameter for NaCl from Helgeson et al. (1981) and Oelkers and Helgeson (1990, 1991). The model involved the following species: H_2O, H^+, OH^-, O_2, H_2, Na^+, $NaOH^0$, $NaCl^0$, Cl^-, and HCl^0 and the thermodynamic data required for modeling the behavior of the solutions at each of the experimental temperatures were taken from Johnson et al. (1992), Sverjensky et al. (1997), and Tagirov et al. (1997). The adjustment of pH to temperatures used in the experiments involved determining the concentrations of HCl in the experimental solutions, based on the values of pH measured at 25 °C after the re-equilibrated solutions were quenched, and incorporating these concentrations into the above model, which was used to derive the pH_T of each experimental solution, as listed in Table 2.1. In order to evaluate the stoichiometry of the dominant Th species, the logarithms of the concentrations of Th obtained in the experimental solutions were plotted as a function of the logarithms of the NaCl concentrations (Fig. 2.4) and pH_T (Fig. 2.5). From Fig. 2.4, it can be seen for each of the isotherms, the concentrations of Th are independent of the concentration of NaCl. In contrast, Fig. 2.5 shows that the concentration of ThO_2 decreases linearly with pH (slope of ~-2) at low pH (pH < ~4), whereas at higher pH Th concentration is independent of pH.

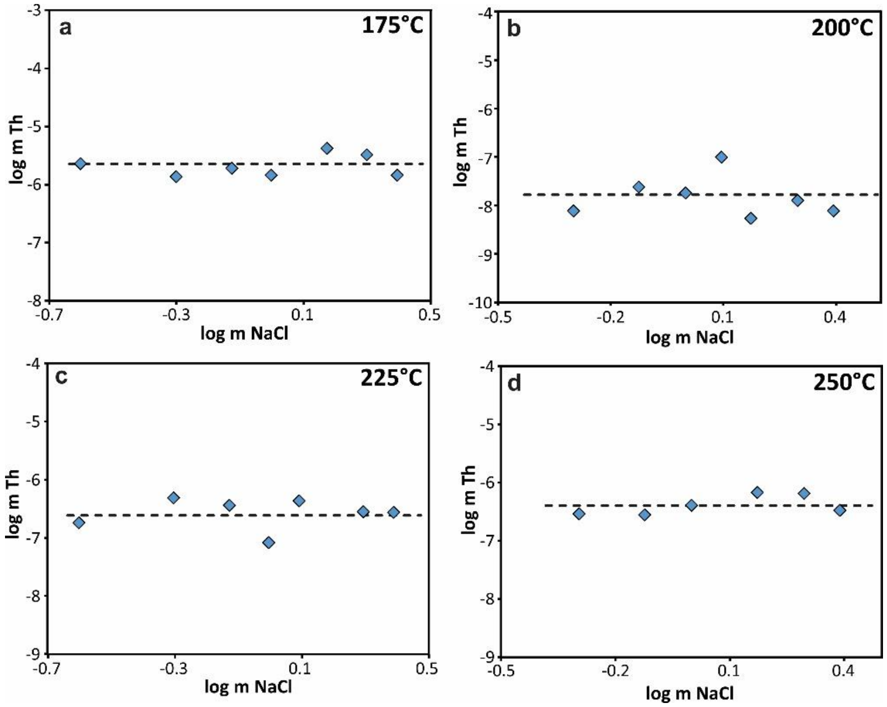

Figure 2.4a-d. The logarithm of Th molality as a function of increasing NaCl content at (a) 175, (b) 200, (c) 225, and (d) 250 °C.

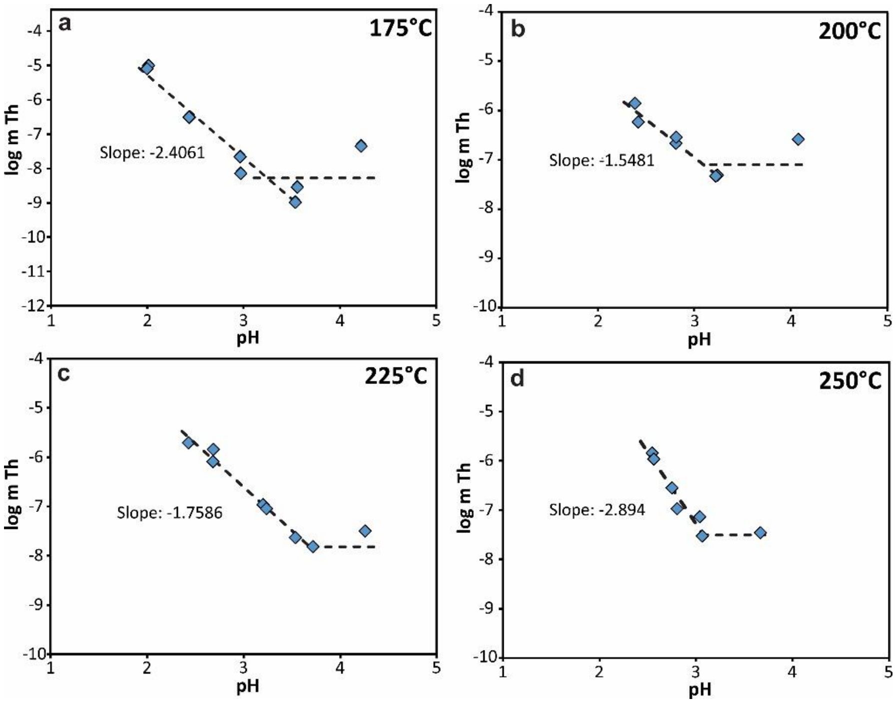

Figure 2.5a-d. The logarithm of Th molality with respect to pH at (a) 175, (b) 200, (c) 225, and (d) 250 °C.

Table 2.2 Logarithms of the formation constants for the species $Th(OH)_2^{2+}$ (log β_2) and $Th(OH)_4^o$ (log β_4) determined in this study.

T (°C)	175	200	225	250
log β_2	23.91 ± 0.05	24.79 ± 0.07	25.78 ± 0.05	25.85 ± 0.05
log β_4	42.18 ± 0.06	43.50 ± 0.07	43.17 ± 0.08	43.74 ± 0.11

2.3.1 Derivation of formation constants

Based on the slopes of the pH-dependent data, we interpret the solubility of Th under each experimental temperature to have been controlled by the formation of two aqueous Th-hydroxyl species. One of these hydroxyl species is considered to be the $Th(OH)_2^{2+}$ species formed through the reaction:

$$ThO_2 + 2H^+ \leftrightarrow Th(OH)_2^{2+} \tag{2}$$

for which the slope of the dependence of log m Th on pH is -2. This is consistent with the distribution of the solubility data at low pH in Fig. 2.5. The other species is $Th(OH)_4^0$, which formed through the reaction:

$$ThO_2 + 2H_2O \leftrightarrow Th(OH)_4^0 \tag{3}$$

This is independent of pH and explains the zero slope of Th concentration as a function of pH in Fig. 2.5.

Formation constants were determined iteratively for each of the isothermal solubility series using the program OptimA, which is part of the HCh software package (Shvarov, 2010). In conjunction with the HCh package, which is used to describe the system of interest (i.e., species, substances; Shvarov, 2008), the program derives standard Gibbs free energies of formation of aqueous species by minimizing the sum of squared deviations of the experimental concentrations of the species of interest in an aqueous solution from their concentrations obtained by calculation of the equilibrium composition of the solution in all experiments performed at the P-T conditions of the experiment (Shvarov, 2015). In addition to the species specified in the model used for the calculation of pH_T (see above), the model also included the following species: ThO_2, Th^{4+}, $Th(OH)_2^{2+}$, and $Th(OH)_4^0$. The thermodynamic properties of water and its dissociation constant were calculated using the Haar-Gallagher-Kell model (Kestin et al., 1984) and the Marshall and Franck (1981) model, respectively. The data for thorianite (ThO_2) and Th^{4+} were taken from Robie and Hemingway (1995) and Shock et al. (1997), respectively. The activity coefficients of the charged species were calculated using the aforementioned extended Debye-Huckel equation (Eq.(1)). Neutral aqueous species activity coefficients were determined following the simplified version of the extended Debye-Huckel equation:

$$log_{\gamma} = \Gamma_{\gamma} + b_{\gamma} I \tag{4}$$

The adjustable parameters in the model were the Gibbs free energies for $Th(OH)_2^{2+}$ and $Th(OH)_4^0$ at each experimental temperature. To compare the derived values of $\Delta G_f(T)$ with the data reported in the literature (which are mostly hydroxyl-explicit), we used the Gibbs free energies to calculate thermodynamic formation constants for these species based on the following reactions:

$$Th^{4+} + 2OH^{-} \leftrightarrow Th(OH)_2^{2+} \tag{5}$$

$$log\beta_2 = loga_{Th(OH)_2^{2+}} - loga_{Th^{4+}} - 2loga_{OH^{-}} \tag{6}$$

$$Th^{4+} + 4OH^{-} \leftrightarrow Th(OH)_4^{0} \tag{7}$$

$$log\beta_4 = loga_{Th(OH)_4^{0}} - loga_{Th^{4+}} - 4loga_{OH^{-}} \tag{8}$$

The resulting formation constants are reported in Table 2.2 together with their associated uncertainty.

Table 2.3 Logarithms of the formation constants for the species $Th(OH)_2^{2+}$ (log β_2) and $Th(OH)_4^o$ (log β_4) at 25 °C reported by other researchers.

References	*log* β_2	*log* β_4
Baes et al. 1965; Baes and Mesmer, 1976	22.2 ± 0.2	40.1 ± 0.3
Moon (1989)	22.46 ± 0.15	42.58 ± 0.08
Ekberg and Albinsson (2000)	21.4 ± 0.2	39 ± 0.5
Moriyama et al., 1999	23.84	40.4
Neck and Kim (2001)	22 ± 0.6	38.5 ± 1.0
Grenthe and Lagerman (1991)		42.4 ± 0.4

2.4 Discussion

The behavior of Th in aqueous solutions at ambient temperature has been described by numerous experimental studies, with most focused on the hydrolysis of Th^{4+}. The solubility products and formation constants derived for the Th species, however, reveal large inconsistencies among the different studies, involving orders of magnitude discrepancies. This disparity among solubility studies has been attributed largely to the improper characterization and variable nature of the reference solids (i.e., ThO_2(crystalline), $Th(OH)_4$(amorphous)), as well as to the possible presence of polynuclear aqueous species and uncertainties over which species to incorporate into the fitting models.

To a large extent, the scatter in solubility data at ambient temperature can be attributed to the nature of the reference solid used in the experiments. Although we have demonstrated clearly that our system attained steady-state immediately at elevated temperatures, solubility studies performed at ambient temperature have failed to reach equilibrium after durations of experiments longer than a year (Neck et al., 2003). These authors attributed the large amount of time required to attain equilibrium to the use of well-crystallized ThO_2 in the experiments, which leads to slow dissolution kinetics at low temperatures (Greiling and Lieser, 1984). In addition to kinetic impediments, experimental studies of ThO_2 solubility and speciation at room temperature are complicated by the formation of amorphous layers on the surface of the reference phase. Even experiments performed with well-characterized crystalline ThO_2 have rendered solubility values that correspond to equilibrium with an amorphous ThO_2 phase rather than crystalline ThO_2 (Neck and Kim, 2001). This has been shown to lead to solubility products that exceed those for crystalline ThO_2 by up to 12 orders of magnitude (Rai et al., 2000). Consequently, the quality of the solubility data is highly dependent on the state of the reference solid, and many authors have noted that its accurate characterization is essential for the interpretation of ambient temperature experimental data. However, as observed by Rai et al. (2000), amorphous ThO_2 transforms to crystalline ThO_2 at temperatures above 90 °C (see also Betterman and Liebau, 1975; Greiling and Lieser, 1984), and therefore amorphitization of the reference solid should not present a problem for experiments at high temperatures (this is supported by the SEM imaging; Fig. 2.3). Moreover, as shown in Fig. 2.2, the constancy of Th concentration in our kinetic series after 24 h is evidence of the absence of any recrystallization to another phase that would arise if there had been a metastable reference phase.

In addition to the aforementioned problems, the disparity among data describing the hydrolysis of Th(IV) has been attributed to the inclusion of inconsistent sets of species in the chemical models. A number of Th-hydroxide complexes ($Th_x(OH)_y^{4x-y}$), including monomeric (1,1), (2,1), (3,1) and (4,1) species; dimeric (1,2), (2,2), (3,2), (4,2) and (7,2) species; trimeric (3,3), (5,3) and (6,3) species; tetrameric (8,4) and (12,4) species; and hexameric (14,6) and (15,6) species have been reported (Zanonato et al., 2016). However, different experimental methods and differences in the range of Th concentrations, and the ionic media used in the experiments (Zanonato et al., 2016) have made it difficult, if not impossible, to select and interpret the data needed to produce the ‘‘best” chemical model. The incorporation of aqueous polynuclear species in modeling Th solubility at ambient temperature is a topic that remains a subject of debate. For example, it has been suggested that under the conditions of some potentiometric studies (e.g., $pH_{25°C}$ 2.4−4, Th concentrations of 10^{-4}–10^{-2} mol/l), polynuclear species dominate, and mononuclear species are negligible (Neck and Kim, 2001). Nevertheless, in many studies, polynuclear species are omitted, thereby potentially yielding unreliable stability constants. In the simplest of models, such as that of Rai et al. (1997), the solubility of ThO_2 was evaluated assuming that only Th^{4+} ions are present in solution, i.e., that hydroxyl species are absent. At the other extreme, up to five species, including multiple polynuclear species, have been proposed in some models, for example, that presented by Grenthe and Lagerman (1991). It can be assumed that the contribution of polynuclear species to the mass balance of a dissolved element will decrease sharply with increasing temperatures due to the large increase of electrostatic repulsion associated with the decrease of the dielectric constant of water (Brugger et al., 2014; Seward et al., 2014). This destabilization has been demonstrated for polynuclear Bi species up to 150 °C (Brugger et al., 2014). Admittedly, our experimental technique does not permit the differentiation between mononuclear and polynuclear species, however, the reasoning provided above suggests that polynuclear species do not play a significant role in the mass balance of dissolved thorium at the temperatures of our experiments, and we thus propose mononuclear species to be the predominate Th species in solution, as supported by data reported in our study (see discussion below).

This study is, to the best of our knowledge, the first to investigate the behavior of Th in aqueous solutions at elevated temperatures (150–250 °C). The studies that do report higher temperature (up to 95 °C) data (Baes Jr. et al., 1965; Rai et al., 2000; Zanonato et al., 2016), do not report formation constants of the species of interest in the present study. As a result, we can only compare our data to those performed at low temperatures (Table 2.3). In order to compare the formation constants derived in this study with those from low-temperature studies, our formation constants were extrapolated to 25 °C by fitting our formation constants to the Ryzhenko–Bryzgalin (MRB) model (Ryzhenko et al., 1985) modified by Borisov and Shvarov (1992) as described in Shvarov and Bastrakov (1999). The MRB model was developed to fit the temperature and pressure dependence of dissociation constants for ion pairs through the following equation:

$$logK_{(T,P)} = \frac{T_r}{T} logK_{(T_r P_r)} + B_{(T,P)} \left(A_{zz/a} + \frac{B_{zz/a}}{T} \right) \tag{9}$$

where K is the dissociation constant of the ion pair, T_r and P_r are the reference temperature and pressure, and $A_{zz/a}$ and $B_{zz/a}$ are fitting parameters. The term $B_{(T, P)}$ accounts for the properties of water at temperature T and pressure P, which was calculated from the data of Marshall and Franck (1981). The parameters derived from this model for $Th(OH)_2^{2+}$ and $Th(OH)_4^0$ are listed in Table 2.4.

The formation constants extrapolated to 25 °C using the MRB model are compared with the formation constant for this temperature reported by other studies in Fig. 2.6a and b. From these figures, it is evident that the extrapolated formation constants for both $Th(OH)_2^{2+}$ and $Th(OH)_4^0$ are in good agreement with those from the most recent ambient temperature studies, i.e., the studies of Ekberg et al. (2000) and Neck and Kim (2001). The convergence of our stability constants for the selected mononuclear species with published low-temperature values validates the selection of species incorporated into our model. It also justifies the exclusion of polynuclear species for temperatures above 175 °C, which we predicted to be unstable under the conditions of our experiments. We have not reported the stability constants calculated for 150 °C. This is because of the poor convergence of the data during the iterative stages of the derivation process. The values obtained for these formation constants deviate considerably from the trend observed for the other temperatures, raising the possibility that polynuclear species were present at 150 °C.

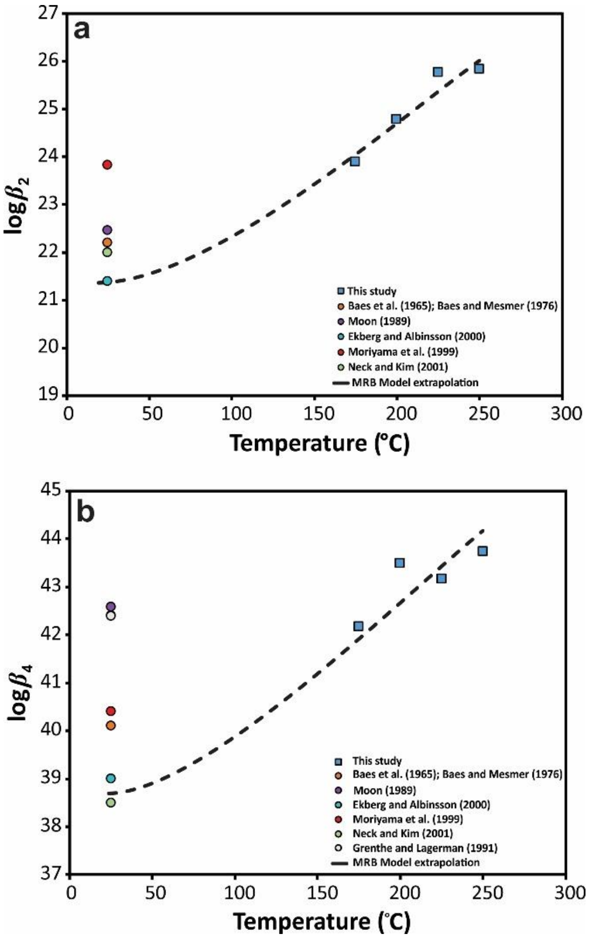

Figure 2.6a-b. Logarithms of formation constants from this study (solid squares) for (a) $Th(OH)_2^{2+}$ and (b) $Th(OH)_4^0$ as a function of temperature and extrapolated to 25 °C using the Ryzhenko-Bryzgalin model (dashed line). Also shown for comparison are the corresponding formation constants at 25 °C reported by other studies.

The data collected in our study suggest that the stability of Th-chloride complexes is weak and that these species, therefore, do not contribute significantly to the mass balance of Th in aqueous solutions at T < 250 °C, mNaCl < 2.5 and $pH_{25°C} < 3.8$. Thus, unlike the REE, for which chloride complexes are believed to be one of the main transport ligands (Migdisov et al., 2016), the behavior of Th in solutions containing considerable concentrations of chloride is mostly controlled by $Th(OH)_2^{2+}$ and $Th(OH)_4^0$ (Fig. 2.5 and 2.7). However, we do not rule out the possibility that Th may show a higher affinity for chloride at a higher temperature, as is the case for U^{4+} (Timofeev et al., 2018).

Table 2.4 Ryzhenko–Bryzgalin (MRB) model parameters derived for temperatures between 175 and 250 °C based on the results of the experiments reported in this study.

	log β				pK(298)	A(zz/a)	B(zz/a)
	175 °C	200 °C	225 °C	250 °C			
$Th(OH)_2^{2+}$	24.13	24.72	25.37	26.12	-20.468	1.755	1458.67
$Th(OH)_4^o$	42.55	42.92	43.32	43.81	-37.610	-0.873	4135.10

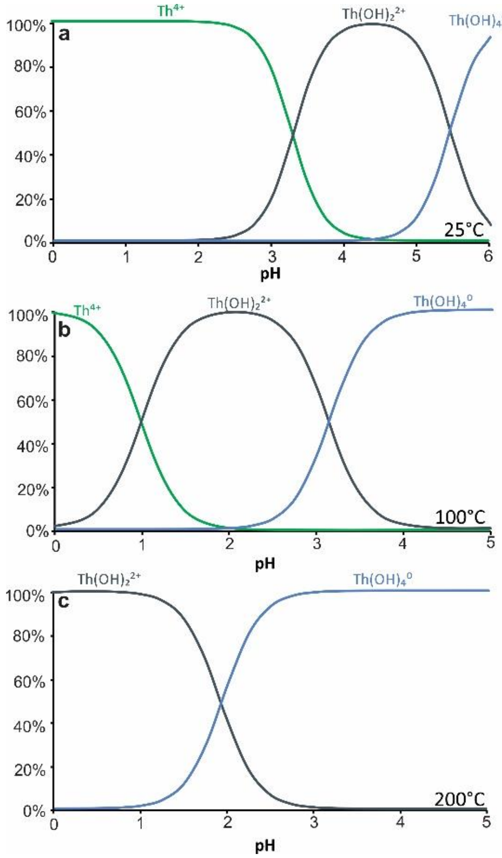

Figure 2.7a-c. Activity speciation diagrams derived from the formation constants calculated from the results of our experiments, illustrating the dominant fields of the different aqueous Th species as a function of pH at (a) 25, (b) 100, and (c) 200 °C.

In more general terms, it is likely that the stability of the above hydroxyl species defines the lowest ‘‘background” solubility level that can be developed in natural hydrothermal solutions in equilibrium with Th-bearing minerals. As chloride does not show significant affinity to Th (at least at T≤ 250 °C), other ligands abundant in natural solutions, such as sulfate or carbonate, can potentially play the role of a transporting agent for this element. Indeed, the data available for the stability of Th sulfate complexes at ambient conditions suggest a significant predominance over chloride and hydroxyl species under acidic conditions (Langmuir and Herman, 1980). Similarly, carbonate complexes are known to be among the strongest for the entire group of actinides (Edelstein and Lander, 2006), and at ambient conditions, the solubility of Th has been shown to increase by orders of magnitude in the presence of carbonates in solution (Rai et al., 1994). If these stability relationships persist at elevated temperatures, it is logical to suspect that for Th, the variability in mobilization capabilities of different natural fluids will be controlled by relative concentrations of these ligands. Evidently, additional studies are necessary for a deeper understanding of its mobility in natural systems.

2.5 Conclusions

The experimental data obtained in this study show that, unlike the REE with which Th is commonly associated in hydrothermal ore deposits, Th-chloride complexation is negligible at the conditions of transport and ore formation. Instead, Th solubility is controlled by the hydrolysis and the formation of the complexes, $Th(OH)_4^0$ and $Th(OH)_2^{2+}$. Formation constants of these complexes were derived from our experimental data for temperatures >175 °C and when extrapolated to 25 °C show good agreement with values reported for ambient temperature. The concentration levels of Th observed in solution represent a solubility minimum, suggested to be reflected in hydrothermal systems of similar conditions.

2.6 Acknowledgments

Research presented in this article was supported by the Laboratory Directed Research and Development program of Los Alamos National Laboratory under project number 20180007DR and by the Los Alamos National Laboratory (LANL) to A.M. through its Center for Space and Earth Science (CSES). CSES is funded by LANL's Laboratory Directed Research and Development (LDRD) program under project number 20180475D.

2.7 References

Andreoli M. A. G., Smith C. B., Watkeys M., Moore J. M., Ashwal L. D. and Hart R. J. (1994) The geology of the Steenkampskraal monazite deposit, South Africa; implications for REE-Th-Cu mineralization in charnockite-granulite terranes. Econ. Geol. 89, 994–1016.

Baes Jr. C. F., Meyer N. J. and Roberts C. E. (1965) The Hydrolysis of Thorium(1V) at 0 and 95°C. Inorg. Chem. 4, 518–527.

Betterman P. and Liebau F. (1975) The transformation of amorphous silica to crystalline silica under hydrothermal conditions. Contrib. Mineral. Petrol. 53, 25–36.

Borisov M. V. and Shvarov Y. V. (1992) Thermodynamics of geochemical processes. Mosc. Mosc. State Univ. Publ. House, 254.

Brugger J., Tooth B., Etschmann B., Liu W., Testemale D., Hazemann J.-L. and Grundler P. V. (2014) Structure and Thermal Stability of Bi(III) Oxy-Clusters in Aqueous Solutions. J. Solut. Chem. 43, 314–325.

Chao E. C. T., Back J. M., Minkin J. A. and Yinchen R. (1992) Host-rock controlled epigenetic, hydrothermal metasomatic origin of the Bayan Obo REEFe-Nb ore deposit, Inner Mongolia, P.R.C. Appl. Geochem. 7, 443–458.

Edelstein N. M. and Lander G. H. (2006) The Chemistry of the Actinide and Transactinide Elements. 3rd ed.,

Ekberg C., Albinsson Y., Comarmond M. J. and Brown P. L. (2000) Study on the complexation behavior of thorium(IV).1. Hydrolysis equilibria. J. Solut. Chem. 29, 63–86.

Findeib M. and Schaffer A. J. (2017) Fate and environmental impact of thorium residues during rare earth processing. J. Sustain. Metall. 3, 179–189.

Greiling H.-D. and Lieser K. H. (1984) Properties of ThO_2, UO_2 and PuO_2 as function of pretreatment and their dissolution in HNO_3. Radiochim. Acta 35, 79–89.

Grenthe I., Fuger J., Konings R. J. M., Lemire R. J., Muller A. B., Nguyen-Trung C. and Wanner H. (1992) Chemical Thermodynamics of Uranium., Nuclear Energy Agency.

Grenthe I. and Lagerman B. (1991) Studies on metal carbonate equilibria: 23. Complex formation in the Th(IV)-H_2O-CO_2(g) system. Acta Chem. Scand. 45, 231–238.

Guillaumont R., Fanghanel T., Fuger J., Grenthe I., Neck V., Palmer D. A. and Rand M. H. (2003) Update on the Chemical Thermodynamics of Uranium, Neptunium, Plutonium, Americium and Technetium., OECD Nuclear Energy Agency.

Helgeson H. C., Kirkham D. H. and Flowers G. C. (1981) Theoretical prediction of the thermodynamic behavior of aqueous electrolytes at high pressures and temperatures: IV. Calculation of activity coefficients, osmotic coefficients, and apparent molal and standard and relative partial molal properties to 600°C. Am. J. Sci. 281, 1249–1516.

Johansson G., Magini M. and Ohtaki H. (1991) Coordination around thorium (IV) in aqueous perchlorate, chloride and nitrate solutions. J. Solut. Chem. 20, 775–792.

Johnson J. W., Oelkers E. H. and Helgeson H. C. (1992) SUPCRT92: a software package for calculating the standard molal thermodynamic properties of minerals, gases, aqueous species, and reactions from 1 to 5000 bar and 0 to 1000 °C. Comput. Geosci. 18, 899–947.

Kestin J., Sengers J. V., Kamgar-Parsi B. and Levelt Sengers J. M. H. (1984) Thermophysical properties of fluid H2O. J. Phys. Chem. Ref. Data 13, 601–609.

Langmuir D. and Herman J. S. (1980) The mobility of thorium in natural waters at low temperatures. Geochim. Cosmochim. Acta 44, 1753–1766.

Lemire R. J., Fuger J., Nitsche H., Potter P. E., Rand M. H., Rydberg J., Spahiu K., Sullivan J. C., Ullman W. J., Vitorge P. and Wanner H. (2001) Chemical Thermodynamics of Neptunium and Plutonium.,

Marshall W. L. and Franck E. U. (1981) Ion product of water substance, 0-1000 °C, 1-10,000 bars new International Formulation and its background. J. Phys. Chem. Ref. Data 10, 295–304.

Migdisov A. A. and Williams-Jones A. E. (2002) A spectrophotometric study of neodymium(III) complexation in chloride solutions. Geochim. Cosmochim. Acta 66, 4311–4323.

Migdisov A. and Williams-Jones A. E. (2008) A spectrophotometric study of Nd(III), Sm(III) and Er(III) complexation in sulfate-bearing solutions at elevated temperatures. Geochim. Cosmochim. Acta 72, 5291–5303.

Migdisov A. and Williams-Jones A. E. (2014) Hydrothermal transport and deposition of the rare earth elements by fluorine-bearing aqueous liquids. Miner. Deposita 49, 987–997.

Migdisov A., Williams-Jones A. E., Brugger J. and Caporuscio F. A. (2016) Hydrothermal transport, deposition, and fractionation of the REE: experimental data and thermodynamic calculations. Chem. Geol. 439, 13–42.

Moon H. (1989) Equilibrium ultrafiltration of hydrolyzed thorium(IV) solutions. Bull. Korean Chem. Soc. 10, 270–272.

Moriyama H., Kitamura A., Fujiwara K. and Yamana H. (1999) Analysis of mononuclear hydrolysis constants of actinide ions by hard sphere model. Radiochim. Acta 87, 97–104.

Neck V., Altmaier M., Muller R., Bauer A., Fanghanel Th. and Kim J. I. (2003) Solubility of crystalline thorium dioxide. Radiochim. Acta 91, 253–262.

Neck V. and Kim J. I. (2001) Solubility and hydrolysis of tetravalent actinides. Radiochim. Acta 89, 1–16.

Oelkers E. H. and Helgeson H. C. (1991) Calculation of activity coefficients and degrees of formation of neutral ion pairs in supercritical electrolyte solutions. Geochim. Cosmochim. Acta 55, 1235–1251.

Oelkers E. H. and Helgeson H. C. (1990) Triple-ion anions and polynuclear complexing in supercritical electrolyte solutions. Geochim. Cosmochim. Acta 54, 727–738.

Rai D., Felmy A. R., Moore D. A. and Mason M. J. (1994) The Solubility of Th(IV) and U(IV) Hydrous Oxides in Concentrated $NaHCO_3$ and Na_2CO_3 Solutions. MRS Proc. 353, 1143.

Rai D., Felmy A. R., Sterner S. M., Moore D. A. and Mason M. J. (1997) The Solubility of Th(IV) and U(IV) Hydrous Oxides in Concentrated NaCl and $MgCl_2$ Solutions. Radiochim. Acta 79, 239–247.

Rai D., Moore D. A., Oakes C. S. and Yui M. (2000) Thermodynamic model for the solubility of thorium dioxide in the Na^+-$Cl^–$-$OH^–$-H_2O system at 23 °C and 90°C. Radiochim. Acta 88, 297–306.

Robie R. A. and Hemingway B. S. (1995) Thermodynamic properties of minerals and related substances at 298.15 K and 1 Bar (10^5 Pascals) pressure and at higher temperatures. US Geol. Survet Bull. 2131, 461.

Ryzhenko B. N., Bryzgalin O. V., Artamkina I. Y., Spasennykh M. Y. and Shapkin A. I. (1985) An electrostatic model for the electrolytic dissociation of inorganic substances dissolved in water. Geochem. Int. 22, 138–144.

Seward T. M., Williams-Jones A. E. and Migdisov A. A. (2014) The Chemistry of Metal Transport and Deposition by Ore-Forming Hydrothermal Fluids. In Treatise on Geochemistry Elsevier. pp. 29–57.

Seydoux-Guillaume A.-M., Wirth R., Heinrich W. and Montel J.-M. (2002) Experimental determination of Thorium partitioning between monazite and xenotime using analytical electron microscopy and X-ray diffraction Rietveld analysis. Eur. J. Mineral. 14, 869–878.

Shock E. L., Sassani D. C., Willis M. and Sverjensky D. A. (1997) Inorganic species in geologic fluids: Correlations among standard molal thermodynamic properties of aqueous ions and hydroxide complexes. Geochim. Cosmochim. Acta 61, 907–950.

Shvarov Y. V. (2015) A suite of programs, OptimA, OptimB, OptimC, and OptimS compatible with the Unitherm database, for deriving the thermodynamic properties of aqueous species from solubility, potentiometry and spectroscopy measurements. Appl. Geochem. 55, 17–27.

Shvarov Y. V. (2008) HCh: new potentialities for the thermodynamic simulation of geochemical systems offered by Windows. Geochem. Int. 46, 898–903.

Shvarov Y. V. (2010) OptimA: A program for the calculation of the free energies of dissolved aqueous species from the results of chemical experiments.

Shvarov Y. V. and Bastrakov E. (1999) HCh, A Software Package for Geochemical Equilibrium Modeling: User’s Guide.

Smith M. P., Campbell L. S. and Kynicky J. (2015) A review of the genesis of the world class Bayan Obo Fe–REE–Nb deposits, Inner Mongolia, China: Multistage processes and outstanding questions. Ore Geol. Rev. 64, 459–476.

Smith M. P., Henderson P. and Campbell L. S. (2000) Fractionation of the REE during hydrothermal processes: constraints from the Bayan Obo Fe-REE-Nb deposit, Inner Mongolia, China. Geochim. Cosmochim. Acta 64, 3141–3160.

Sverjensky D. A., Shock E. L. and Helgeson H. C. (1997) Prediction of the thermodynamic properties of aqueous metal complexes to 1000 °C and 5 kb. Geochim. Cosmochim. Acta 61, 1359–1412.

Tagirov B. R., Zotov A. and Akinfiev N. (1997) Experimental study of dissociation of HCl from 350 to 500 °C and from 500 to 2500 bars: thermodynamic properties of HCl°(aq). Geochim. Cosmochim. Acta 61, 4267–4280.

Timofeev A., Migdisov A., Williams-Jones A. E., Roback R., Nelson A. and Xu H. (2018) Uranium transport in acidic brines under reducing conditions. Nat. Commun. 9.

U.S. Department of Energy (2011) Critical Materials Strategy.,

Zanonato P. L., Bernardo P. D., Zhang Z., Gong Y., Tian G., Gibson J. K. and Rao L. (2016) Hydrolysis of thorium(IV) at variable temperatures. Dalton Trans. 45, 12763–12771.

Preface to Chapter 3

In the previous chapter, we determined that Th-chloride complexation is negligible at elevated temperatures, and, instead, identified two Th-hydroxyl complexes that predominated in the experimental solutions. These complexes, however, did not lead to the significant dissolution of ThO_2. Thus, the question remains as to which aqueous complexes are responsible for mobilizing and concentrating Th to the elevated levels observed in some natural hydrothermal systems.

The sulfate ligand is known to form highly stable complexes with Th at ambient conditions. For this reason, we have dedicated the following chapter to evaluating whether Th-sulfate complexes are also stable at higher temperatures and whether sulfate-bearing hydrothermal fluids can promote the significant mobilization of Th. Autoclave solubility experiments were carried out between 175 and 250 °C and the complexation of Th was determined. The complex, $Th(SO_4)_2$, predominates in all experimental solutions. Thermodynamic formation constants are derived for this species and incorporated into predictive thermodynamic models to identify conditions under which Th-depleted REE deposits can form. Guidelines for the strategic exploration of these deposits are outlined.

Chapter 3

Challenging the thorium-immobility paradigm

Haylea Nisbet[1,2*], Artas Migdisov[1], Anthony Williams-Jones[2], Hongwu Xu[1],
Vincent van Hinsberg[2], Robert Roback[1]

[1]Earth and Environmental Sciences Division, Los Alamos National Laboratory, Los Alamos, NM 87545, USA.

[2] Department of Earth and Planetary Sciences, McGill University, 3450 University Street, Montreal, QC, H3A 0E8, Canada.

*haylea.nisbet@mail.mcgill.ca

Published in Scientific Reports, November 2019

DOI: https://doi.org/10.1038/s41598-019-53571-x

Abstract

Thorium is the most abundant actinide in the earth's crust and has universally been considered one of the most immobile elements in natural aqueous systems. This view, however, is based almost exclusively on solubility data obtained at low temperatures and their theoretical extrapolation to elevated temperature. The occurrence of hydrothermal deposits with high concentrations of Th challenges the Th immobility paradigm and strongly suggests that Th may be mobilized by some aqueous fluids. Here, we demonstrate experimentally that Th, indeed, is highly mobile at temperatures between 175 and 250 °C in sulfate-bearing aqueous fluids due to the formation of the highly stable $Th(SO_4)_2$ aqueous complex. The results of this study indicate that current models grossly underestimate the mobility of Th in hydrothermal fluids, and thus the behavior of Th in ore-forming systems and the nuclear fuel cycle needs to be re-evaluated.

3.1 Introduction

Thorium is primarily concentrated in highly evolved geologic systems, owing to its high charge/radius ratio, which inhibits incorporation into common rock-forming minerals. A consequence is the association of Th with other incompatible elements, particularly the rare earth elements (REE). In the past decade, a mounting interest in the REE (elements that have become critical commodities for a wide range of advanced technologies (Ault et al., 2015)), has prompted researchers and the mining industry to address the behavior of Th. This element, and to a lesser extent U, is known to incorporate into REE ore minerals and, in some cases, reach concentrations in these minerals exceeding 20 wt. % ThO_2 (e.g. monazite). Owing to its intrinsic radioactivity, Th can dictate the economic viability of an ore deposit, making some impossible to mine. Therefore, the ability to predict the behavior of Th in natural systems and identify the conditions at which Th-depleted REE ores can form is crucial for the discovery of new, economic deposits of these highly sought-after elements. As many REE ore deposits are known to have formed by hydrothermal fluids (Chao et al., 1992; Olivo and Williams-Jones, 1999; Cook et al., 2013), knowledge of Th solubility and mobility in these fluids is essential.

Evidence of hydrothermal deposits with high concentrations of Th (Blackburn et al., 1994; Kerr and Rafuse, 2012; Ault et al., 2015) and rocks to which Th has been added or removed hydrothermally (Valsami-Jones and Ragnardottir, 1997) argues convincingly that this actinide can be readily mobilized in hot, aqueous solutions. However, existing models which rely on extrapolations of low-temperature solubility data (Grenthe and Lagerman, 1991; Moriyama et al., 1999; Ekberg et al., 2000; Rai et al., 2000; Neck and Kim, 2001; Zanonato et al., 2016) to high temperatures are unable to explain the observed mobility of Th in both natural and man-made settings. This contradiction arises because information on the behavior of Th in hydrothermal fluids is effectively non-existent, for lack of data on aqueous Th speciation at elevated temperatures and pressures. This information gap has led us to recently begin investigating the solubility and speciation of Th in aqueous solutions at elevated temperatures (Nisbet et al., 2018; Migdisov et al., 2019).

In addition to its role in ore-forming hydrothermal systems, understanding the behavior of Th is relevant for nuclear energy and other nuclear applications (Guo et al., 2016). While underappreciated in the past, Th is now considered to be one of the most promising alternative fuels for the nuclear industry, which is undergoing a major transformation as it seeks to become safer, cleaner, and more sustainable. Not only is Th four times more abundant in nature than uranium, but it also offers a cleaner energy source that produces significantly less waste and is highly resistant to nuclear proliferation (OECD, 2015). Although the concept of Th nuclear reactors is not new and, indeed, has been discussed since the introduction of nuclear energy, the push to develop Th nuclear technology has been particularly strong in the past few decades (OECD, 2015), requiring that we greatly expand our knowledge of Th chemistry at relevant conditions.

The experimental study reported in this contribution presents essential high temperature (175−250 °C) thermodynamic data on the stability of Th-sulfate species in sulfate-bearing solutions; sulfate because of its high affinity for Th at ambient temperatures (Rand et al., 2008) and because sulfate is known to occur in high concentrations in some hydrothermal fluids (Williams-Jones et al., 2000; Walter et al., 2017).

3.2 Results

In this study, we determined the solubility of Th dioxide (ThO_2) in aqueous solutions as a function of sulfate concentration from 0.05 to 0.5m Na_2SO_4 at temperatures between 175 and 250

°C and at the pressure of saturated water vapor. Our results indicate that the amount of Th that can be dissolved in sulfate-bearing solutions is remarkably high, and, moreover, increases with the activity of sulfate at each temperature investigated (Fig. 3.1). This dependence provides compelling evidence that Th forms very stable complexes with sulfate. For each isotherm, the concentration of Th increases with respect to the activity of sulfate at a ratio of 2:1. Based on this ratio, the species controlling the ThO_2 solubility in our experiments is interpreted to be $Th(SO_4)_2$, which formed via the reaction:

$$ThO_2(s) + 2SO_4^{2-} + 4H^+ \leftrightarrow Th(SO_4)_2 + 2H_2O \tag{1}$$

The experimental data (Sup Table 3.1) plotted in Figure 3.1 were used to calculate equilibrium constants (log K) for the above reaction at each temperature. Formation constants (log β_2) relating the predominant species in solution, $Th(SO_4)_2$, to the activity of Th^{4+} and SO_4^{2-} were calculated using the following reaction (Table 3.1):

$$Th^{4+} + 2SO_4^{2-} \leftrightarrow Th(SO_4)_2 \tag{2}$$

$$log\beta_2 = \log a_{Th(SO_4)_2} - \log a_{Th^{4+}} - 2\log a_{SO_4^{2-}} \tag{3}$$

For further information on the calculation of the formation constants, readers are referred to the Supplementary Information file.

Table 3.1 Calculated logarithm of equilibrium constants (log K) and formation constants (log β). Equilibrium constants calculated according to the associated reaction for each experimental temperature investigated, along with the derived uncertainty.

Reaction		175 °C	200 °C	225 °C	250 °C
$ThO_2 + 2SO_4^{2-} + 4H^+ \leftrightarrow Th(SO_4)_2 + 2H_2O$	log K	12.79	14.45	15.67	15.86
$Th^{4+} + 2SO_4^{2-} \leftrightarrow Th(SO_4)_2$	log β_2	17.48	19.83	21.70	22.50
	Uncertainty	± 0.47	± 0.53	± 0.25	± 0.52

The results indicate that under the conditions of our experiments, Th-sulfate complexes completely predominate over Th-hydroxyl complexes, rendering ThO_2 extremely soluble. It should be noted that the contribution of Th-chloride complexes to the solubility of Th has been ignored in our data treatment as we have shown previously (Nisbet et al., 2018) that Th-chloride complexes have very low stability. It is well-known that with decreasing pH, the total concentration of dissolved Th increases as a result of the higher concentration of Th^{4+} (Rand et al., 2008), and that this leads to a higher concentration of Th complexes (e.g. Reaction 2). Indeed, based on our stability constants at 200 °C and a pH of 2, 1 L of solution with the activity of HSO_4^- fixed at 0.1 is predicted to dissolve more than 2 kg of ThO_2 (Fig. 3.2). This exceptionally high solubility is comparable to that of sugar (2039 g/L at 20 °C) (Browne, 1912) in water at room temperature! Although such high Th concentrations are highly unlikely in natural systems (they would require that a stoichiometric equivalent amount of sulfate be present in the solution), these simplistic calculations illustrate the conditions that lead to the exceptionally high solubility of ThO_2, even at temperatures as low as 200 °C. It should be noted that in addition to Th and SO_4^{2-}, our system also contains Si and Ti. However, the observed trends in the experimental data (Fig. 3.1) do not suggest any significant contribution of these elements to the solubility of Th.

Our results suggest that previous studies have grossly underestimated the mobility of Th in natural systems, requiring that existing hypotheses for the behavior of Th in nature be re-evaluated. It also requires that the implementation of nuclear protocols that may lead to the interaction of Th and sulfate be carefully assessed.

3.3 Discussion

Given that the feasibility of exploiting a REE deposit economically is largely governed by the concentration of Th, identifying conditions under which Th-depleted REE deposits form is a pre-

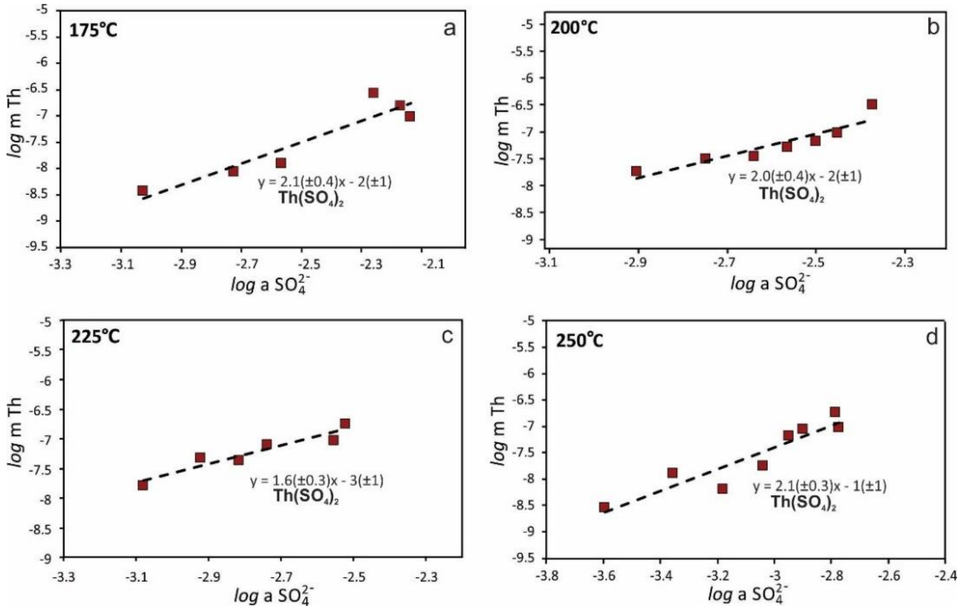

Figure 3.1 The solubility of ThO_2 as a function of sulfate activity. The concentration of Th plotted as a function of the activity of sulfate determined at a) 175 °C, b) 200 °C, c) 225 °C, and d) 250 °C. Each data point represents the concentration of dissolved Th measured in an individual autoclave. The trend lines represent the fit of the data and have a slope of ~2. The error (SD) associated with the individual points is smaller than the markers.

requisite for successful exploration. Modern exploration is based on genetic models that predict geochemical controls on metal enrichment. In the case of REE exploration, an additional requirement is that the models also predict the geochemical controls on Th depletion. Existing models for REE ore genesis have been unable to discriminate between Th-rich and Th-depleted deposits because of the false assumption that Th is effectively immobile in hydrothermal fluids (Migdisov et al., 2019).

To identify conditions in nature, which can lead to the separation of Th from the REE, we simulated the one-directional hydrothermal alteration of a column of rock containing 0.5 wt. % apatite-OH (Ca-hydroxy-phosphate, to allow for the formation of REE phosphates) by a REE and Th-bearing solution. To avoid alteration of the observed trends by pH and other buffering parameters, the rock was assumed to be chemically inert, and the only chemically active component was apatite, which supplied the P needed to form two primary REE ore minerals, monazite (LREEPO$_4$) and xenotime (HREEPO$_4$). The association of these minerals in natural systems have been described previously (Harlov et al., 2002; Harlov and Förster, 2003). The solution altering the rock contained 10 wt.% NaCl, 2 wt.% SO_4^{2-}, and had a pH of 2, consistent with the composition of some natural hydrothermal REE ore systems (e.g. Bayan Obo, Gallinas Mountains; Smith and Henderson, 2000; A. E. Williams-Jones et al., 2000). The simulation uses a step-flow reactor approach ("box model"; Fig. 3.3), which involves the interaction and initial equilibration of a 1 kg aliquot of solution with 1 kg of rock ("Step 1"). Monazite and xenotime were deposited as a result of the initial interaction. The equilibrated fluid then moved to the next reactor where it equilibrated with 1 kg of unaltered rock. This was repeated 15 times, creating a column of rock altered by an initial passage of the first fluid aliquot ("Wave 1"). After completion of this first wave, a new aliquot of fluid (1 kg) of identical composition was flushed through the newly altered column of rock in an identical manner ("Wave 2"). This process was repeated for a total of 10 waves, allowing us to predict how Th and the REE are likely to behave in well-evolved hydrothermal systems that experience continuous flushing of solution. For a complete description of the model, readers are referred to the Supplementary Information files.

At the temperature considered (225 °C), the simulation shows that Th is highly mobile in the modeled solution owing to the high stability of the $Th(SO_4)_2$ complex. Indeed, whereas Th-bearing monazite and xenotime solid solutions precipitated initially, subsequent flushing of the sulfate-bearing fluid through a REE deposit promoted the mobilization and concentration of Th in the wavefront, resulting in the near-complete removal of Th from the ore and the crystallization of Th-depleted monazite and xenotime behind the alteration front (Fig. 3.3). Our simulation provides two important guidelines for an exploration strategy for Th-depleted REE ore deposits. The first of these guidelines is that in choosing among potentially REE-rich targets, preference should be given to targets for which there is evidence of the passage of sulfate-rich fluids (e.g., the presence of sulfate minerals such as barite, anhydrite, and gypsum, or from fluid inclusion studies). The second is that there should be evidence of intensive, pervasive alteration by fluids having the composition required for the mobilization of Th from the ore. In contrast, if the object of exploration is the discovery of a Th deposit that can be used as a raw material for nuclear fuel, the alteration front, enriched with Th (Fig. 3.3), should be in close proximity to the zones depleted with Th; the latter could provide important vectors to economically exploitable Th mineralization.

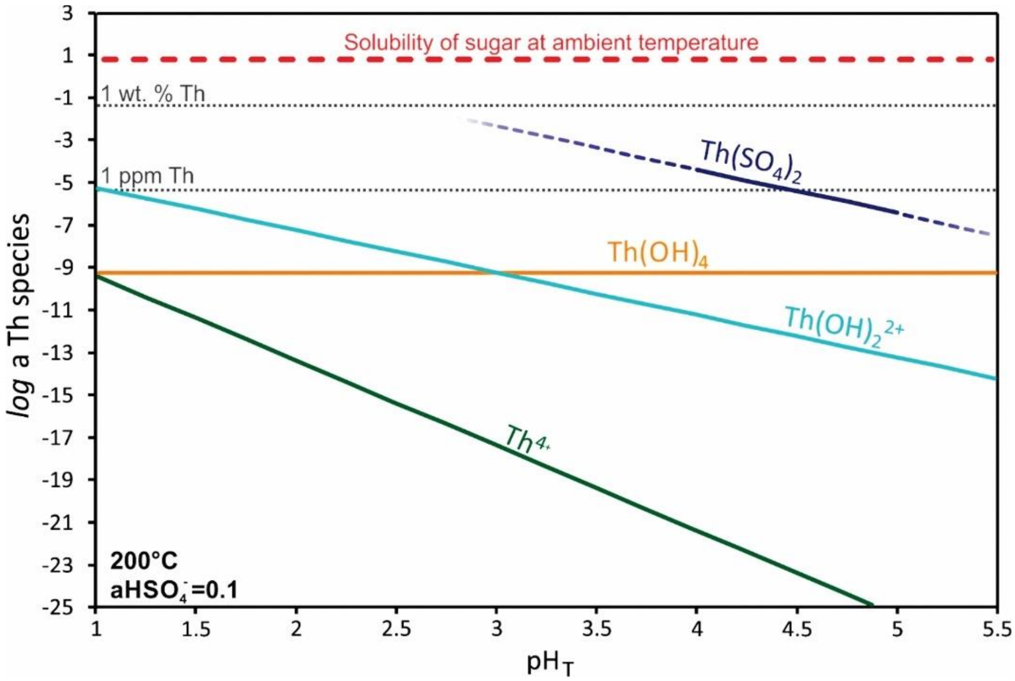

Figure 3.2 A model of aqueous Th speciation. The modeled stability of aqueous Th species as a function of pH in a 1 L solution with an activity of HSO_4^- fixed at 0.1 (activities are after the formation of sulfate complexes of Th) at 200 °C. The solid line for $Th(SO_4)_2$ corresponds to the experimentally investigated range of pH, whereas the dashed lines indicate estimates of Th concentration beyond the measured range.

The mechanism proposed in this model is dependent on the presence of SO_4^{2-} as a ligand in the solution. The potential reduction of SO_4^{2-} in natural systems can lead to the destabilization of Th-sulfate complexes and promote the deposition of Th-bearing minerals. It is known, however, that the thermal reduction of sulfate (TSR) is kinetically inhibited up to 300 °C (Goldstein and

Aizenshtat, 1994) and therefore the reduction of SO_4^{2-} will likely not occur in many natural systems. Furthermore, it is worth noting that a potential restriction on the sulfate-mediated transport of Th is the retrograde solubility of most sulfate solids with temperature. In the calculations reported in this study, however, the concentrations of sulfate considered were taken directly from fluid inclusions of a natural REE hydrothermal system (Banks et al., 1994). A related consideration is the reported occurrence of liquid-liquid immiscibility observed in multiple sulfate-bearing systems (e.g. UO_2, Li, Mg; Wang et al., 2013, 2016, 2017) at elevated temperatures (>285.8 °C, >336.5 °C, and >259.5 °C, respectively) (Weingärtner and Franck, 2005), which may serve to provide a source of excess sulfate for complexation. In these studies, aqueous sulfate solutions were observed to separate into a high density, sulfate-rich (up to 70% of total sulfate) phase and a low-density sulfate-depleted aqueous phase. Whether such liquid-liquid immiscibility can occur in nature or in nuclear industry applications and impact on the transport of Th in high temperature fluids is an intriguing question worthy of study.

This paper reports the first investigation of the behavior of Th at temperatures representative of hydrothermal systems. Contrary to the widely held view that Th is an immobile element, our results demonstrate that in high temperature sulfate-bearing solutions, ThO_2 is extremely soluble, and therefore that Th is highly mobile. This is an important discovery in the field of actinide science that advances our understanding of the behavior of Th. Moreover, it is one that could promote the successful exploration for new, economically viable sources of the REE, facilitate the removal of Th from REE minerals, and potentially lead to new approaches in the fabrication and development of Th-based fuels.

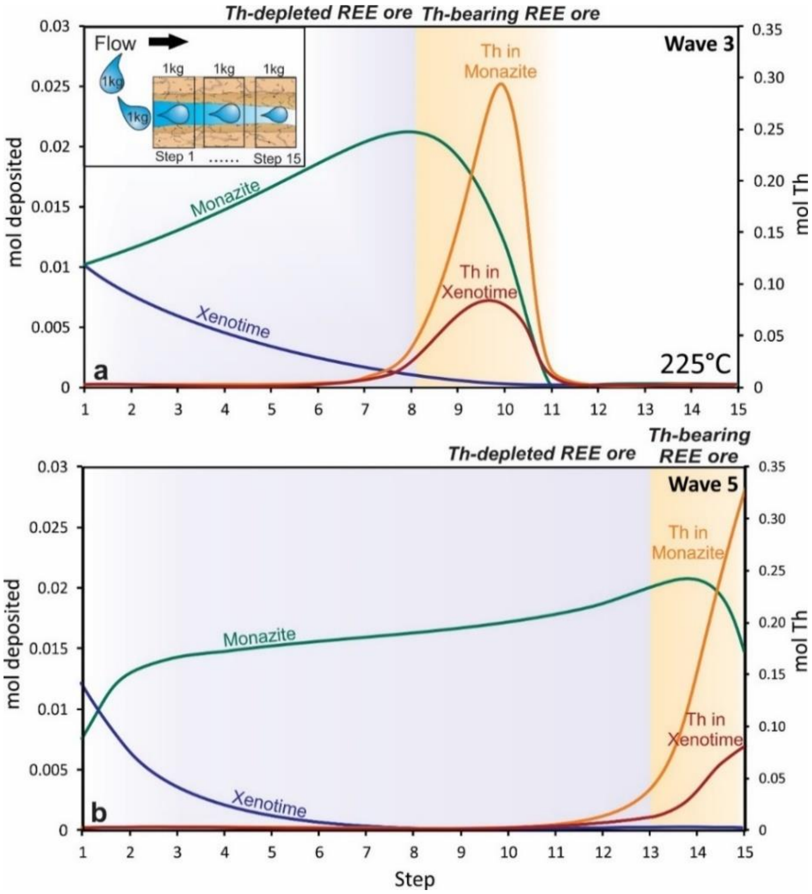

Figure 3.3. Results of flow-through model simulation of hydrothermal alteration. A step-flow reactor model was employed to investigate the fractionation of Th and the REE. The distribution of the REE-minerals, monazite, and xenotime, and their Th contents at a) wave 3 and b) wave 5 in a column of apatite-bearing rock at 225 °C. From this figure, it is evident that Th is concentrated at the alteration wave front due to its high mobility. After successive waves of fluid, Th is transported beyond the column, leaving behind REE-minerals depleted in Th.

3.4 Materials and Methods

3.4.1 Experimental procedure

The experiments involved investigating the solubility of Th dioxide (ThO_2) in solutions as a function of varying sulfate concentration (0.05–0.5 m Na_2SO_4) at elevated temperatures (175, 200, 225, 250 °C) and the pressure of saturated water vapor. The experimental solutions were contained in Teflon reactors (50 mL PFA test tubes), which were placed inside Ti autoclaves treated with nitric acid to ensure their inertness (by creating a dense layer of TiO_2 on the internal surfaces). Prior to each experiment, ThO_2 powder (IBI Labs, Technical Grade 99.8%), was placed inside small quartz tubes capped with silica wool and was exposed to conditions promoting hydrothermal re-crystallization until the grain sizes reached 10–50 μm. Thereafter, the tubes were placed in the Teflon reactors and submerged in their respective solutions (10−12 mL). The autoclaves were then sealed with a Teflon O-ring and placed in a Muffle Furnace inside an Al box (with 1.5 cm thick walls to reduce temperature gradients) for 1−2 weeks. After heating, the autoclaves were removed from the furnace and immediately quenched in a stream of cold air (solutions reached ambient conditions in <25min). The quartz tubes containing ThO_2 were removed from the Teflon reactors, and the pH of the solutions was measured using a calibrated glass electrode. The electrode was calibrated with a set of $NaCl/Na_2SO_4/HCl$ solutions having concentrations identical to those used in our experiments. Ion Chromatography (IC) was used to verify the sulfate content in the solution. Subsequently, 2 mL of sulfuric acid (Fisher Scientific, TraceMetal Grade) was added to the experimental solutions and left for 24 hours to dissolve any Th that may have precipitated on the walls of the Teflon reactors during quenching. Finally, the concentrations of Th in each solution were measured via Inductively Coupled Plasma Mass Spectrometry (ICP-MS) at the Geochemical and Geomaterials Research Laboratories of Los Alamos National Laboratory. A sketch of the experimental setup is shown in Supplementary Figure 3.1.

The experimental solutions were prepared with a constant 1 molal NaCl concentration and Na_2SO_4 concentration varying from 0.05−0.5 molal to determine the solubility of Th as a function of sulfate activity. The addition of NaCl (Fisher Scientific, A.C.S. Grade) was necessary to satisfy the activity model used in our calculations, information for which can be found in the Supplementary Information file. The solutions were prepared with deionized water acidified with HCl (Fisher Scientific, TraceMetal Grade) to a $pH_{25^\circ C}$ range of 2.01−2.67. Predetermined amounts of Na_2SO_4 (Fisher Scientific, A.C.S. Grade) were added to the solutions to set the activity of sulfate. Experimental parameters for each solution, including the calculated pH_T and activity of sulfate at the experimental temperatures, are reported in Supplementary Table 3.1.

The time required to attain equilibrium was determined in our previous study (Nisbet et al., 2018) for NaCl-bearing solutions, to be less than 1 day at 175 °C, and thus we infer that for each of our experiments which lasted >6 days and at $T \geq 175$ °C, the concentration of Th achieved an equilibrium/steady state. Phase characterization of the reference solid (ThO_2) was performed by X-ray diffraction (XRD) to ensure that there was no phase change during the experiments (Sup Fig. 3.2).

3.5 Data availability

All data generated or analyzed during this study are included in this published article (and its Supplementary Information files).

3.6 Acknowledgments

The research was supported by the G.T Seaborg Institute through a Summer Research Fellowship (Awarded to H.N.), the Laboratory Directed Research and Development program of Los Alamos National Laboratory (20180007DR) to H.X., and by the Los Alamos National Laboratory to A.M. through its Center for Space and Earth Sciences (CSES). CSES is funded by LANL’s Laboratory Directed Research and Development program under project number 20180475DR. We also thank Nicholas Wozniak for conducting the XRD analysis.

3.7 Author contributions

H.N. and A.M. conceptualized the ideas. H.N. performed the experiments and wrote the manuscript with input from all authors. Critical revision was provided by A.W-J, V.V., and H.X. and funding was acquired through H.X. and R.R.

3.8 Competing interests

The authors declare no competing interests.

3.9 References

Ault Timothy, Krahn S. and Croff A. (2015) Radiological Impacts and Regulation of Rare Earth Elements in Non-Nuclear Energy Production. Energies 8, 2066–2081.

Ault T, Van Gosen B., Krahn S. and Croff A. (2015) Natural thorium resources and recovery: options and impacts. Nucl. Technol. 194, 136–151.

Banks D. A., Yardley B. W. D., Campbell A. R. and Jarvis K. E. (1994) REE composition of an aqueous magmatic fluid: A fluid inclusion study from the Capitan Pluton, New Mexico, U.S.A. Chem. Geol. 113, 259–272.

Blackburn W. H., Metcalf R. V. and Ragland P. C. (1994) Geochemical evolution of the Precambrian Old Rag Granite, Virginia, U.S.A.: testing a U-Th exploration model. Chem. Geol. 111, 177–206.

Browne C. A. (1912) A Handbook of Sugar Analysis., J. Wiley & sons.

Chao E. C. T., Back J. M. and Minkin J. A. (1992) Host-rock controlled epigenetic, hydrothermal metasomatic origin of the Bayan Obo REE-Fe-Nb ore deposit, Inner Mongolia, P.R.C. Appl. Geochem. 7, 443–458.

Cook N. J., Ciobanu C. L., O'Rielly D., Wilson R., Das K. and Wade B. (2013) Mineral chemistry of Rare Earth Element (REE) mineralization, Browns Ranges, Western Australia. Lithos 172–173, 192–213.

Ekberg C., Albinsson Y., Comarmond M. J. and Brown P. L. (2000) Study on the complexation behavior of thorium(IV).1. Hydrolysis equilibria. J. Solut. Chem. 29, 63–86.

Grenthe I. and Lagerman B. (1991) Studies on metal carbonate equilibria: 23. Complex formation in the Th(IV)-H_2O-CO_2(g) system. Acta Chem. Scand. 45, 231–238.

Guo X., Szenknect S., Mesbah A., Clavier N., Poinssot C., Wu D., Xu H., Dacheux N., Ewing R. C. and Navrotsky A. (2016) Energetics of Uranothorite (Th 1– xUxSiO 4) Solid Solution. Chem. Mater. 28, 7117–7124.

Kerr A. and Rafuse H. (2012) Rare Earth Element geochemistry of the strange lake deposits: Implications for resource estimation and metallogenic models. Curr. Res. Nfld. Labrador Dep. Nat. Resour. Geol. Surv., 39–60.

Migdisov A., Guo X., Nisbet H., Xu H. and Williams-Jones A. E. (2019) Fractionation of REE, U, and Th in natural ore-forming hydrothermal systems: Thermodynamic modeling. J. Chem. Thermodyn. 128, 305–319.

Moriyama H., Kitamura A., Fujiwara K. and Yamana H. (1999) Analysis of mononuclear hydrolysis constants of actinide ions by hard sphere model. Radiochim. Acta 87, 97–104.

Neck V. and Kim J. I. (2001) Solubility and hydrolysis of tetravalent actinides. Radiochim. Acta 89, 1–16.

Nisbet H., Migdisov A., Xu H., Guo X., van Hinsberg V., Williams-Jones A. E., Boukhalfa H. and Roback R. (2018) An experimental study of the solubility and speciation of thorium in chloride-bearing aqueous solutions at temperatures up to 250 °C. Geochim. Cosmochim. Acta 239, 363–373.

OECD (2015) Introduction of Thorium in the Nuclear Fuel Cycle: Short- to long-term considerations. Nucl. Sci.

Olivo G. R. and Williams-Jones A. E. (1999) Hydrothermal REE-rich Eudialyte from the Pilanesberg Complex, South Africa. Can. Mineral. 37, 653–663.

Rai D., Moore D. A., Oakes C. S. and Yui M. (2000) Thermodynamic model for the solubility of thorium dioxide in the Na^+-Cl^--OH^--H_2O system at 23 °C and 90°C. Radiochim. Acta 88, 297–306.

Rand M. H., Mompean F. J., Perrone J. and Illemassene M. (2008) Chemical Thermodynamics of Thorium., OECD, NEA.

Smith M. P. and Henderson P. (2000) Preliminary Fluid Inclusion Constraints on Fluid Evolution in the Bayan Obo Fe-REE-Nb Deposit, Inner Mongolia, China. Econ. Geol. 95, 1371–1388.

Valsami-Jones E. and Ragnardottir K. V. (1997) Controls on uranium and thorium behavior in ocean-floor hydrothermal systems: examples from the Pindos ophiolite, Greece. Chem. Geol. 135, 263–274.

Walter B. F., Steele-MacInnis M. and Markl G. (2017) Sulfate brines in fluid inclusions of hydrothermal veins: Compositional determinations in the system H_2O-Na-Ca-Cl-SO_4. Geochim. Cosmochim. Acta 209, 184–203.

Wang X., Chou I.-M., Hu W. and Burruss R. C. (2013) In situ observations of liquid–liquid phase separation in aqueous $MgSO_4$ solutions: Geological and geochemical implications. Geochim. Cosmochim. Acta 103, 1–10.

Wang X., Wan Y., Hu W., Chou I.-M., Cai S., Lin N., Zhu Q. and Li Z. (2016) Visual and in situ Raman spectroscopic observations of the liquid–liquid immiscibility in aqueous uranyl sulfate solutions at temperatures up to 420°C. J. Supercrit. Fluids 112, 95–102.

Wang Xiaolin, Wang Xiaoyu, Chou I.-M., Hu W., Wan Y. and Li Z. (2017) Properties of lithium under hydrothermal conditions revealed by in situ Raman spectroscopic characterization of Li_2O-SO_3-H_2O (D_2O) systems at temperatures up to 420 °C. Chem. Geol. 451, 104–115.

Weingärtner H. and Franck E. U. (2005) Supercritical Water as a Solvent. Angew. Chem. Int. Ed. 44, 2672–2692.

Williams-Jones A. E., Samson I. M. and Olivo G. R. (2000) The genesis of hydrothermal fluorite-REE deposits in the Gallinas Mountains, New Mexico. Econ. Geol. 95, 327–341.

Zanonato P. L., Bernardo P. D., Zhang Z., Gong Y., Tian G., Gibson J. K. and Rao L. (2016) Hydrolysis of thorium(IV) at variable temperatures. Dalton Trans. 45, 12763–12771.

3.10 Supplementary information

3.10.1 Results and data treatment

Phase characterization of the reference solid (ThO_2) was performed by X-ray diffraction (XRD) in order to ensure no phase change occurred (i.e. $Th(SO_4)_{2(solid)}$) during the experiments. An example of the XRD spectra obtained from solids taken at the end of multiple experiments is illustrated in Supplementary Figure 3.2 and shows that, indeed, the solid remained ThO_2 and that there are no peaks for $Th(SO_4)_2$.

The results of the solubility experiments are presented in Supplementary Table 3.1, which lists the experimental parameters for each solution, the logarithm of molality of Th measured, the activity of sulfate calculated at the experimental conditions, the pH measured after completion of the experiments ($pH_{25°C}$), and the pH extrapolated to the experimental temperature (pH_T). The pH at the experimental temperature (pH_T) differs from the pH measured at ambient conditions ($pH_{25°C}$) owing to changes in the dissociation constant of water and the dissolved species. In order to determine the pH_T, the thermodynamic modeling software HCh was used (Shvarov, 2010). The thermodynamic model employed for these calculations involved the following species: H_2O, H^+, OH^-, O_2, H_2, Na^+, $NaOH°$, $NaSO_4^-$, $NaCl°$, SO_4^{2-}, HSO_4^-, Cl^-, and $HCl°$ and thermodynamic data for modeling the aqueous solutions at each experimental temperature were taken from Johnson et al. (1992), Sverjensky et al. (1997), and Tagirov et al. (1997). The dissociation constant and thermodynamic properties of water were calculated using the Marshall and Frank model (Marshall and Franck, 1981) and the Haar-Gallagher-Kell model (Kestin et al., 1984), respectively. Initially, the composition of the experimental solution was modeled to determine the concentration of HCl at 25 °C corresponding to the experimentally measured $pH_{25°C}$. Subsequently, the pH was recalculated at the experimental temperature (pH_T) using the measured concentrations of HCl. The activity model used in these and all subsequent calculations (see below) was the Debye-Hückel model modified by Helgeson et al. (1981), and Oelkers and Helgeson (1990, 1991), recommended for NaCl-dominated solutions up to I=6 and temperatures up to 600 °C:

$$\log \gamma_i = -\frac{AZ_i^2\sqrt{I}}{1+B\dot{a}\sqrt{I}} + b_\gamma I + \Gamma \tag{S1}$$

where A and B are the Debye-Hückel solvent parameters, γ_i, Z_i and $\dot{a}_i$ are the individual molal activity coefficient, the charge, and the distance of the closest approach of an ion *i*, respectively. The effective ionic strength calculated using the molal scale is I, Γ is a molarity to molality conversion factor, and b_γ is the extended-term parameter for NaCl from Oelkers and Helgeson (1990, 1991).

3.10.2 Calculation of equilibrium constants

As shown in Supplementary Table 3.1, the pH of the experimental solutions varied within 0.5 log units for the range of our experimental solutions. In order to identify the Th-sulfate species from the stoichiometric slope of our experimental data, we normalized the pH based on the two species that have been observed in sulfate-bearing solutions at acidic to moderately acidic conditions ($ThSO_4^{2+}$ and $Th(SO_4)_2$):

$$ThO_2(s) + 2SO_4^{2-} + 4H^+ \leftrightarrow Th(SO_4)_2 + 2H_2O \tag{S2}$$

$$ThO_2(s) + SO_4^{2-} + 4H^+ \leftrightarrow Th(SO_4)^{2+} + 2H_2O \tag{S3}$$

As shown in Figure 3.1, which plots the normalized values for the logarithm of the concentration of Th as a function of the logarithm of the activity of sulfate, for each isotherm, the concentration of Th increases with increasing activity of sulfate with a slope of approximately 2. Based on the stoichiometric slope, the results suggest that the aqueous species controlling the solubility of ThO_2 in our experiments is most likely $Th(SO_4)_2$, formed through Reaction S2.

The activity of sulfate was calculated using the same model as that employed for the pH_T calculations. The activity values, which are listed in Supplementary Table 3.1, differ significantly from the total sulfate molality in the solutions. This difference is primarily due to the range of pH_T of the experimental solutions, which is primarily in the predominance field of HSO_4^-, but extends into the sulfate field at a lower temperatures (Supplementary Figure 3.3). Thus, the concentrations of sulfate in most cases represent a minor proportion of the total concentration of sulfate. In addition, because sulfate is a charged species, it is strongly influenced by the ionic strength of the solutions.

The experimental data reported in Supplementary Table 3.1 were used to calculate equilibrium constants for Reaction S2 for each isotherm investigated. The values of the derived constants are reported in Table 3.1. The calculations accounted for the following species: Th^{4+}, ThO_2, $Th(OH)_2^{2+}$, $Th(OH)_4$, and $Th(SO_4)_2$. Data for Th^{4+} and thorianite (ThO_2) were taken from Shock et al. (1997) and Robie and Hemingway (1995), respectively. Data for Th hydroxyl species were taken from Nisbet et al. (2018). The contribution of polynuclear species to the solubility of Th was not considered as it can be assumed that these species become unstable at high temperature due to the large increase of electrostatic repulsion associated with the decrease of the dielectric constant of water (Seward et al., 2013), as demonstrated in Nisbet et al. (2018).

3.10.3 Extrapolation to low temperature and comparison to previous studies

To the best of our knowledge, this is the first study to investigate Th-sulfate speciation at hydrothermal conditions. The other thermodynamic data for $Th(SO_4)_2$ are restricted to ambient conditions, and are reported in an extensive review performed by the Nuclear Energy Agency (NEA) (Rand et al., 2008). This report cites several studies that have derived equilibrium constants at ambient conditions for $Th(SO_4)_2$ and $ThSO_4^{2+}$; the species expected to predominate in an aqueous solution at low temperature (Zebroski et al., 1951; Maiorova and Fomin, 1958; Zielen, 1959; Patil and Ramakrishna, 1972). These studies invoked liquid-liquid extraction methods with thenoyltrifluoroacetone (TTA) or dinonyl naphthalene sulphonic acid (DNNS) as extracting ligands, and by using ion-exchange. The experiments involved fluids with relatively high acidity and a near-constant ionic strength of 1.7−2.0 M (Rand et al., 2008). Variation among the derived equilibrium constants for the $Th(SO_4)_2$ complex from these studies is small. However, in order to accurately compare these values, they were recalculated to zero ionic strength by NEA using a modified NONLINT-SIT code (Felmy, 1995). These values were then averaged and combined with the equilibrium constant for the protonation of sulfate to obtain a thermodynamic formation constant of log β_2 = 9.69 ± 0.27. Recently, Di Bernardo et al. (2018) reported results of calorimetric titration experiments for temperatures between 10−70 °C and derived equilibrium constants and enthalpies of complexation for the Th-sulfate complexes. The reported formation constants for $Th(SO_4)_2$ at 10, 25, 40, 55, and 70 °C were 9.48 ± 0.09, 9.99 ± 0.10, 10.45 ± 0.10, 10.56 ± 0.10, and 11.10 ± 0.10, respectively. In order to compare our data with those reported in previous studies, the formation constants obtained from this study were extrapolated to low temperature by fitting the log β_2 for each temperature to the Ryzhenko-Bryzgalin model (MRB) (Ryzhenko et al., 1985) modified by Borisov and Shvarov (1992) as described in Shvarov and Bastrakov (1999). This model fits the temperature and pressure dependence of the dissociation constant for ion pairs through the following equation:

$$logK_{(T,P)} = \frac{T_r}{T} logK_{(T_r P_r)} + B_{(T,P)} \left(A_{zz/a} + \frac{B_{zz/a}}{T} \right) \tag{S4}$$

where K is the dissociation constant of the ion pair, T_r and P_r are the reference temperature and pressure, $B_{(T,P)}$ accounts for the property of water at temperature and pressure calculated from data contained in Marshall and Franck (1981), and $A_{zz/a}$ and $B_{zz/a}$ are the fitting parameters. The parameters derived from this model for $Th(SO_4)_2$ are found in Supplementary Table 3.2. Supplementary Figure 3.4 shows the thermodynamic formation constants from this study extrapolated to 10 °C for comparison with the selected constant from the NEA review (Rand et al., 2008), and values derived from Di Bernardo et al. (2018). As shown in this figure, the formation constants calculated in this study systematically increase with temperature, and when back-extrapolated to low temperature, show excellent agreement with the previously reported values.

3.10.4 Modeling

The model presented in this contribution simulates progressive hydrothermal alteration and re-distribution of REE and Th by an acidic solution in a one-dimensional column of a rock containing 0.5 wt. % apatite-OH (Ca-hydroxy-phosphate, to allow for the formation of REE phosphates), which was evaluated using a step-flow reactor approach (‘‘box model”, Figure 3.3). The calculations were performed for 225 °C to be within the range of experimental data for Th. To avoid changes in the observed trends by pH, and other buffering parameters, the rock was assumed to be chemically inert and the only chemically active component of it was apatite, which supplied the P needed to form monazite or xenotime. The composition of the altering solution corresponded to compositions documented for fluids associated with natural REE ore forming systems. Fluid inclusion studies indicate that the Bayan Obo deposit in China was formed from brines containing 7–10 wt.% NaCl equivalent (Smith and Henderson, 2000), whereas fluids responsible for ore deposition at Gallinas Mountains contained 12–18 wt.% NaCl equivalent (Williams-Jones et al., 2000). To avoid uncertainties associated with poorly defined activity models for highly saline brines at elevated temperatures, the solution selected for calculations contained only 10 wt. % NaCl (1.72 mol/kg). The initial concentrations of REE in the solution associated with the initial depositional event (‘‘step 1”) were closely approximated to the fluid inclusions from the Capitan

Pluton REE prospect (Banks et al., 1994) (Supplementary Table 3.3). This publication, however, did not report the concentrations of Y, the main component of xenotime solid solutions. In our simulations, the concentrations of this element was set to be one-third of the concentrations of La and Ce. The concentration of Th in the solution was fixed by its saturation with respect to thorianite (ThO_2) at 225 °C. The pH_T of the initial solution was set at ~2 by adding the required amount of HCl.

A full list of aqueous species employed in the calculations, the parameters for the equations of state used to extrapolate their properties to elevated temperature, and their data sources, are provided in the Supplementary Excel spreadsheet. Calculations of the thermodynamic properties of the species and the H_2O dissociation constant were performed using the same models as those mentioned above. Similarly, the activity of the individual ions was calculated using the modified extended Debye-Hückel model (Eqn. S1). The thermodynamic properties of basic aqueous species ${O^o_2}_{aq}$, ${H^o_2}_{aq}$, Na^+, $NaOH^o_{aq}$, $NaSO_4^-$, $NaCl^o_{aq}$, and Cl^- were taken from Johnson et al. (1992), Sverjensky et al. (1997) and Shock et al. (1997). The stability of the HCl^o_{aq} ion pair was evaluated using the combined data from Tagirov et al. (1997) and Ho et al. (2001). The properties of simple hydrated ions REE^{3+} and Th^{4+} were taken from Shock et al. (1997). The thermodynamic data for REE and Th aqueous species incorporated in this model are identical to those described in Migdisov et al. (2019). Exceptions are the REE-sulfate complexes, $REESO_4^+$ and $REE(SO_4)_2^-$ (Migdisov et al., 2016) and the data derived in this contribution for $Th(SO_4)_2$. For more detail on the sources and selection of thermodynamic data, readers are referred to Migdisov et al. (2016, 2019).

The model mainly investigates the incorporation of Th in REE phosphate solid solutions and co-existing aqueous phases. Additionally, it incorporates co-existing thorianite (ThO_2 (Robie and

Hemingway, 1995)), solid REE-hydroxides (Migdisov et al., 2016), apatite-OH, whitlockite ($Ca_5(PO_4)_2$), halite (NaCl), hydrophilite ($CaCl_2$), and portlandite ($Ca(OH)_2$) (Robie and Hemingway, 1995). Except for thorianite, apatite-OH, and whitlockite, all phases mentioned above were unstable under the conditions employed in our model. Thermodynamic properties for monazite end-members ($LaPO_4$ to $GdPO_4$) were derived based on calorimetric measurements by Popa and Konings (2006), Popa et al. (2006), and Navrotsky et al. (2015) and solubility products determined for REE phosphates at 25 °C (Liu and Byrne, 1997). Thermodynamic properties for xenotime were derived from calorimetric data reported in Gavrichev et al. (2006, 2010, 2012, 2013) and Navrotsky et al. (2015) and solubility products at 25 °C reported in Liu and Byrne, (1997). For details on data selection, readers are referred to Migdisov et al. (2019).

To determine the mixing systematics of L/MREE in monazite and HREE in xenotime, a regular solid solution model was employed in which the excess enthalpy of mixing ΔH_{mix}^{E} is expressed as $W \cdot x(1-x)$, where W is the interaction parameter and x is the portion of one REE over the cation site. The interaction parameters for the monazite system were derived based on *ab initio* calculations from Mogilevsky (2007) and Kowalski and Li (2016), where the excess mixing properties of two REE in monazite were expressed as a function of volume mismatch from the two end-members, proportional to the average Young's modulus $\bar{E}$. The derivation of the xenotime system interaction parameters first involved the calculation of $\bar{E}$ values, which were estimated based on their near linear correlation with the ionic radii of the cations (Mogilevsky, 2007). These values were then used to calculate W for each substituting pair of HREE. The incorporation of Th into monazite and xenotime was modeled through the brabantitic substitution, in which the extra charge, introduced by the tetravalent actinide, is accommodated via incorporation of Ca^{2+} into the structure. Thermodynamic properties of the pure $(Ca,Th)PO_4$ end-member were taken from Popa et al. (2008) and Rawat et al. (2017). For a detailed description of the solid solution model, readers are referred to Migdisov et al. (2019).

The most common varieties of monazite in nature are monazite-(Ce) and monazite-(La). Monazite-(Nd) is also found in natural systems but is much rarer. Thus, in our model we accounted for two types of monazite: monazite-(Ce), containing $CePO_4$, $PrPO_4$, $NdPO_4$, $SmPO_4$, $GdPO_4$, and $(Ca,Th)PO_4$, and monazite-(La) containing $LaPO_4$, $PrPO_4$, $NdPO_4$, $SmPO_4$, $GdPO_4$, and $(Ca,Th)PO_4$. This separation into two types of monazites is necessary, due in part to limitations of the software (HCh) (Shvarov and Bastrakov, 1999), which cannot account for solid solutions having more than seven components. Formation of monazite-(Nd) was assumed when NdPO4 predominated in one of the above solid solutions. The xenotime solid solution contained YPO_4, $TbPO_4$, $DyPO_4$, $ErPO_4$, $YbPO_4$, and $(Ca,Th)PO_4$.

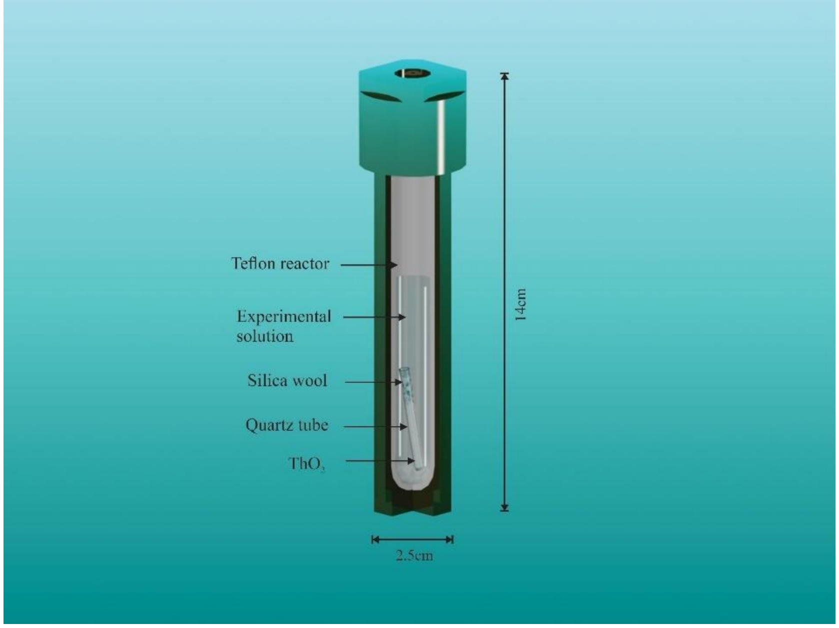

Supplementary Figure 3.1 A sketch of the experimental setup. Experimental solutions were contained in titanium autoclaves lined with Teflon. ThO_2 was placed inside a small quartz tube capped with silica wool. Approximately 10 ml of the experimental solution was added.

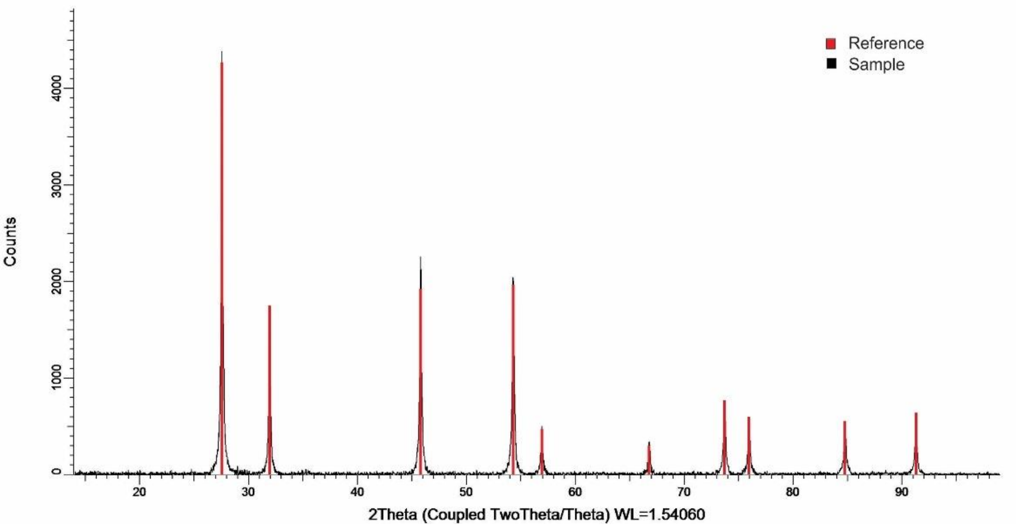

Supplementary Figure 3.2 X-ray diffraction (XRD) analysis of ThO_2 after completion of experiments. ThO_2 was analyzed at the end of multiple experiments by XRD to determine whether the phase remained the same. As illustrated, the solid is ThO_2.

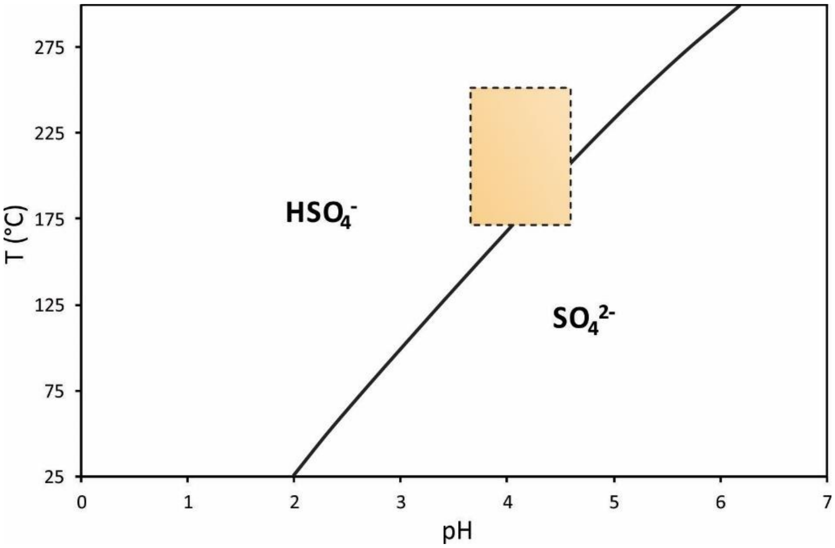

Supplementary Figure 3.3 Sulfate predominance diagram with respect to temperature and pH. The orange box corresponds to the field of our experimental data, showing that both sulfate species were present under the experimental solutions.

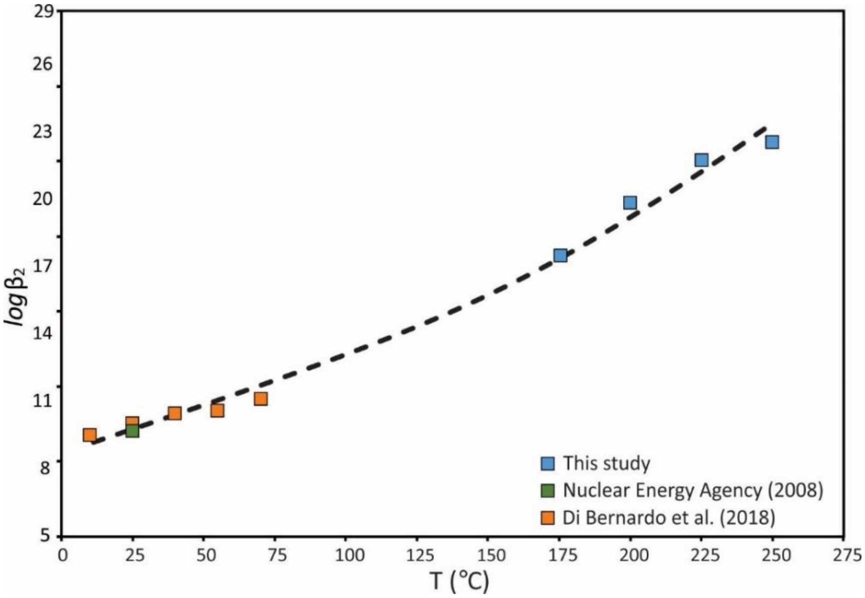

Supplementary Figure 3.4 Extrapolation and comparison of calculated thermodynamic formation constants from this study to low temperature. Formation constants ($log\,\beta_2$) for $Th(SO_4)_2$ plotted as a function of temperature. The experimental data obtained in this study (blue squares) were fitted to the Bryzgalin–Ryzhenko model (dashed line) to compare with the selected data from the Nuclear Energy Agency (Rand et al., 2008) (green square) and data collected from Di Bernardo et al. (2018) (orange squares). The error (SD) associated with the individual points is smaller than the size of the markers. Our data show excellent agreement with the low-temperature values

Supplementary Table 3.1 The composition of the experimental solutions. Concentrations of the components in the experimental solutions and pH values measured after quenching (25 °C) and extrapolated to the temperature of the experiments (pH_T).

T (°C)	log m Na_2SO_4	log a SO_4^{2-}	$pH_{25°C}$	pH_T	log m Th	log m Th (pH corrected)
175	-1.301	-3.030	2.44	3.69	-8.466	-8.466
175	-1.0	-2.739	2.66	3.88	-8.467	-8.096
175	-0.824	-2.586	2.55	3.85	-8.247	-7.935
175	-0.456	-2.289	2.47	3.89	-7.012	-6.608
175	-0.347	-2.204	2.63	4.08	-7.604	-6.838
175	-0.301	-2.172	2.63	4.09	-7.834	-7.046
200	-1.301	-3.181	2.71	3.99	-7.766	-7.766
200	-1.0	-2.895	2.67	4.13	-8.026	-7.750
200	-0.824	-2.740	2.55	4.16	-7.845	-7.509
200	-0.699	-2.632	2.63	4.25	-7.971	-7.461
200	-0.602	-2.557	2.60	4.20	-7.703	-7.287
200	-0.523	-2.493	2.67	4.30	-7.805	-7.185
200	-0.456	-2.443	2.63	4.31	-7.652	-7.026
200	-0.347	-2.365	2.67	4.38	-7.267	-6.495
225	-1.0	-3.079	2.56	4.26	-7.762	-7.762
225	-0.824	-2.922	2.54	4.32	-7.432	-7.300
225	-0.699	-2.815	2.56	4.40	-7.621	-7.345
225	-0.602	-2.737	2.57	4.44	-7.445	-7.073
225	-0.347	-2.554	2.54	4.48	-7.458	-7.010
225	-0.301	-2.522	2.58	4.54	-7.283	-6.721
250	-1.301	-3.595	2.44	4.16	-8.567	-8.567
250	-1.0	-3.356	2.09	3.96	-7.525	-7.922
250	-0.824	-3.180	2.09	4.08	-8.058	-8.222
250	-0.699	-3.041	2.29	4.36	-8.170	-7.770
250	-0.602	-2.947	2.49	4.61	-8.106	-7.198
250	-0.523	-2.899	2.32	4.46	-7.667	-7.071
250	-0.347	-2.785	2.20	4.38	-7.198	-6.758
250	-0.347	-2.773	2.36	4.55	-7.824	-7.044

Supplementary Table 3.2 The Ryzhekno-Bryzgalin model (MRB) parameters. Thermodynamic formation constants derived in this study for $Th(SO_4)_2$ fitted to the Ryzhekno-Bryzgalin model and model parameters.

	log β				pK(298)	A(zz/a)	B(zz/a)
	175 °C	200 °C	225 °C	250 °C			
$Th(SO_4)_2$	17.93	19.51	21.16	22.93	9.763	7.231	-877.53

Supplementary Table 3.3 The concentrations of REE in the initial modeling solution. Initial concentrations of the REE in the solution are associated with the initial depositional event (‘‘step 1”). These values are close to those of the Capitan Pluton REE fluid (Banks et al., 1994).

Element	La	Ce	Pr	Nd	Sm	Gd	Y	Tb	Dy	Er	Yb
Concentration (ppm)	300	300	35	150	20	20	100	6	45	33	33

3.11 Supplementary References

Banks D. A., Yardley B. W. D., Campbell A. R. and Jarvis K. E. (1994) REE composition of an aqueous magmatic fluid: A fluid inclusion study from the Capitan Pluton, New Mexico, U.S.A. Chem. Geol. 113, 259–272.

Borisov M. V. and Shvarov Y. V. (1992) Thermodynamics of geochemical processes. Mosc. Mosc. State Univ. Publ. House, 254.

Di Bernardo P., Endrizzi F., Melchior A., Zhang Z., Zanonato P. L. and Rao L. (2018) Complexation of Th(IV) with sulfate in aqueous solution at 10–70 °C. J. Chem. Thermodyn. 116, 273–278.

Felmy A. R. (1995) A Computerized chemical equilibrium program using a constrained minimization of the Gibbs free energy: Summary report. SSSA Spec. Publ. Soil Sci. Soc. Am. Am. Soc. Agron., 377–407.

Gavrichev K. S., Ryumin M. A., Tyurin A. V., Gurevich V. M., Khoroshilov A. V. and Komissarova L. N. (2012) Thermodynamic functions of erbium orthophosphate $ErPO_4$ in the temperature range of 0–1600K. Thermochim. Acta 535, 1–7.

Gavrichev K. S., Ryumin M. A., Tyurin A. V., Gurevich V. M. and Komissarova L. N. (2010) Heat capacity and thermodynamic functions of xenotime $YPO_{4(c)}$ at 0–1600 K. Geochem. Int. 48, 932–939.

Gavrichev K. S., Ryumin M. A., Tyurin A. V., Gurevich V. M., Nikiforova G. E. and Komissarova L. N. (2013) Heat capacity and thermodynamic functions of $YbPO_4$ from 0 to 1800 K. Inorg. Mater. 49, 701–708.

Gavrichev K. S., Smirnova N. N., Gurevich V. M., Danilov V. P., Tyurin A. V., Ryumin M. A. and Komissarova L. N. (2006) Heat capacity and thermodynamic functions of $LuPO_4$ in the range 0–320K. Thermochim. Acta 448, 63–65.

Helgeson H. C., Kirkham D. H. and Flowers G. C. (1981) Theoretical prediction of the thermodynamic behavior of aqueous electrolytes at high pressures and temperatures: IV. Calculation of activity coefficients, osmotic coefficients, and apparent molal and standard and relative partial molal properties to 600°C. Am. J. Sci. 281, 1249–1516.

Ho P. C., Palmer D. A. and Gruszkiewicz M. S. (2001) Conductivity Measurements of Dilute Aqueous HCl Solutions to High Temperatures and Pressures Using a Flow-Through Cell. J. Phys. Chem. B 105, 1260–1266.

Johnson J. W., Oelkers E. H. and Helgeson H. C. (1992) SUPCRT92: a software package for calculating the standard molal thermodynamic properties of minerals, gases, aqueous species, and reactions from 1 to 5000 bar and 0 to 1000 °C. Comput. Geosci. 18, 899–947.

Kestin J., Sengers J. V., Kamgar-Parsi B. and Levelt Sengers J. M. H. (1984) Thermophysical properties of fluid H_2O. J. Phys. Chem. Ref. Data 13, 601–609.

Kowalski P. M. and Li Y. (2016) Relationship between the thermodynamic excess properties of mixing and the elastic moduli in the monazite-type ceramics. J. Eur. Ceram. Soc. 36, 2093–2096.

Liu X. and Byrne R. H. (1997) Rare earth and yttrium phosphate solubilities in aqueous solution. Geochim. Cosmochim. Acta 61, 1625–1633.

Maiorova E. P. and Fomin V. V. (1958) Extraction of thorium with tributyl phosphate. III. Effect of sulfate ions on the distribution of thorium. Russ. J. Inorg. Chem. 3, 295–316.

Marshall W. L. and Franck E. U. (1981) Ion product of water substance, 0-1000 °C, 1-10,000 bars new International Formulation and its background. J. Phys. Chem. Ref. Data 10, 295–304.

Migdisov A., Guo X., Nisbet H., Xu H. and Williams-Jones A. E. (2019) Fractionation of REE, U, and Th in natural ore-forming hydrothermal systems: Thermodynamic modeling. J. Chem. Thermodyn. 128, 305–319.

Migdisov A., Williams-Jones A. E., Brugger J. and Caporuscio F. A. (2016) Hydrothermal transport, deposition, and fractionation of the REE: experimental data and thermodynamic calculations. Chem. Geol. 439, 13–42.

Mogilevsky P. (2007) On the miscibility gap in monazite–xenotime systems. Phys. Chem. Miner. 34, 201–214.

Navrotsky A., Lee W., Mielewczyk-Gryn A., Ushakov S. V., Anderko A., Wu H. and Riman R. E. (2015) Thermodynamics of solid phases containing rare earth oxides. J. Chem. Thermodyn. 88, 126–141.

Nisbet H., Migdisov A., Xu H., Guo X., van Hinsberg V., Williams-Jones A. E., Boukhalfa H. and Roback R. (2018) An experimental study of the solubility and speciation of thorium in chloride-bearing aqueous solutions at temperatures up to 250 °C. Geochim. Cosmochim. Acta 239, 363–373.

Oelkers E. H. and Helgeson H. C. (1991) Calculation of activity coefficients and degrees of formation of neutral ion pairs in supercritical electrolyte solutions. Geochim. Cosmochim. Acta 55, 1235–1251.

Oelkers E. H. and Helgeson H. C. (1990) Triple-ion anions and polynuclear complexing in supercritical electrolyte solutions. Geochim. Cosmochim. Acta 54, 727–738.

Patil S. K. and Ramakrishna V. V. (1972) Study of the sulphate complexing of Th(IV) by solvent extraction with dinonyl naphthalene sulphonic acid. Radiochim. Acta 18, 190–192.

Popa K. and Konings R. J. M. (2006) High-temperature heat capacities of $EuPO_4$ and $SmPO_4$ synthetic monazites. Thermochim. Acta 445, 49–52.

Popa K., Sedmidubský D., Beneš O., Thiriet C. and Konings R. J. M. (2006) The high-temperature heat capacity of $LnPO_4$ (Ln=La, Ce, Gd) by drop calorimetry. J. Chem. Thermodyn. 38, 825–829.

Popa K., Shvareva T., Mazeina L., Colineau E., Wastin F., Konings R. J. M. and Navrotsky A. (2008) Thermodynamic properties of $CaTh(PO_4)_2$ synthetic cheralite. Am. Mineral. 93, 1356–1362.

Rand M. H., Mompean F. J., Perrone J. and Illemassene M. (2008) Chemical Thermodynamics of Thorium., OECD, NEA.

Rawat D., Phapale S., Mishra R. and Dash S. (2017) Thermodynamic studies on charge-coupled substituted synthetic monazite. J. Nucl. Mater. 487, 406–417.

Robie R. A. and Hemingway B. S. (1995) Thermodynamic properties of minerals and related substances at 298.15 K and 1 Bar (10^5 Pascals) pressure and at higher temperatures. US Geol. Survet Bull. 2131, 461.

Ryzhenko B. N., Bryzgalin O. V., Artamkina I. Y., Spasennykh M. Y. and Shapkin A. I. (1985) An electrostatic model for the electrolytic dissociation of inorganic substances dissolved in water. Geochem. Int. 22, 138–144.

Seward T. M., Williams-Jones A. E. and Migdissov A. A. (2013) The Chemistry of Metal Transport and Deposition by Ore-Forming Hydrothermal Fluids. Treatise Geochem. 10, 29–57.

Shock E. L., Sassani D. C., Willis M. and Sverjensky D. A. (1997) Inorganic species in geological fluids: Correlations among standard molal thermodynamic properties of aqueous ions and hydroxide complexes. Geochim. Cosmochim. Acta 61, 907–950.

Shvarov Y. V. (2010) OptimA: A program for the calculation of the free energies of dissolved aqueous species from the results of chemical experiments.

Shvarov Y. V. and Bastrakov E. (1999) HCh, A Software Package for Geochemical Equilibrium Modeling: User's Guide.

Smith M. P. and Henderson P. (2000) Preliminary Fluid Inclusion Constraints on Fluid Evolution in the Bayan Obo Fe-REE-Nb Deposit, Inner Mongolia, China. Econ. Geol. 95, 1371–1388.

Sverjensky D. A., Shock E. L. and Helgeson H. C. (1997) Prediction of the thermodynamic properties of aqueous metal complexes to 1000 °C and 5 kb. Geochim. Cosmochim. Acta 61, 1359–1412.

Tagirov B. R., Zotov A. and Akinfiev N. (1997) Experimental study of dissociation of HCl from 350 to 500 °C and from 500 to 2500 bars: thermodynamic properties of HCl°(aq). Geochim. Cosmochim. Acta 61, 4267–4280.

Williams-Jones A. E. and Samson I. M. The Genesis of Hydrothermal Fluorite-REE Deposits in the Gallinas Mountains, New Mexico, 16.

Zebroski E. L., Alter H. W. and Heumann F. K. (1951) Thorium Complexes with Chloride, Fluoride, Nitrate, Phosphate and Sulfate. J. Am. Chem. Soc. 73, 5646–5650.

Zielen A. J. (1959) Thermodynamics of the sulfate complexes of thorium. J. Am. Chem. Soc. 81, 5022–5028.

Preface to Chapter 4

The experimental study reported in the previous chapter challenges the long-standing paradigm that thorium behaves as an immobile element in nature. It was shown that Th-sulfate complexes are highly stable at elevated temperatures, promoting the significant dissolution of Th. Furthermore, thermodynamic modeling determined that sulfate-bearing hydrothermal fluids can mobilize and fractionate Th from the REE, which can ultimately lead to the formation of a REE ore deposit depleted in Th. A considerable gap remains in our ability to model Th transport in natural hydrothermal systems, and that is its behavior in carbonate-bearing hydrothermal fluids. At ambient conditions, Th-carbonate complexes are among the strongest, and it is thus imperative that the stability of these complexes be assessed at elevated temperatures as well.

To bridge this knowledge gap, in Chapter 4, we provide a comprehensive study on the solubility and speciation of Th in carbonate-bearing solutions at 175−250 °C using the autoclave solubility technique. Thorium-carbonate complexes were not detected under the experimental conditions, and rather, two Th-hydroxyl species predominate, for which, thermodynamic data are derived. We conclude that carbonate-bearing solutions are unlikely to transport significant quantities of Th in natural hydrothermal systems.

Chapter 4

The solubility of thorium in carbonate-bearing solutions at hydrothermal conditions

Haylea Nisbet[1,2*], Artas Migdisov[1], Anthony Williams-Jones[2], Vincent van Hinsberg[2], Hongwu Xu[1], Robert Roback[1]

[1]Earth and Environmental Sciences Division, Los Alamos National Laboratory, Los Alamos, NM 87545, USA.

[2] Department of Earth and Planetary Sciences, McGill University, 3450 University Street, Montreal, QC, H3A 0E8, Canada.

*haylea.nisbet@mail.mcgill.ca

In Press in Geochimica et Cosmochimica Acta, Special Issue "Metals-Fluids-Minerals", May 2021

DOI: https://doi.org/10.1016/j.gca.2021.04.035

Abstract

Thorium mineralization is frequently hosted in carbonate-bearing rocks, and thorium commonly substitutes into the structures of carbonate-bearing minerals that have precipitated from or been modified by hydrothermal fluids. Given this common association, it is reasonable to consider the hypothesis that the presence of carbonate ligands in hydrothermal solutions promotes the transport of Th through the formation of stable aqueous complexes. Our ability to evaluate this hypothesis, however, is hindered by the lack of experimental data for Th-carbonate species at conditions beyond ambient. The low-temperature data indicate that carbonate is a strong complexing agent for Th. In this contribution, we investigate the solubility of Th in carbonate-bearing fluids relevant to natural systems (0.05−0.5m $NaHCO_3/Na_2CO_3$; pH_T ~7.8−9.8) at elevated temperatures (175−250 °C). We demonstrate that, in contrast to the behavior of Th at low temperatures, the stability of Th-carbonate complexes is not sufficient for them to predominate at these conditions. Instead, the solubility of Th is governed by hydrolysis reactions. Under the experimental conditions investigated, the predominant hydroxyl complexes are $Th(OH)_4^0$ and $Th(OH)_5^-$. Thermodynamic formation constants were derived for these species at the temperatures considered in our experiments ($\log \beta_4$=43.34 and 44.31 at 175 and 200 °C, respectively, and $\log \beta_5$= 46.15 and 47.9 at 225 and 250 °C, respectively) to permit forward modeling of Th mobility in natural systems. Our study indicates that carbonate ions are unlikely to play a role in transporting Th in hydrothermal fluids. Summarizing the results of this study and our previous studies of the solubility of Th in hydrothermal fluids, we conclude that SO_4^{2-} is the primary ligand responsible for the hydrothermal transport of Th.

4.1 Introduction

Thorium, the most abundant actinide in the Earth's crust, is generally considered to be immobile in nature, based on data collected at ambient conditions (Rand et al., 2008). This interpretation, however, conflicts with observations of hydrothermal Th mineralization, including that of REE ore deposits produced by hydrothermal fluids (Castor, 2008; Sheard et al., 2012; Cook et al., 2013). Owing to its radioactivity, Th is viewed as an unfavorable contaminant, and its enrichment, therefore, impacts negatively on the feasibility of mining endeavors. There has been growing interest in the past few decades, however, in the possibility of exploiting deposits of Th to substitute for or enhance U nuclear fuels. Consequently, it is necessary to determine the mechanisms responsible for the mobilization, enrichment, and depletion of Th in hydrothermal fluids.

The main impediment to evaluating the transport and deposition of Th by hydrothermal solutions is a lack of information on the behavior and properties of Th-bearing aqueous species at elevated temperatures. The published data on Th speciation are restricted almost entirely to temperatures below 100 °C, with most of the data being for ambient conditions (Rand et al., 2008). We recently launched a research program to address this knowledge gap by conducting solubility experiments involving crystalline ThO_2 at temperatures >175 °C in chloride- and sulfate-bearing systems, i.e., systems containing ligands expected to be important in natural hydrothermal systems (Nisbet et al., 2018, 2019). These experiments indicated that sulfate has a major impact on the solubility and mobility of Th at elevated temperatures (175−250 °C), even if the concentrations of SO_4^{2-} (>0.5m) are modest (Nisbet et al., 2019). A notable gap in our current knowledge is a lack of understanding of the behavior of Th in carbonate-bearing systems. Among the possible complexing ligands, the carbonate anion has been shown to form very stable complexes with actinides, such as Th, at ambient conditions (Rand et al., 2008), and it is logical to speculate, as many researchers have (Wood, 1990b; Haas et al., 1995), that this complex may also play a significant role in Th mobility at elevated temperature. Indeed, it is noteworthy that, in nature, thorium tends to concentrate in highly evolved systems that have elevated carbonate concentrations including carbonatites (>50 % carbonate) (Ault et al., 2015). Many of these systems were formed and/or altered by hydrothermal fluids (e.g., Mountain Pass, Bear Lodge; Castor, 2008; Andersen et al., 2017); yet, to date, there have been no investigations of Th solubility and speciation in carbonate-bearing fluids at high temperature. Consequently, the role of carbonate species in the mobilization of Th in these systems cannot be evaluated.

The thermodynamic data for Th-carbonate speciation have been summarized in a thorough review by the Nuclear Energy Agency (NEA) (Rand et al., 2008). Results of 19 sets of experiments have been reported for aqueous solutions at ambient conditions, all of which show that Th has a strong affinity for carbonate anions. Indeed, reactions involving the complexation of actinides with carbonate have been considered “some of the most important reactions in aqueous systems” (Altmaier et al., 2005). However, there have been serious inconsistencies in the identification of the dominant Th-carbonate species. Altmaier et al. (2005; 2006) identified the ternary complexes $Th(OH)(CO_3)_4^{5-}$ and $Th(OH)_2(CO_3)_2^{2-}$ as the dominant species with minor contributions from $Th(OH)_2(CO_3)_{(aq)}$, $Th(OH)_3(CO_3)^-$ and $Th(OH)_4(CO_3)^{2-}$ in solutions with an ionic strength of 0.5 M. In contrast, Osthols et al. (1994), Felmy et al. (1997) and Felmy and Rai, (1999) proposed that $Th(CO_3)_6^{5-}$ is the dominant complex in solutions containing 0.1−2.0 M CO_3^{2-} and $Th(OH)_3(CO_3)^-$ to dominate at lower carbonate concentrations and near-neutral pH conditions. It should be noted that the above-mentioned studies were all conducted using an amorphous ThO_2 reference phase, which has been shown to lead to discrepancies of several orders of magnitude in the measured concentrations of dissolved Th relative to those using crystalline ThO_2, owing to the higher solubility of amorphous solids (Rand et al., 2008).

Even at ambient conditions, there is uncertainty regarding Th-carbonate speciation, and at elevated temperatures, thermodynamic data are simply non-existent. The purpose of this study is to investigate the speciation of Th in carbonate-bearing fluids at hydrothermal conditions and to derive the thermodynamic properties of the dominant complexes to permit forward modeling of Th mobility in natural, carbonate-bearing hydrothermal systems.

4.2 Methods

To investigate the speciation of Th in carbonate-bearing solutions, solubility experiments were performed in solutions of varying carbonate concentration (0.05−0.5m $NaHCO_3$/Na_2CO_3, pH_T 7.83−9.82) at elevated temperatures (175−250 °C) and the pressure of saturated water vapor, with crystalline thorium dioxide (ThO_2) as the solid reactant (particle size >10 μm). The experimental solutions were contained in Teflon-lined titanium autoclaves. Before each experiment, small Teflon tubes containing crystalline ThO_2 (IBI Labs, Technical Grade 99.8%), capped with a porous Teflon film, were placed in the Teflon reactors and submerged in 10 mL of solution. The autoclaves were then sealed with a Teflon O-ring, and placed in a Muffle Furnace for 12−14 days. At the end of an experiment, the autoclaves were removed from the furnace and immediately quenched in a stream of cold air (the quench time was < 25min). The Teflon tubes were removed as soon as the solutions were quenched. The addition of the Teflon film ensured that the exchange between the ThO_2 and the experimental solution was slowed down such that the measured solubility was not altered during quenching and heating. Considering that equilibrium with the solution was reached within 3 days (see below) and quenching and heating take less than 25 min, we consider the concentrations measured in the quenched aqueous solutions to correspond to isothermal solubility. A 3mL aliquot of sulfuric acid (Fisher Scientific, TraceMetal Grade) was then added to the solutions and left for 24 hours to dissolve any Th that may have precipitated on the walls of the reactor. Finally, Th concentrations in the resulting solutions were measured via Inductively Coupled Plasma Mass Spectrometry (ICP-MS) at the Geochemical and Geomaterials Research Laboratories of the Los Alamos National Laboratory. A sketch of the experimental setup is shown in Figure 4.1.

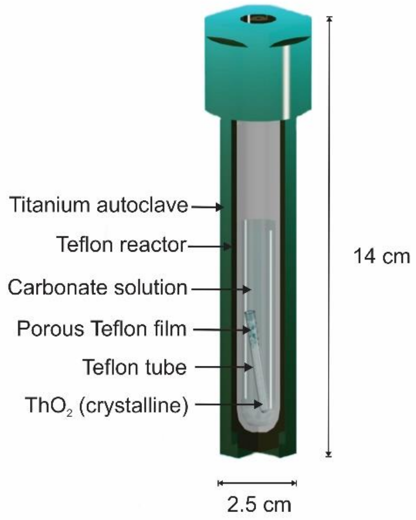

Figure 4.1 Sketch showing the autoclave set-up used in the experiments.

Two sets of experimental solutions were prepared to determine the solubility of Th as a function of carbonate activity: 1) solutions containing 0.05−0.5 m $NaHCO_3$ and 2) solutions containing 0.05−0.5 m Na_2CO_3, each with a constant 1 m concentration of NaCl. The pH of the experimental solutions was calculated based on the concentrations of $NaHCO_3$ and Na_2CO_3 added, as described below. The presence of NaCl in the experimental solutions was required to satisfy the activity model used in our calculations. Targeted amounts of $NaHCO_3$ (Acros Organics, A.C.S. grade), Na_2CO_3(anhydrous, Fisher Chemical, A.C.S. grade), and NaCl (Fisher Chemical, A.C.S. grade) were added to vacuum-degassed deionized water (DI) that was flushed with argon gas immediately before sealing off the autoclaves to minimize the exchange of CO_2 between the fluid and the atmosphere. Parameters for each experiment are reported in Table 4.1.

Table 4.1 The compositions of the experimental solutions in this study, the calculated activity of HCO_3^- and pH_T, the measured concentration of Th, and the temperature. All experimental solutions contained 1m NaCl.

T (°C)	m $NaHCO_3$	m Na_2CO_3	log a HCO_3^-	pH_T	log m Th
175	0.05		-1.678	7.837	-6.695
175	0.1		-1.380	7.855	-6.568
175	0.15		-1.208	7.857	-6.726
175	0.25		-0.993	7.853	-6.690
175	0.3		-0.917	7.85	-6.609
175	0.35		-0.854	7.846	-6.398
175	0.4		-0.799	7.842	-6.826
175		0.05	-2.053	9.337	-6.791
175		0.15	-1.792	9.594	-7.272
175		0.2	-1.730	9.653	-6.890
175		0.25	-1.685	9.696	-6.909
175		0.4	-1.595	9.780	-7.173
175		0.45	-1.574	9.799	-6.972
175		0.5	-1.555	9.816	-6.849
200	0.15		-1.268	7.961	-5.501
200	0.2		-1.148	7.962	-5.855
200	0.25		-1.055	7.96	-5.876
200	0.3		-0.980	7.958	-5.584
200	0.35		-0.918	7.954	-5.685
200	0.4		-0.863	7.951	-5.304
200	0.45		-0.816	7.947	-5.764
200		0.15	-1.757	9.505	-6.311
200		0.25	-1.649	9.61	-5.824
200		0.3	-1.614	9.645	-6.392
200		0.35	-1.585	9.673	-6.021
200		0.4	-1.560	9.696	-6.120
200		0.45	-1.540	9.716	-5.988
200		0.45	-1.540	9.716	-6.547
225	0.05		-1.808	8.028	-6.125
225	0.10		-1.512	8.070	-6.485
225	0.15		-1.341	8.082	-6.254
225	0.20		-1.221	8.086	-6.414
225	0.25		-1.129	8.086	-6.046
225	0.30		-1.055	8.084	-6.449
225	0.35		-0.993	8.082	-6.297
225	0.40		-0.940	8.079	-6.771
225	0.45		-0.893	8.075	-5.912
225		0.05	-2.031	9.175	-5.065
225		0.10	-1.847	9.357	-4.802
225		0.15	-1.750	9.453	-4.871
225		0.25	-1.641	9.562	-4.993

225		0.30	-1.605	9.597	-5.151
225		0.40	-1.552	9.650	-4.997
225		0.45	-1.532	9.670	-4.975
225		0.50	-1.515	9.687	-4.758
250	0.15		-1.428	8.222	-5.675
250	0.20		-1.309	8.229	-5.543
250	0.25		-1.218	8.231	-5.900
250	0.30		-1.144	8.230	-5.493
250	0.35		-1.083	8.229	-5.407
250	0.40		-1.031	8.226	-5.937
250	0.45		-0.985	8.223	-5.438
250	0.05	0.05	-1.701	8.961	-5.190
250	0.075	0.075	-1.558	9.022	-5.247
250	0.1	0.1	-1.457	9.055	-4.925
250	0.15	0.15	-1.318	9.086	-4.882
250	0.175	0.175	-1.265	9.094	-4.941
250	0.2	0.2	-1.220	9.098	-5.232
250	0.225	0.225	-1.181	9.1	-5.404
250	0.25	0.25	-1.146	9.101	-5.139
250		0.05	-2.062	9.154	-4.820
250		0.1	-1.871	9.341	-4.650
250		0.15	-1.772	9.440	-4.745
250		0.2	-1.707	9.505	-4.827
250		0.25	-1.660	9.552	-4.530
250		0.3	-1.625	9.588	-4.693
250		0.35	-1.596	9.617	-4.690
250		0.45	-1.553	9.661	-4.536
250		0.5	-1.536	9.679	-4.742

To prevent contamination between experiments, the Teflon reactors and titanium autoclaves were soaked in a 5% nitric acid solution (Fisher Chemical, TraceMetal Grade) prepared with deionized water. A series of washing solutions were analyzed alongside the experimental solutions to verify there was no residual Th in the vessels. The time required to reach a steady-state concentration was determined through a time series of experiments, in which autoclaves containing solutions of identical composition (0.25m $NaHCO_3$) were heated at 175 °C and removed sequentially over 14 days (Table 4.2). A steady-state concentration was reached within 3 days; the time would be less at a higher temperatures because of a higher rate of reaction. All the experiments had a minimum duration of 12 days. As in our previous experiments (Nisbet et al., 2018; 2019), the solid reactant (crystalline ThO_2) was analyzed by X-ray diffraction (XRD) to ensure that no new crystalline phases formed during the experiments and that the solubility measured corresponded to saturation of the fluid with respect to this phase.

Table 4.2 The composition of the time series experimental solutions and the measured concentration of Th collected sequentially over 14 days. All solutions contained 1 m NaCl.

T (°C)	m $NaHCO_3$	Time (days)	log a HCO_3^-	pH_T	log m Th
175	0.25	0.94	-0.9932	7.853	-6.308
175	0.25	1.93	-0.9932	7.853	-6.203
175	0.25	2.93	-0.9932	7.853	-6.178
175	0.25	3.94	-0.9932	7.853	-6.142
175	0.25	6.92	-0.9932	7.853	-6.002
175	0.25	7.93	-0.9932	7.853	-5.823
175	0.25	13.93	-0.9932	7.853	-6.107

4.3 Results and data treatment

The results of the solubility experiments are reported in Table 4.1. This table lists the concentration of $NaHCO_3$ and Na_2CO_3 in the solution added to each autoclave, the logarithm of the concentration of Th measured in the solutions after each experiment, the calculated activity of HCO_3^- and the pH calculated for the experimental temperature (pH_T). To determine the pH_T and the activity of HCO_3^-, we used the thermodynamic modeling software, HCh (Shvarov and Bastrakov, 1999). The model that was employed included the following species: H_2O, H^+, OH^-, O_2, H_2, Na^+, NaOH°, NaCl°, Cl^-, HCl°, CO, CO_2, CO_3^{2-}, HCO_3^-, $NaCO_3^-$, $NaHCO_{3(aq)}$, $NaHCO_{3(s)}$ $Na_2CO_{3(s)}$, with thermodynamic data taken from Johnson et al. (1992), Shock et al. (1997), Sverjensky et al. (1997), and Tagirov et al. (1997). Aqueous Th species were not included in these initial calculations as it was assumed that the low concentration of Th dissolved in the solution did not make a significant contribution to the pH of the solution. The thermodynamic properties of water and its dissociation constant were calculated using the Haar-Gallagher-Kell model (Kestin et al., 1984) and the Marshall and Franck model (Marshall and Franck, 1981), respectively. To date, the most reliable and accurate high-T thermodynamic calculations are those performed in

NaCl-dominant solutions. This limitation is due to the relative paucity of activity models tuned and experimentally verified at elevated temperatures for other background electrolytes. The need for an experimentally proven activity model is why all the experiments were designed to be NaCl-dominant. The model used in these, and all subsequent calculations was the extended Debye-Hückel model modified by Helgeson et al. (1981), Oelkers and Helgeson (1990), and Oelkers and Helgeson (1991), which is recommended for NaCl-dominated solutions up to an ionic strength of 6, and a temperature up to 600 °C:

$$\log \gamma_i = -\frac{A Z_i^2 \sqrt{I}}{1 + B \dot{a} \sqrt{I}} + b_\gamma I + \Gamma \qquad (1)$$

where A and B are the Debye-Hückel solvent parameters, γ_i, Z_i and $\dot{a}_i$ are the individual molal activity coefficient, the charge, and the distance of closest approach of an ion i, respectively. The effective ionic strength calculated using the molal scale is I, Γ is a molarity to molality conversion factor, $\Gamma = -log_{10}(1 + 0.0180153 m_\Sigma)$, where m_Σ is the sum of molalities of all dissolved species, and b_γ is the extended-term parameter for NaCl from Helgeson et al. (1981). Using this model, the pH_T and the $aHCO_3^-$ was calculated for each experimental temperature. The solution compositions fixed the pH_T range between 7.8 and 9.8 for each temperature.

4.3.1 Determination of predominant aqueous species

Irrespective of whether $NaHCO_3$ or Na_2CO_3 was added to the solution, each of the experiments was conducted in the predominance field of HCO_3^- (Fig. 4.2). It should be noted that, although our experiments do not fall within the predominance field of CO_3^{2-}, such conditions are also very unlikely to occur in natural hydrothermal systems. Considering that the pK of water is 11.4 at 175 °C and 11.2 at 250 °C, the condition of neutrality at these temperatures corresponds to pH_T values of 5.7 and 5.6, respectively. Therefore, the conditions tested in our experiments (pH_T 7.8–9.8) were extremely alkaline. Moreover, it has been shown that the formation constant of $An(HCO_3)^+$ for trivalent actinides is 4−5 orders of magnitude lower than that of $An(CO_3)^+$at ambient conditions (Ciavatta et al., 1981; Spahiu, 1985; Guillaumont and Mompean, 2003) and it is expected that the difference will be even larger for the formation of tetravalent metal ion bicarbonate complexes, such as those of Th (Rand et al. 2008). Therefore, to evaluate whether Th-carbonate species predominate in solution, the logarithm of the concentration of Th was plotted as a function of the activity of HCO_3^- for both sets of experiments (Fig. 4.3 and 4.4). As shown in Figures 4.3 and 4.4, the concentration of Th is independent of the activity of HCO_3^- over the entire temperature range, and for each set of experiments.

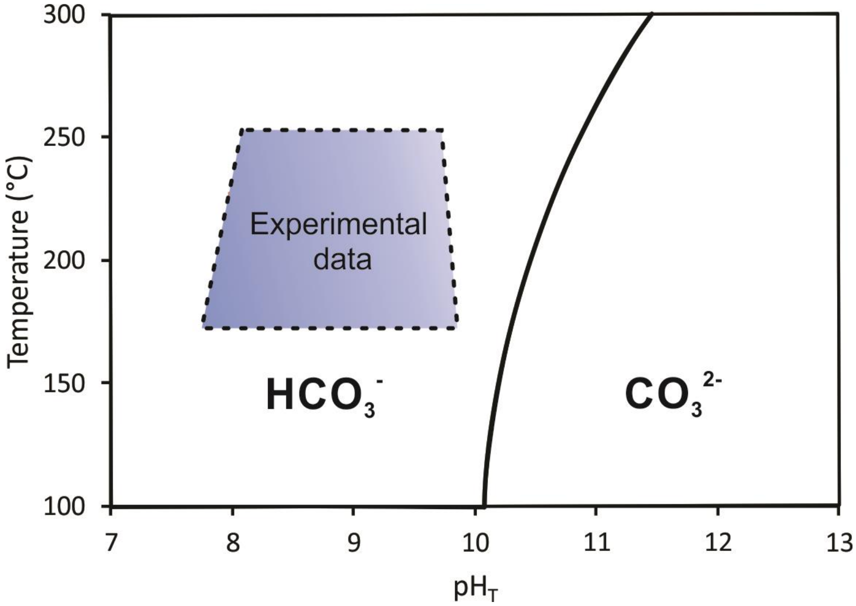

Figure 4.2 Carbonate predominance diagram with respect to temperature and pH, calculated based on activity using the data of Johnson et al. (1992). The blue area corresponds to the field of our experimental data, demonstrating that all the experiments were conducted in the predominance field of HCO_3^-.

The lack of dependence of the measured Th concentration on the activity of carbonate indicates that Th-carbonate complexes were not present in detectable concentrations at the conditions investigated in our experiments. Moreover, although Cl^- is an important ligand in the experimental system and, in principle, could form stable complexes with Th, Th-chloride complexes have not been detected in previous experiments at comparable experimental conditions (Nisbet et al., 2018).

This suggests, as in the experiments of Nisbet et al. (2018), that Th-hydroxyl complexes predominated in the experiments conducted in the current study. We tested this hypothesis by analyzing the pH_T dependency of the saturation concentration of Th in our experimental solutions, each of which had a specific pH_T that depended on the molality of $NaHCO_3$ or Na_2CO_3 in the starting solutions. To determine if Th-hydroxyl complexes did, indeed, predominate at the experimental conditions, the logarithm of the measured concentrations of Th for the sets of experiments were plotted as a function of the pH_T at each temperature (Fig. 4.5).

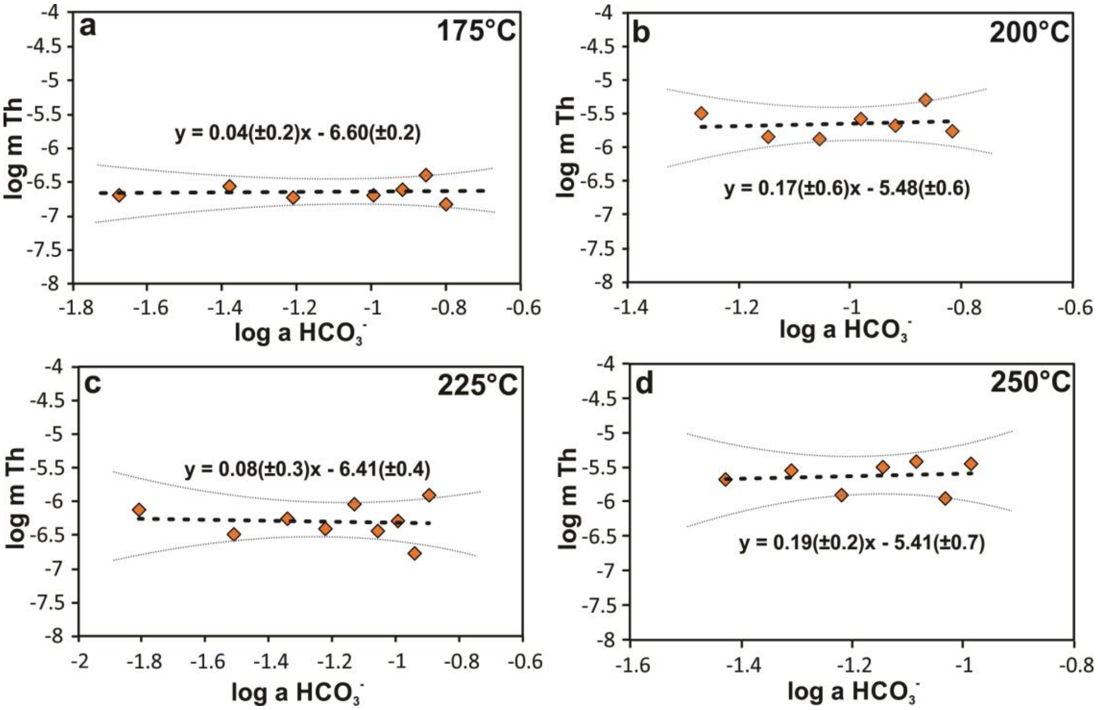

Figure 4.3a-d. The solubility of Th in $NaHCO_3$ solutions plotted as a function of the logarithm of the activity of HCO_3^- at (a)175 °C, (b) 200 °C, (c) 225 °C, and (d) 250 °C. Each data point represents the logarithm of the concentration of Th (in molality) measured in each autoclave. The trend lines represent a linear least-squares fit of the data and are accompanied by an error envelope of 95% confidence. In all plots, the slope is not significantly different from 0.

As shown in the plots presented in Figure 4.5, the concentration of Th defines two trends: 1) at the lower experimental temperatures (175 and 200 °C), the concentration of Th is nearly independent of pH_T (it decreases slightly with increasing pH_T and 2) at the higher temperatures (225 and 250 °C), it increases linearly with pH_T at a slope of approximately +1 (0.71 and 0.91). This suggests that the dominant Th-hydroxyl species in solution are $Th(OH)_4^0$ and $Th(OH)_5^-$ at the lower and higher temperatures, respectively, and that they formed via the reactions:

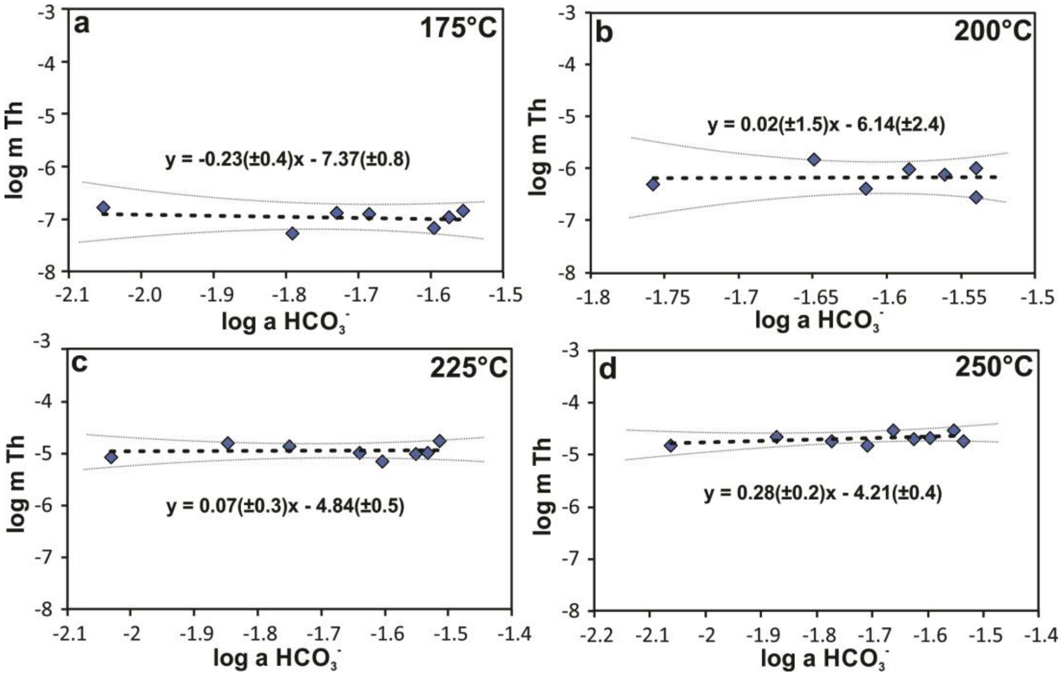

Figure 4.4a-d. The solubility of Th in Na_2CO_3 solutions plotted as a function of the logarithm of the activity of HCO_3^- at (a) 175 °C, (b) 200 °C, (c) 225 °C, and (d) 250 °C. Each data point represents the logarithm of the concentration of Th (in molality) measured in each autoclave. The trend lines represent the linear least-squares fit of the data and are accompanied by an error envelope of 95% confidence. In all plots, the slope is not significantly different from 0.

$$ThO_2 + 2H_2O \leftrightarrow Th(OH)_4^0 \tag{2}$$

$$ThO_2 + 3H_2O \leftrightarrow Th(OH)_5^- + H^+. \tag{3}$$

An additional set of experiments was performed at 250 °C, using solutions containing a mixture of $NaHCO_3$ and Na_2CO_3 (0.05–0.5m), to establish an intermediate pH and better constrain the trend in the data.

Although the slopes observed in these figures deviate a little from the stoichiometric slope suggested by Reactions 2 and 3, due possibly to a change in the activity of the Th species, it needs to be emphasized that this graphical analysis is a preliminary, semi-quantitative step designed to determine the probable stoichiometry of the species. Reliable determination of the stoichiometry of the predominant species and evaluation of their stability requires a more complex numerical fitting that accounts for all the factors influencing the concentration of Th in the experimental solutions. This fitting is reported in the following section.

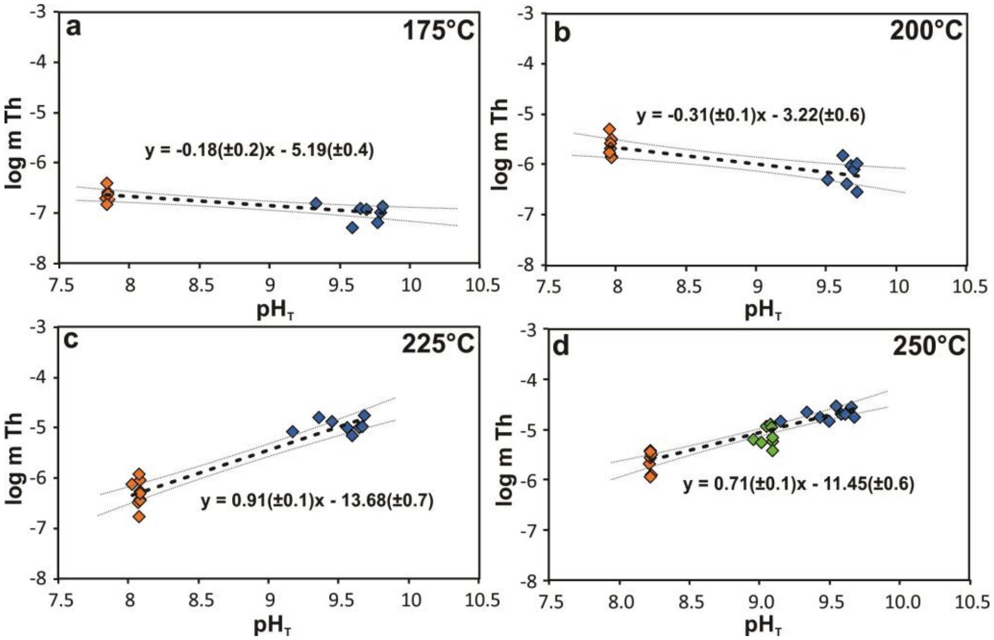

Figure 4.5a-d. The solubility of Th in $NaHCO_3$ and Na_2CO_3 solutions as a function of the pH at the experimental temperature (a) 175 °C, (b) 200 °C, (c) 225 °C, and (d) 250 °C. The slope of the linear least-squares fit to the data (dashed lines) provides a preliminary indication of the dominant Th hydroxyl species in the solution. The small change in the concentration of Th with pH_T in plots a and b suggests independence of pH (slope ~0), and the predominance of $Th(OH)_4^0$. In contrast, the slope of the data in plots c and d is ~1, suggesting that $Th(OH)_5^-$ was predominant. An error envelope of the fit at 95% confidence is shown by the fine dotted lines in each plot.

4.3.2 Derivation of formation constants

The experimental data reported in Table 4.1 were used to confirm the stoichiometry of the predominant species interpreted from the simple graphical analysis discussed above, and to calculate thermodynamic formation constants for these species. As discussed below, these species were confirmed to be $Th(OH)_4^0$ and $Th(OH)_5^-$, for which the corresponding formation reactions are:

$$Th^{4+} + 4OH^- \leftrightarrow Th(OH)_4^0 \tag{4}$$

$$\log \beta_4 = \log a_{Th(OH)_4^0} - \log a_{Th^{4+}} - 4 \log a_{OH^-} \tag{5}$$

and

$$Th^{4+} + 5OH^- \leftrightarrow Th(OH)_5^- \tag{6}$$

$$\log \beta_5 = \log a_{Th(OH)_5^-} - \log a_{Th^{4+}} - 5 \log a_{OH^-}. \tag{7}$$

In our earlier study (Nisbet et al., 2018), we reported thermodynamic formation constants for $Th(OH)_4^0$ from solubility experiments conducted in chloride-bearing solutions under acidic conditions (pH_T ~1.7–4.0). However, it should be noted that owing to the experimental conditions, these constants were based on limited data. Thus, in this contribution, we have combined the data from the current set of experiments in which our graphical analysis predicted that $Th(OH)_4^0$ is the dominant complex (175 and 200 °C), with the data from our previous experiments (Nisbet et al., 2018) to better constrain the thermodynamic parameters and extract more reliable stability constants. The calculations were performed using the program, OptimA, which is part of the HCh software package (Shvarov and Bastrakov, 1999). OptimA iteratively derives the standard Gibbs free energies of formation of aqueous species by minimizing the sum of the squared deviations of the experimental concentrations for the species of interest from their concentrations calculated using the equilibrium composition of the solution in all experiments at the relevant P-T conditions (Shvarov, 2015). In addition to the species specified in the model described above, the model also included the following species: $ThO_{2(s)}$, Th^{4+}, $Th(OH)_2^{2+}$, and $Th(OH)_4^0$. Data for $ThO_{2(s)}$ and Th^{4+} were taken from Robie and Hemingway (1995) and Shock et al. (1997), respectively, and data for

$Th(OH)_2^{2+}$ and $Th(OH)_4^0$ were taken from Nisbet et al. (2018); the stability parameters of $Th(OH)_4^0$ and $Th(OH)_5^-$ were adjustable. Considering that we did not observe any dependency of the solubility of ThO_2 on the carbonate concentration in the experimental solutions, Th-carbonate species were deemed insignificant to the mass balance of dissolved Th and were not included in the model. Likewise, as Nisbet et al. (2018), did not detect Th-chloride species in their experiments, these species were also not accounted for in the model. It should be noted that the contribution of polynuclear species to the solubility of Th was also not considered in our model, as it can be assumed that these species become unstable at high temperatures due to the decrease in the dielectric constant of water and the associated increase in electrostatic repulsion at elevated temperatures (Brugger et al., 2014; Seward et al., 2014). This is further supported by previous analyses conducted using Extended X-Ray Absorption Fine Structure (EXAFS), which found no evidence for the formation of polynuclear species in bicarbonate and carbonate solutions at concentrations above 0.1 M at ambient conditions (Felmy et al., 1997; Altmaier et al., 2006). The resulting formation constants for $Th(OH)_4^0$ and $Th(OH)_5^-$ derived for their respective experimental temperatures are reported in Table 4.3, together with their uncertainties.

Table 4.3 The logarithm of the thermodynamic formation constants for $Th(OH)_4^0$ (log β_4) and $Th(OH)_5^-$ (log β_5) derived in this study.

	175 °C	200 °C	225 °C	250 °C
log β_4	43.34 ± 0.5*	44.31 ± 0.3*		
log β_5			46.15 ± 0.09	47.9 ± 0.1

4.3.3 Derivation of MRB parameters

The revised thermodynamic formation constants for $Th(OH)_4^0$ derived in this study for 175 and 200 °C are an average of 1.1 log units higher than those published in Nisbet et al. (2018). This is not surprising considering that the values reported in Nisbet et al. (2018) for these temperatures were derived from only a few experimental data points. To refine these values, the new thermodynamic formation constants were combined with our previous values for 225 and 250 °C (43.17 and 43.74, respectively), in a fit to the Ryzhenko-Bryzgalin model (MRB) (Ryzhenko et al., 1985), modified by Borisov and Shvarov (1992) as described in Shvarov and Bastrakov (1999). This allowed us to interpolate the data and also extrapolate them to ambient temperature for comparison to previously reported formation constants for 25 °C. The MRB model fits the temperature and pressure dependence of the dissociation constant for ion pairs through the following equation:

$$logK_{(T,P)} = \frac{T_r}{T} logK_{(T_r,P_r)} + B_{(T,P)}(A_{zz/a} + \frac{B_{zz/a}}{T}) \qquad (8)$$

where K is the dissociation constant of the ion pair, T_r and P_r are the reference temperature and pressure, respectively, $B_{(T,P)}$ accounts for the property of water at the temperature and pressure calculated from the data in Marshall and Franck (1981), and $A_{zz/a}$ and $B_{zz/a}$ are the fitting parameters. The revised MRB parameters for $Th(OH)_4^0$ are reported in Table 4.4, and Figure 4.6 shows the results of the optimization as well as data previously reported for ambient conditions (Baes Jr. et al., 1965; Baes and Mesmer, 1976; Moon, 1989; Grenthe and Lagerman, 1991; Moriyama et al., 1999; Ekberg et al., 2000; Neck and Kim, 2001). As can be seen from Figure 4.6, the revised log β values are consistent with those published for 25 °C. However, given the high degree of extrapolation required, the reliability of the fit at 25 °C is lower than that interpolated within the experimental temperature range.

Table 4.4 Revised Ryzhenko–Bryzgalin (MRB) model parameters for $Th(OH)_4^0$ (from Nisbet et al., 2018)) derived from experimental data collected in this study at 175 and 200 °C, and data collected by Nisbet et al. (2018) at 225 and 250 °C.

	pK (298)	A(zz/a)	B(zz/a)
$Th(OH)_4^0$	39.769	-1.045	4139.69

Thermodynamic formation constants were derived for $Th(OH)_5^-$ at 225 and 250 °C. To the best of our knowledge, the only study that has reported the presence of $Th(OH)_5^-$ in an aqueous solution is that of Gayer and Leider (1954), who conducted solubility experiments with $ThO(OH)_2$(s) in $HClO_4$ and NaOH solutions at 25 °C. The equilibrium constant presented in this study, however, was considered unreliable in a subsequent review of the chemical thermodynamics of thorium because the study did not involve filtration or centrifugation steps following the experiments and, therefore, may have overestimated the concentration of Th due to the presence of colloids (Rand et al., 2008). The absence of a reliable formation constant for $Th(OH)_5^-$ at ambient conditions makes it challenging to extrapolate our high-temperature formation constants for this species to 25 °C with any confidence. In order to try and overcome this limitation, we estimated the thermodynamic formation constant of $Th(OH)_5^-$ at 25 °C from the change in the stability of Th-hydroxyl species with the degree of hydrolysis, using log β values reported for 25 °C in Neck and Kim (2001) for $Th(OH)^{3+}$ and $Th(OH)_3^+$, for $Th(OH)_2^{2+}$ in Nisbet et al. (2018) and $Th(OH)_4^0$ (this

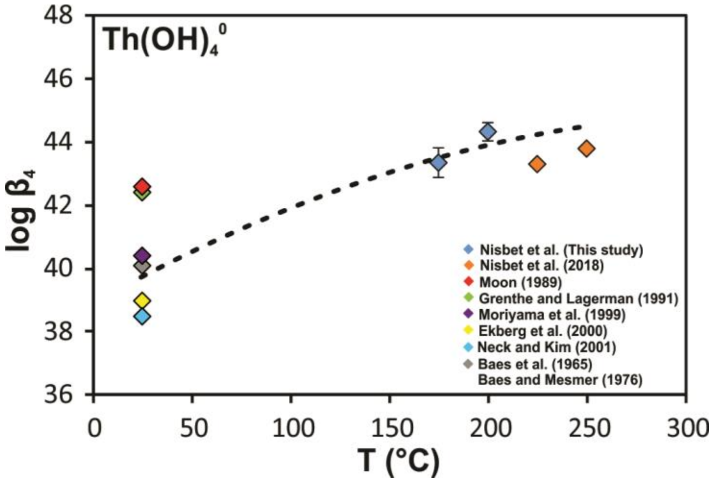

Figure 4.6 Thermodynamic formation constants for $Th(OH)_4^0$ from our previous study (225 and 250 °C) (Nisbet et al., 2018) and values refined in the current study (175 and 200 °C), extrapolated to 25 °C using the Ryzhenko-Bryzgalin model (dashed line). The error bars for 225 and 250 °C are less than the diameters of the symbols. Formation constants reported for 25 °C from ambient temperature experiments are shown for comparison.

study). The polynomial fit of these data is shown in Figure 4.7, together with the estimated value for $Th(OH)_5^-$. Using this log β at 25 °C and the experimentally derived values at 225 and 250 °C, the data were interpolated using the MRB model, as described above (Fig. 4.8). A set of MRB parameters were derived for $Th(OH)_5^-$ and are reported in Table 4.5.

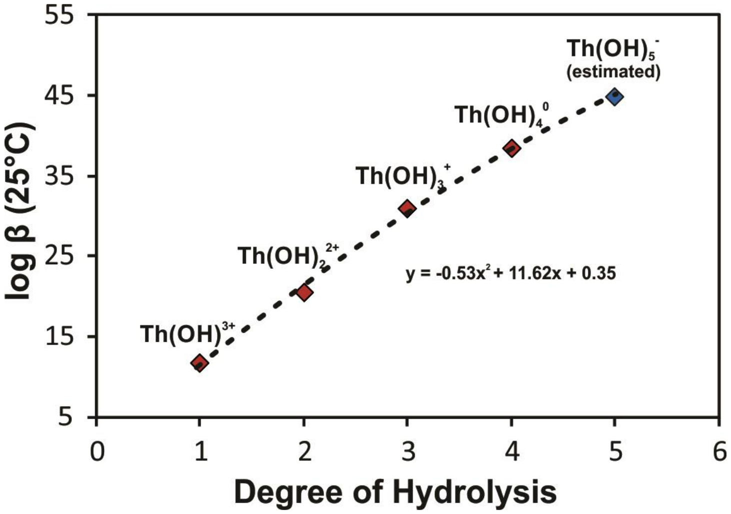

Figure 4.7 Thermodynamic formation constants for Th hydroxyl species at 25 °C plotted as a function of the degree of hydrolysis. Data for $Th(OH)^{3+}$ and $Th(OH)_3^+$ were taken from Neck and Kim (2001), data for $Th(OH)_2^{2+}$ was taken from Nisbet et al. (2018) and the value for $Th(OH)_4^0$ is the value derived in this study. The equation of the polynomial fit was used to derive the formation constant of $Th(OH)_5^-$ at 25 °C.

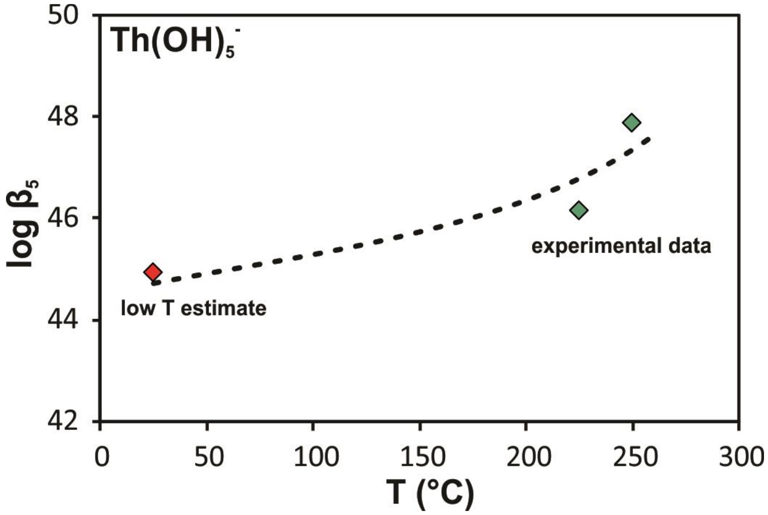

Figure 4.8 Thermodynamic formation constants for $Th(OH)_5^-$ derived in this study, and an estimate of the formation constant for this species at 25 °C (as described in the text and illustrated in Figure 4.7) fitted to the Ryzhenko-Bryzgalin model (dashed line). The error bars for the formation constants derived in this study are less than the diameters of the symbols.

4.4 Discussion

The relative proportions of the various Th-hydroxyl species as a function of pH at the temperature of our experiments are illustrated in Figure 4.9. As is evident from this figure, there is a progressive shift in the predominance of the complexes from $Th(OH)_2^{2+}$ at low pH to $Th(OH)_4^0$ and $Th(OH)_5^-$ at high pH. This increase in the degree of the hydrolysis of ThO_2 with increasing pH is a predictable consequence of the increase in the concentration of OH^- ions available for complexation with Th^{4+} in the solution. The most notable change with temperature is the shift in the predominance of $Th(OH)_5^-$ to lower pH as temperature increases and a related decrease in the size of the $Th(OH)_4^0$ predominance field.

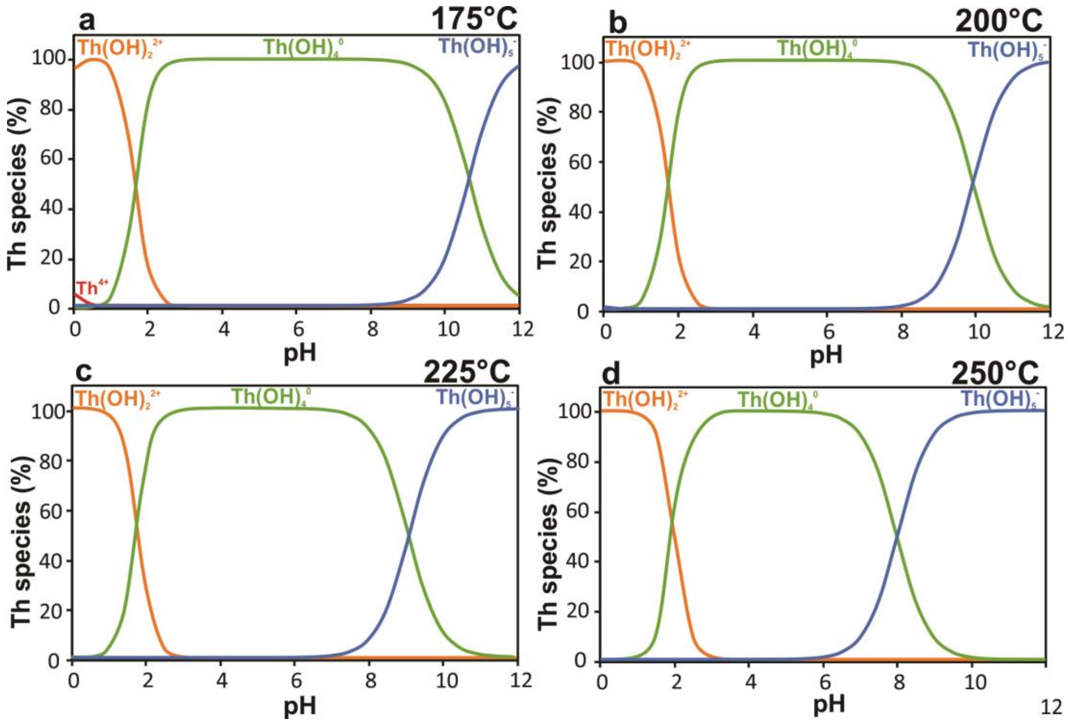

Figure 4.9 Diagrams showing the proportions of the different Th-hydroxyl species as a function of pH at the temperatures investigated in this study: (a) 175 °C, (b) 200 °C, (c) 225 °C, and (d) 250 °C. The diagrams were constructed using thermodynamic data derived in this study and Nisbet et al. (2018) studies.

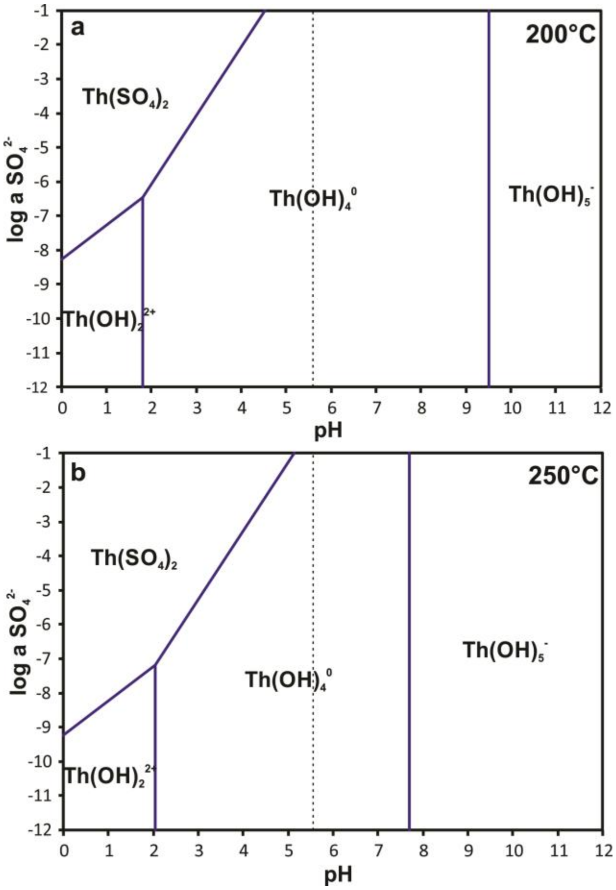

Figure 4.10 Diagrams showing the predominance fields of thorium aqueous species for (a) 200 °C and (b) 250 °C. The dashed line represents neutral pH at the respective temperatures. Data used to construct the diagrams were taken from Shock et al. (1997), Nisbet et al. (2018), Nisbet et al. (2019), and this study.

Hard Soft Acid Base (HSAB) theory (Pearson, 1963) predicts that strong acids, such as the Th^{4+} ion, will preferentially react and form stable complexes with hard bases. In general, hard bases are ligands that have low polarizability, a small ionic radius, and a high oxidation state (Pearson, 1963), and these include the anions CO_3^{2-} and SO_4^{2-} that are abundant in nature. Our previous experiments on Th speciation in sulfate-bearing fluids at elevated temperatures demonstrated that Th has a very high affinity for SO_4^{2-}, with the stable $Th(SO_4)_2$ complex predominating over the entire temperature range (175–250 °C; Nisbet et al., 2019). In contrast, the data reported in this study indicate that aqueous Th-carbonate complexes do not predominate at temperatures >175 °C. Instead, the solubility of ThO_2 is governed by hydrolysis reactions and the species $Th(OH)_4^0$ and $Th(OH)_5^-$. The failure to detect the formation of Th-carbonate complexes at elevated temperatures is in stark contrast to the results of studies conducted at ambient conditions, which showed that carbonate ions form strong complexes with Th. Irrespective of the reason for the sharp decrease in the stability of Th-carbonate complexes at elevated temperatures, the essential finding of our experiments is that carbonate-bearing solutions are unlikely to transport Th in hydrothermal systems. To identify the species that may be responsible for the transport of Th in hydrothermal fluids, we constructed diagrams showing the predominance of various Th complexes at 200 and 250 °C as a function of pH_T and the logarithm of the activity of SO_4^{2-} (Fig. 4.10). The diagrams shown in this figure consider all the Th species for which there are currently high T data: Th^{4+}, $Th(OH)_2^{2+}$, $Th(OH)_4^0$, $Th(OH)_5^-$ and $Th(SO_4)_2$. Under acidic conditions, $Th(OH)_2^{2+}$ is predicted to dominate only when the sulfate concentration is extremely low. In the presence of even minor sulfate, $Th(SO_4)_2$ is predicted to be more stable. Concentrations of sulfate in hydrothermal solutions frequently go unreported, and where mentioned are commonly based on the presence of minerals such as anhydrite and gypsum. Some authors, however, have reported concentrations of sulfate from fluid inclusion studies, primarily from REE-bearing hydrothermal fluids; these fluids are relevant to Th transport as these systems have been shown to have higher than average Th concentrations due to the similar ionic radii and charges of Th and the REE. These authors have reported concentrations of sulfate that range from 0.2−2.5m (Banks et al., 1994; Anthony E Williams-Jones et al., 2000) which, based on the predominance diagrams (Fig. 4.10), indicates that Th will be transported as a sulfate complex under acidic to moderately acidic conditions (modeled in Nisbet et al. 2019). As pH increases to neutral and alkaline conditions, the speciation of Th is dominated by the Th-hydroxyl species, $Th(OH)_4^0$ and $Th(OH)_5^-$. Under these conditions, the concentration of Th in solution is expected to be low, owing to the relatively low stability of these complexes. Therefore, given the data available to date for Th speciation at elevated temperatures, we predict that the $Th(SO_4)_2^0$ complex is one of the major vehicles for the transport of Th, that Th-hydroxyl species play a minor role in this transport, and that carbonate species are insignificant.

4.5 Conclusions

The experimental data collected in this study demonstrate that there is negligible Th-carbonate complexation at elevated temperatures (>175 °C) in carbonate-bearing solutions (0.05−0.5m $NaHCO_3/Na_2CO_3$). This result is in sharp contrast to the results of experiments performed at ambient conditions for which Th-carbonate species are reported to be highly stable. Instead, hydrolysis of Th is the major control on the solubility of ThO_2, with $Th(OH)_4^0$ predominating at 175 and 200 °C and $Th(OH)_5^-$ at 225 and 250 °C. Thermodynamic formation constants were derived for these complexes at their respective temperatures. Based on the data currently available for Th complexation at elevated temperatures, our results indicate that carbonate is unlikely to play a role in the transport of Th in natural hydrothermal systems and that the $Th(SO_4)_2^0$ complex is the main species controlling the mobilization of Th.

4.6 Acknowledgments

We would like to thank Joshua White for conducting the XRD analyses, and Oana Marina and Chelsea Neil for performing the ICP-MS analyses. We thank three anonymous reviewers for their comments and suggestions.

Funding: This work was supported by the Laboratory Directed Research and Development (LDRD) program of Los Alamos National Laboratory (LANL), New Mexico, USA (project number 20180007DR), and by LANL's Center for Space and Earth Sciences (CSES). CSES is funded by LANL’s LDRD program under project number 20180475DR.

4.7 References

Altmaier M., Neck V., Denecke M. A., Yin R. and Fanghänel T. (2006) Solubility of $ThO_2 \cdot xH_2O$(am) and the formation of ternary Th(IV) hydroxide-carbonate complexes in NaHCO3-Na2CO3 solutions containing 0–4 M NaCl. Radiochim. Acta 94.

Altmaier M., Neck V., Müller R. and Fanghänel T. (2005) Solubility of $ThO_2 \cdot xH_2O$(am) in carbonate solution and the formation of ternary Th(IV) hydroxide-carbonate complexes. Radiochim. Acta 93.

Andersen A. K., Clark J. G., Larson P. B. and Donovan J. J. (2017) REE fractionation, mineral speciation, and supergene enrichment of the Bear Lodge carbonatites, Wyoming, USA. Ore Geol. Rev. 89, 780–807.

Ault T., Van Gosen B., Krahn S. and Croff A. (2015) Natural thorium resources and recovery: options and impacts. Nucl. Technol. 194, 136–151.

Baes C. F. and Mesmer R. S. (1976) The hydrolysis of cations. Ber Bunsenges Phys Chem 81, 245–246.

Baes Jr. C. F., Meyer N. J. and Roberts C. E. (1965) The Hydrolysis of Thorium(1V) at 0 and 95°C. Inorg. Chem. 4, 518–527.

Banks D. A., Yardley B. W. D., Campbell A. R. and Jarvis K. E. (1994) REE composition of an aqueous magmatic fluid: A fluid inclusion study from the Capitan Pluton, New Mexico, U.S.A. Chem. Geol. 113, 259–272.

Borisov M. V. and Shvarov Y. V. (1992) Thermodynamics of geochemical processes. Mosc. Mosc. State Univ. Publ. House, 254.

Brugger J., Tooth B., Etschmann B., Liu W., Testemale D., Hazemann J.-L. and Grundler P. V. (2014) Structure and Thermal Stability of Bi(III) Oxy-Clusters in Aqueous Solutions. J. Solut. Chem. 43, 314–325.

Castor S. B. (2008) The Mountain Pass rare-earth carbonatite and associated ultrapotassic rocks, California. Can. Mineral. 46, 779–806.

Ciavatta L., Ferri D., Grenthe I., Salvatore F. and Spahiu K. (1981) Studies on Metal Carbonate Equilibria. 3. The Lanthanum(III) Carbonate Complexes in Aqueous Perchlorate Media. Acta Chem. Scand. 35a, 403–413.

Cook N. J., Ciobanu C. L., O'Rielly D., Wilson R., Das K. and Wade B. (2013) Mineral chemistry of Rare Earth Element (REE) mineralization, Browns Ranges, Western Australia. Lithos 172–173, 192–213.

Ekberg C., Albinsson Y., Comarmond M. J. and Brown P. L. (2000) Study on the complexation behavior of thorium(IV).1. Hydrolysis equilibria. J. Solut. Chem. 29, 63–86.

Felmy A. R. and Rai D. (1999) Application of Pitzer's Equations for Modeling the Aqueous Thermodynamics of Actinide Species in Natural Waters: A Review. J. Solut. Chem. 28, 533–553.

Felmy A. R., Rai D., Sterner S. M., Mason M. J., Hess N. J. and Conradson S. D. (1997) Thermodynamic models for highly charged aqueous species: Solubility of Th(IV) hydrous oxide in concentrated $NaHCO_3$ and Na_2CO_3 solutions. J. Solut. Chem. 26, 233–248.

Gayer K. H. and Leider H. (1954) The Solubility of Thorium Hydroxide in Solutions of Sodium Hydroxide and Perchloric Acid at 25°C. J. Am. Chem. Soc. 76, 5938–5940.

Grenthe I. and Lagerman B. (1991) Studies on metal carbonate equilibria: 23. Complex formation in the Th(IV)-H_2O-$CO_{2(g)}$ system. Acta Chem. Scand. 45, 231–238.

Guillaumont R., Fanghanel T., Fuger J., Grenthe I., Neck V., Palmer D. A. and Rand M. H. (2003) Update on the Chemical Thermodynamics of Uranium, Neptunium, Plutonium, Americium and Technetium., OECD Nuclear Energy Agency.

Haas J. R., Shock E. L. and Sassani D. C. (1995) Rare earth elements in hydrothermal systems: Estimates of standard partial molal thermodynamic properties of aqueous complexes of the rare earth elements at high pressures and temperatures. Geochim. Cosmochim. Acta 59, 4329–4350.

Helgeson H. C., Kirkham D. H. and Flowers G. C. (1981) Theoretical prediction of the thermodynamic behavior of aqueous electrolytes at high pressures and temperatures: IV. Calculation of activity coefficients, osmotic coefficients, and apparent molal and standard and relative partial molal properties to 600°C. Am. J. Sci. 281, 1249–1516.

Johnson J. W., Oelkers E. H. and Helgeson H. C. (1992) SUPCRT92: a software package for calculating the standard molal thermodynamic properties of minerals, gases, aqueous species, and reactions from 1 to 5000 bar and 0 to 1000 °C. Comput. Geosci. 18, 899–947.

Kestin J., Sengers J. V., Kamgar-Parsi B. and Levelt Sengers J. M. H. (1984) Thermophysical properties of fluid H2O. J. Phys. Chem. Ref. Data 13, 601–609.

Marshall W. L. and Franck E. U. (1981) Ion product of water substance, 0-1000 °C, 1-10,000 bars new International Formulation and its background. J. Phys. Chem. Ref. Data 10, 295–304.

Moon H. (1989) Equilibrium ultrafiltration of hydrolyzed thorium(IV) solutions. Bull. Korean Chem. Soc. 10, 270–272.

Moriyama H., Kitamura A., Fujiwara K. and Yamana H. (1999) Analysis of mononuclear hydrolysis constants of actinide ions by hard sphere model. Radiochim. Acta 87, 97–104.

Neck V. and Kim J. I. (2001) Solubility and hydrolysis of tetravalent actinides. Radiochim. Acta 89, 1–16.

Nisbet H., Migdisov A. A., Williams-Jones A. E., Xu H., van Hinsberg V. J. and Roback R. (2019) Challenging the thorium-immobility paradigm. Sci. Rep. 9, 17035.

Nisbet H., Migdisov A., Xu H., Guo X., van Hinsberg V., Williams-Jones A. E., Boukhalfa H. and Roback R. (2018) An experimental study of the solubility and speciation of thorium in chloride-bearing aqueous solutions at temperatures up to 250 °C. Geochim. Cosmochim. Acta 239, 363–373.

Oelkers E. H. and Helgeson H. C. (1991) Calculation of activity coefficients and degrees of formation of neutral ion pairs in supercritical electrolyte solutions. Geochim. Cosmochim. Acta 55, 1235–1251.

Oelkers E. H. and Helgeson H. C. (1990) Triple-ion anions and polynuclear complexing in supercritical electrolyte solutions. Geochim. Cosmochim. Acta 54, 727–738.

Osthols E., Bruno J. and Grenthe I. (1994) On the influence of carbonate on mineral dissolution: III. The solubility of microcrystalline ThO2 in CO2-H2O media. Geochim. Cosmochim. Acta 58, 613–623.

Pearson R. G. (1963) Hard and soft acids and bases. J. Am. Chem. Soc. 85, 3533–3539.

Rand M. H., Mompean F. J., Perrone J. and Illemassene M. (2008) Chemical Thermodynamics of Thorium., OECD, NEA.

Robie R. A. and Hemingway B. S. (1995) Thermodynamic properties of minerals and related substances at 298.15 K and 1 Bar (10^5 Pascals) pressure and at higher temperatures. US Geol. Survet Bull. 2131, 461.

Ryzhenko B. N., Bryzgalin O. V., Artamkina I. Y., Spasennykh M. Y. and Shapkin A. I. (1985) An electrostatic model for the electrolytic dissociation of inorganic substances dissolved in water. Geochem. Int. 22, 138–144.

Seward T. M., Williams-Jones A. E. and Migdisov A. A. (2014) The Chemistry of Metal Transport and Deposition by Ore-Forming Hydrothermal Fluids. In Treatise on Geochemistry Elsevier. pp. 29–57.

Sheard E. R., Williams-Jones A. E., Heiligmann M., Pederson C. and Trueman D. L. (2012) Controls on the Concentration of Zirconium, Niobium, and the Rare Earth Elements in the Thor Lake Rare Metal Deposit, Northwest Territories, Canada. Econ. Geol. 107, 81–104.

Shock E. L., Sassani D. C., Willis M. and Sverjensky D. A. (1997) Inorganic species in geological fluids: Correlations among standard molal thermodynamic properties of aqueous ions and hydroxide complexes. Geochim. Cosmochim. Acta 61, 907–950.

Shvarov Y. V. (2015) A suite of programs, OptimA, OptimB, OptimC, and OptimS compatible with the Unitherm database, for deriving the thermodynamic properties of aqueous species from solubility, potentiometry and spectroscopy measurements. Appl. Geochem. 55, 17–27.

Shvarov Y. V. and Bastrakov E. (1999) HCh, A Software Package for Geochemical Equilibrium Modeling: User’s Guide.

Spahiu K. (1985) Studies on metal carbonate equilibria. XI: Yttrium (III) carbonate complex formation in aqueous perchlorate media of various ionic strengths. Acta Chem. Scand. A39, 33–45.

Sverjensky D. A., Shock E. L. and Helgeson H. C. (1997) Prediction of the thermodynamic properties of aqueous metal complexes to 1000 °C and 5 kb. Geochim. Cosmochim. Acta 61, 1359–1412.

Tagirov B. R., Zotov A. and Akinfiev N. (1997) Experimental study of dissociation of HCl from 350 to 500 °C and from 500 to 2500 bars: thermodynamic properties of HCl°(aq). Geochim. Cosmochim. Acta 61, 4267–4280.

Williams-Jones A. E., Samson I. M. and Olivo G. R. (2000) The Genesis of Hydrothermal Fluorite-REE Deposits in the Gallinas Mountains, New Mexico. Econ. Geol. 95, 327–342.

Wood S. A. (1990) The aqueous geochemistry of the rare-earth elements and yttrium 2. Theoretical predictions of speciation in hydrothermal solutions to 350°C at saturation water vapor pressure. Chem. Geol. 88, 99–125.

Preface to Chapter 5

In the previous three chapters, we explored the speciation of Th in chloride, sulfate, and carbonate-bearing hydrothermal fluids and considered the potential for these ligands to mobilize and concentrate Th in hydrothermal systems. We determined that Th-chloride and Th-carbonate are not detectable at hydrothermal conditions (175-250 °C) and that hydroxyl and sulfate complexes predominate, the latter being the most stable, and most likely to transport Th.

Although we now have a better understanding of the mobility of Th in hydrothermal fluids such as those associated with REE ore deposits, a key shortcoming remains, and that is a lack of knowledge on the solubility and speciation of the REE in carbonate-bearing solutions at high-temperatures. Considering that many REE ore deposits are hosted in carbonatites and their associated systems, and REE-carbonate minerals are among the most commonly extracted REE ore minerals, it is imperative that we understand the REE-carbonate relationship.

In the following chapter, we investigate the solubility and speciation of Nd, one of the most sought-after REE, in acidic and alkaline carbonate-bearing hydrothermal fluids, using synthesized Nd-hydroxylbastnäsite as a reference phase. We identify two Nd-carbonate complexes and derive solubility constants for each. The potential for REE-carbonate complexes to transport the REE in hydrothermal systems is discussed.

Chapter 5

The solubility and speciation of Nd in carbonate-bearing hydrothermal fluids up to 250 °C

Haylea Nisbet[1,2*], Artas Migdisov[1], Anthony Williams-Jones[2], Vincent van Hinsberg[2]

[1]Earth and Environmental Sciences Division, Los Alamos National Laboratory, Los Alamos, NM 87545, USA.

[2] Department of Earth and Planetary Sciences, McGill University, 3450 University Street, Montreal, QC, H3A 0E8, Canada.

Abstract

Neodymium is one of the most sought-after rare earth elements (REE) as it is an essential component in permanent magnets used in wind turbines and electric motors that are needed to address the issue of climate change. In nature, the enrichment of Nd and the other REE is frequently attributed to their transport and deposition by hydrothermal fluids. Whereas numerous studies have investigated the complexation of Nd with chloride, sulfate, and fluoride in hydrothermal fluids, a major gap in knowledge that hinders our ability to predict the mobility of Nd in ore-forming hydrothermal systems is its behavior in carbonate-bearing fluids at elevated temperatures. In this contribution, we evaluate the speciation of Nd in carbonate-bearing fluids under acidic (pH_T 2−4) and alkaline (pH_T 7.8−9.8) conditions using the autoclave solubility method at temperatures between 175 and 250 °C with synthesized Nd-hydroxylbastnäsite as the reference phase. We demonstrate that the predominant aqueous complexes are $NdCO_3^+$ and $NdCO_3OH^0$ under acidic and alkaline conditions, respectively. Our findings predict that carbonate species have the potential to be important ligands for REE mobilization in hydrothermal fluids.

5.1 Introduction

The rare earth elements (REE) have become an indispensable resource in the 21st-century because of their central role in advanced technologies required to mitigate climate change (wind turbines, electric cars), and address national security issues (satellites, aircraft) (Van Gosen et al., 2017). As a result, the global demand for these elements is increasing strongly, and with it, the need to discover and exploit new resources. Contrary to their name, the REE are relatively abundant in nature and occur in concentrations comparable to those of metals such as Mo, Ni, and Co (Voncken, 2016). Instead, it is their tendency to concentrate into amounts sufficient to achieve "ore" status, that is rare.

Although there are examples of REE ore deposits that have been proposed to have crystallized directly from a magmatic source (e.g., the Sulphide Queen ore body at Mountain Pass, California; Castor, 2008), there is growing evidence that they are mainly concentrated to ore grades by hydrothermal fluids (e.g., Ashram, Strange Lake, Browns Range, Gallinas Mountains, Bayan Obo; Beland and Williams-Jones (2021), Vasyukova and Williams-Jones (2019), Cook et al. (2013), Williams-Jones et al. (2000), Smith et al. (2015)). A large proportion of REE ore deposits are hosted in carbonatites, many of which are proposed to have originated from hydrothermal fluids, including Ashram, Canada (Beland and Williams-Jones, 2021), Bear's Lodge, USA (Andersen et al., 2017), Wicheeda, Brazil (Trofanenko et al., 2016), Barra do Itapirapuã, Brazil (Ruberti et al., 2008), and Amba Dongar, India (Williams-Jones and Palmer, 2002). It is also common for REE-carbonate minerals such as bastnäsite ($REECO_3(F,OH)$) to be the dominant REE ore mineral (Verplanck and Hitzman, 2016). This close association with carbonates raises the possibility that carbonate-bearing solutions may play a key role in transporting the REE. Indeed, carbonate complexes are among the strongest REE-complexes at ambient conditions (Cantrell and Byrne, 1986; Johannesson and Stetzenbach, 1995). Cantrell and Byrne (1987) showed that $REECO_3^+$ and $REE(CO_3)_2^-$ are the principal aqueous REE complexes in seawater, and that the LREE preferentially partition into $REECO_3^+$, and the HREE into $REE(CO_3)_2^-$. Modeling of groundwater from the Nevada Test Site and Yucca Mountain predicted that the same carbonate complexes for Nd have significantly higher concentrations than Nd-fluoride, chloride, sulfate, and phosphate complexes (Johannesson and Stetzenbach, 1995). A more recent experimental study by Luo and Byrne (2004) that used potentiometric measurements corroborated the findings of these studies and derived thermodynamic formation constants for these carbonate species. Thermodynamic data for these complexes at elevated temperatures are limited to theoretical predictions by Wood (1990) and Haas et al. (1995) based on extrapolations from ambient temperature. These extrapolations, however, yielded very different predictions for the stability of REE-carbonate complexes. The current study has been designed to resolve this disagreement experimentally and provide the data on REE-carbonate speciation at elevated temperatures that are required to reliably evaluate the potential for REE transport by carbonate species in hydrothermal systems.

Among the REE, neodymium (Nd) is the most highly sought after, owing to the essential role that it plays in neodymium-iron-boron magnets that are in high demand in a huge variety of technological applications including those related to green energy (Van Gosen et al., 2017). Neodymium is supplied in large part by the REE-carbonate mineral bastnäsite ($REECO_3(F,OH)$), which, in addition to Nd, preferentially hosts light rare earth elements (LREE) including Ce, La, and Pr, as well as Y, a heavy rare earth element (HREE) (Voncken, 2016). Data on the standard thermodynamic properties of bastnäsite are limited to the studies of Gysi and Williams-Jones (2015) and Shivaramaiah et al. (2016). The study of Gysi and Williams-Jones (2015) used Differential Scanning Calorimetry (DSC) to determine the isobaric heat capacity and thermogravimetric analysis to derive a standard enthalpy of formation and estimate entropy for a natural bastnasite-(Ce) sample. Shivaramaiah et al. (2016) reported a value for the standard enthalpy of formation of synthetic Nd-hydroxylbastnäsite based on the results of high-temperature oxide melt solution calorimetry. Our understanding of Nd aqueous complexation at elevated temperatures comes from studies that investigated the speciation of Nd with ligands that are common in natural hydrothermal systems (Cl^-, F^-, and SO_4^{2-}) (Migdisov and Williams-Jones, 2002; Migdisov et al., 2006; Migdissov and Williams-Jones, 2007). The complexation of Nd with carbonate, another ligand that is common in nature, has not yet been investigated experimentally at hydrothermal conditions. Our study corrects this situation by reporting the results of solubility experiments in acidic and alkaline solutions undertaken to investigate the aqueous speciation of Nd in carbonate-bearing solutions at elevated temperatures.

5.2 Methods

Solubility experiments were performed in solutions of varying carbonate concentration (0.05−0.5m $NaHCO_3$/Na_2CO_3) and pH to evaluate the speciation of Nd in carbonate-bearing hydrothermal fluids at acidic to alkaline pH. Each series of experiments was carried out at 175, 200, 225, and 250 °C, and the pressure of saturated water vapor. The experiments used the autoclave solubility technique, described below.

The reference phase used in the experiments was synthesized Nd-hydroxylbastnäsite ($NdCO_3OH$). Bastnäsite, the REE-fluorocarbonate mineral $REECO_3(F,OH)$, is one of the most stable and abundant REE minerals deposited in REE hydrothermal systems (Shivaramaiah et al., 2016). Although bastnäsite invariably occurs in nature as a solid solution that contains multiple LREE and fluorine, we have elected to use the end-member Nd-hydroxylbastnäsite in our experiments to simplify the system. The Nd-hydroxylbastnäsite phase was synthesized hydrothermally using the method of Vallina et al. (2014) and Voigt et al. (2016). A 50 mM solution of $NdCl_3$ was mixed with the a 50 mM Na_2CO_3 solution and immediately precipitated an amorphous REE carbonate phase. The resulting slurry was introduced into Teflon-lined titanium autoclaves capped with a Teflon O-ring and heated in a Muffle Furnace at 165−200 °C (Vallina et al., 2014; Voigt et al., 2016). The autoclaves were gently shaken every 10 min for the first 60−100 min of heating. After heating for ~3 weeks, the autoclaves were removed from the furnace and cooled to room temperature by a stream of cold air (<30 min). Next, the products were filtered through a glass vacuum filter set-up using 2.5 μm filter paper and rinsed several times with deionized water (DI) and isopropyl. The resultant powders were dried overnight at room temperature and analyzed by X-ray diffraction (XRD) to verify that hydroxylbastnäsite had formed and that the low-temperature polymorph of hydroxylbastnäsite, kozoïte, was not present. To do this, samples of the powders were ground to a finer powder, loaded onto a quartz-glass slide, and analyzed by a Bruker D8 Discover X-ray Diffractometer with CuKα radiation (λ = 0.154 nm, 40 kV, and 40 mA) and a LynxEye position-sensitive detector. Scans were carried out from 5 to 70° 2θ with a step interval of 0.02° and a dwell time of 1−2 sec per step. The spectra obtained (Fig. 5.1) matched that of the Nd-hydroxylbastnäsite obtained by Vallina et al. (2015) and Christensen (1973). The phase was also analyzed by XRD after the completion of the experiments to verify that no phase change had occurred.

The autoclave solubility experiments were divided into two sets. The first set of experiments was conducted under acidic conditions. Five solutions of variable $pH_{25°C}$ (1.305, 1.613, 2.098, 2.540, 3.00) were prepared by slowly adding concentrated HCl (Fisher Scientific, TraceMetal Grade) to deionized water (DI). Each solution contained 1 m NaCl to satisfy the activity model used in our calculations (see below). Before each experiment, small quartz tubes containing synthesized Nd-hydroxylbastnäsite, capped with a porous Teflon film, were introduced into Teflon-lined autoclaves and submerged in 10 mL of the experimental solution that had previously

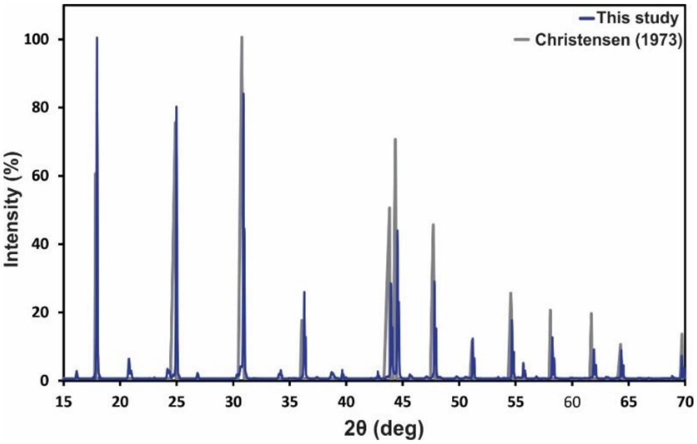

Figure 5.1 An example of an XRD scan of the reference phase after hydrothermal synthesis. The spectrum overlaps that of Christensen (1973) (grey) for Nd-hydroxylbastnäsite ($NdCO_3OH$).

Been introduced into the autoclaves. Next, a small piece of $CO_{2(s)}$ (dry ice; 0.3−1.3 grams) was added to the solutions and the autoclaves were immediately sealed with a Teflon O-ring. The autoclaves were weighed before and after adding the dry ice to determine how much was added to each solution. Dry ice was required in these experiments because of the low solubility of CO_2 under acidic conditions; the experiments were conducted at elevated pressure to ensure CO_2 was dissolved in the solutions. The autoclaves were heated in a Muffle Furnace for 13 days. At the end of the experiments, the autoclaves were removed from the furnace and quenched in a stream of cold air (the quench time was <25 min). The autoclaves were weighed before and after the experiments to ensure there was no loss of CO_2. Next, the holders containing the Nd-hydroxylbastnäsite were removed and a 3 mL aliquot of sulfuric acid was added to the solutions and left for 24 hours to dissolve any Nd that may have precipitated on the walls of the Teflon reactor during the quenching process. Finally, Nd concentrations were measured by Inductively Coupled Plasma Quadrupole Mass Spectrometry (ICP-QMS). A sketch of the experimental setup is shown in Figure 5.2a. Values of the parameters for the first set of experiments are reported in Table 5.1.

Table 5.1 Values of the experimental parameters for the acidic solubility experiments, including the temperature, the amount of $CO_{2(s)}$ added to each autoclave, the calculated pH_T and activity of $CO_{2(aq)}$, and the measured concentration of Nd. All experimental solutions contained 1m NaCl.

T (°C)	$CO_{2(s)}$ added (g)	log a $CO_{2(aq)}$	pH_T	log m Nd
175	0.5	-1.002	2.023	-3.362
175	0.3	-1.128	2.271	-3.539
175	0.6	-0.997	2.779	-3.909
175	0.5	-1.017	3.251	-4.775
175	0.6	-0.997	3.626	-4.881
200	0.6	-0.928	2.032	-3.594
200	1	-0.861	2.287	-3.883
200	0.7	-0.931	2.787	-4.033
200	0.6	-0.926	3.289	-4.309
200	0.3	-1.078	3.587	-4.860
225	0.5	-0.878	2.097	-3.298
225	0.9	-0.765	2.383	-3.587
225	1	-0.772	2.915	-4.036
225	0.5	-0.869	3.464	-4.606
225	0.4	-0.925	3.771	-5.191
250	0.8	-0.757	2.152	-3.278
250	0.5	-0.800	2.483	-3.613
250	0.9	-0.816	3.046	-4.488
250	0.8	-0.767	3.491	-4.781
250	1.3	-0.718	3.837	-5.259

The second set of solubility experiments were performed in alkaline solutions of varying carbonate concentrations and were conducted at the same temperatures as the acidic experiments. Two types of experimental solutions were used to determine the solubility of Nd as a function of carbonate activity and pH: 1) solutions containing 0.05−0.5 m $NaHCO_3$; and 2) solutions containing 0.05−0.5 m Na_2CO_3, each containing 1 m NaCl. Targeted amounts of $NaHCO_3$ (Acros Organics, A.C.S. grade), Na_2CO_3 (anhydrous, Fisher Chemical, A.C.S. grade), and NaCl (Fisher Chemical, A.C.S. grade) were added to vacuum-degassed deionized water (DI) to constrain the pH and composition of the fluid. The fluid was flushed with argon gas immediately before sealing the autoclaves to minimize the exchange of CO_2 between the fluid and the atmosphere. The experiments were heated for 7–21 days. The post-experimental steps were identical to those described above. A sketch of the experimental setup is shown in Figure 5.2b. Values of the parameters for the second set of experiments are reported in Table 5.2.

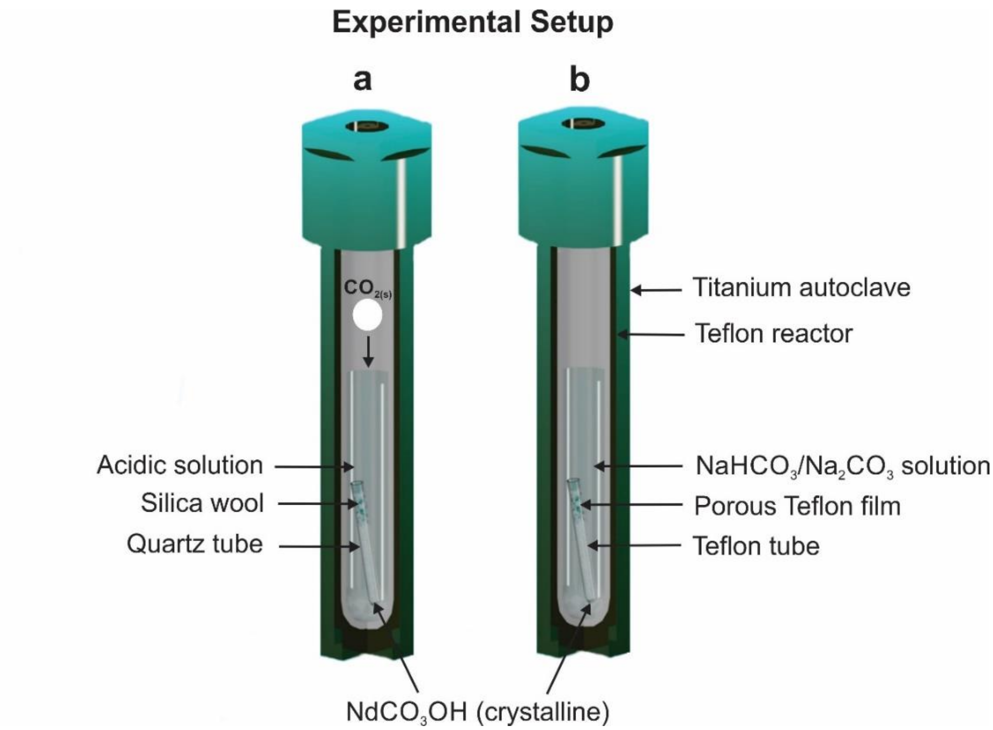

Figure 5.2a-b A schematic cross-section depicting the experimental setup of the autoclave solubility method: a) Experiments conducted under acidic conditions using $CO_{2(s)}$ as the carbonate source and b) Experiments conducted at alkaline conditions using $NaHCO_3$ and Na_2CO_3 as the carbonate source.

The time required to reach a steady-state Nd concentration in the experiments was determined through time-series experiments, in which autoclaves containing solutions of identical composition (e.g. 0.2 m $NaHCO_3$ and 1m NaCl) were heated at 175 °C and removed sequentially over 7 days. It was determined that a steady-state concentration was reached in less than 3 days

Table 5.2 Values of the experimental parameters for the alkaline solubility experiments, including the temperature, the amount of $NaHCO_3$ or Na_2CO_3 added to each autoclave, the calculated activity of HCO_3^- and pH_T, and the measured concentration of Nd. All experimental solutions contained 1m NaCl.

T (°C)	m $NaHCO_3$	m Na_2CO_3	log a HCO_3^-	pH_T	log m Nd
175	0.1		-1.380	7.855	-5.195
175	0.15		-1.208	7.857	-5.657
175	0.2		-1.087	7.856	-5.367
175	0.25		-0.993	7.853	-5.616
175	0.3		-0.917	7.85	-5.402
175	0.4		-0.799	7.842	-5.280
175		0.15	-1.792	9.594	-5.279
175		0.2	-1.730	9.653	-6.244
175		0.25	-1.685	9.696	-5.332
175		0.3	-1.649	9.73	-5.853
175		0.35	-1.620	9.757	-5.163
175		0.4	-1.595	9.78	-5.275
175		0.45	-1.574	9.799	-5.980
200	0.2		-1.148	7.962	-5.851
200	0.25		-1.055	7.96	-5.669
200	0.3		-0.980	7.958	-5.139
200	0.4		-0.863	7.951	-5.752
200	0.45		-0.816	7.947	-5.742
200		0.1	-1.851	9.412	-5.572
200		0.15	-1.757	9.505	-5.626
200		0.2	-1.695	9.566	-5.249
200		0.25	-1.649	9.61	-6.211
200		0.3	-1.614	9.645	-5.216
200		0.35	-1.585	9.673	-5.658
225	0.2		-1.221	8.086	-4.577
225	0.25		-1.129	8.086	-5.517
225	0.3		-1.055	8.084	-5.204
225	0.35		-0.993	8.082	-5.033
225	0.4		-0.940	8.079	-4.367
225	0.45		-0.893	8.075	-5.344
225		0.05	-2.031	9.175	-4.803
225		0.1	-1.847	9.357	-4.392
225		0.15	-1.750	9.453	-4.813
225		0.2	-1.687	9.516	-4.769
225		0.25	-1.641	9.562	-4.692
225		0.3	-1.605	9.597	-4.197
225		0.35	-1.576	9.626	-5.172
225		0.4	-1.552	9.65	-4.943
250	0.05		-1.895	8.15	-5.240
250	0.1		-1.598	8.204	-5.078

250	0.15		-1.428	8.222	-4.909
250	0.2		-1.309	8.229	-5.031
250	0.25		-1.218	8.231	-4.955
250	0.3		-1.144	8.23	-5.068
250	0.35		-1.083	8.229	-4.877
250	0.4		-1.031	8.226	-4.749
250	0.45		-0.985	8.223	-4.871
250		0.1	-1.871	9.341	-4.706
250		0.15	-1.772	9.44	-4.916
250		0.2	-1.707	9.505	-5.228
250		0.25	-1.660	9.552	-4.881
250		0.3	-1.625	9.588	-4.658
250		0.35	-1.596	9.617	-4.921
250		0.4	-1.572	9.641	-4.967
250		0.45	-1.553	9.661	-4.776

for all experimental solutions (Fig. 5.3); the time would have been less at a higher temperatures because of a higher rate of reaction. All the experiments had a minimum duration of 7 days. To prevent contamination, the Teflon reactors and titanium autoclaves were soaked for more than 48 hours in a 5% nitric acid solution (Fisher Chemical, TraceMetal Grade), prepared with deionized water between experiments.

5.3 Results and data treatment

The results of the first set of solubility experiments conducted under acidic conditions are reported in Table 5.1. This table lists the logarithm of the measured concentration of dissolved Nd, the amount of $CO_{2(s)}$ added to each autoclave, the calculated activity of $CO_{2(aq)}$ dissolved in the solution, and the pH of the solution calculated at the experimental temperature (pH_T). We used the thermodynamic modeling software, HCh, to calculate the activity of dissolved $CO_{2(aq)}$ and pH_T, (Shvarov and Bastrakov, 1999). The model that was employed included the following aqueous species: H_2O, H^+, OH^-, O_2, H_2, Na^+, NaOH°, NaCl°, Cl^-, HCl°, $NaCO_3^-$, $NaHCO_3°_{(aq)}$, $CO_{2(aq)}$, CO_3^{2-}, and HCO_3^- with thermodynamic data taken from Johnson et al. (1992), Shock et al. (1997), Sverjensky et al. (1997), Tagirov et al. (1997), and Miron et al. (2017). The thermodynamic properties of water and its dissociation constant were calculated using the Haar-Gallagher-Kell model (Kestin et al., 1984) and the Marshall and Franck model (Marshall and Franck, 1981), respectively. To date, the most reliable and accurate thermodynamic calculations for high temperatures are those performed in NaCl-dominant solutions (Oelkers and Helgeson, 1991). This limitation is due to the relative paucity of activity models tuned and experimentally verified at elevated temperatures for other background electrolytes. The lack of an experimentally proven activity model is the reason why all the experiments were designed to be NaCl-dominant. The model used in these, and all subsequent calculations was the extended Debye-Hückel model modified by Helgeson et al. (1981), Oelkers and Helgeson (1990), and Oelkers and Helgeson (1991), which is recommended for NaCl-dominated solutions up to an ionic strength of 6, and a temperature up to 600 °C:

$$\log \gamma_i = -\frac{A Z_i^2 \sqrt{I}}{1 + B \dot{a} \sqrt{I}} + b_\gamma I + \Gamma \tag{1}$$

where A and B are the Debye-Hückel solvent parameters, γ_i, Z_i and $\dot{a}_i$ are the individual molal activity coefficient, the charge, and the distance of the closest approach of an ion *i*, respectively. The effective ionic strength calculated using the molal scale is I, Γ is a molarity to molality conversion factor, and b_γ is the extended-term parameter for NaCl from Helgeson et al. (1981). The species $CO_{2(gas)}$ (Holland and Powell, 1998) was included in the model as a perfectly mobile component, and the fugacity of CO_2 in the experimental solutions was calculated using the modified Redlich–Rosenfeld equation of Appelo et al. (2014). The activity of dissolved $CO_{2(aq)}$ and pH_T were calculated iteratively and are reported in Table 5.1.

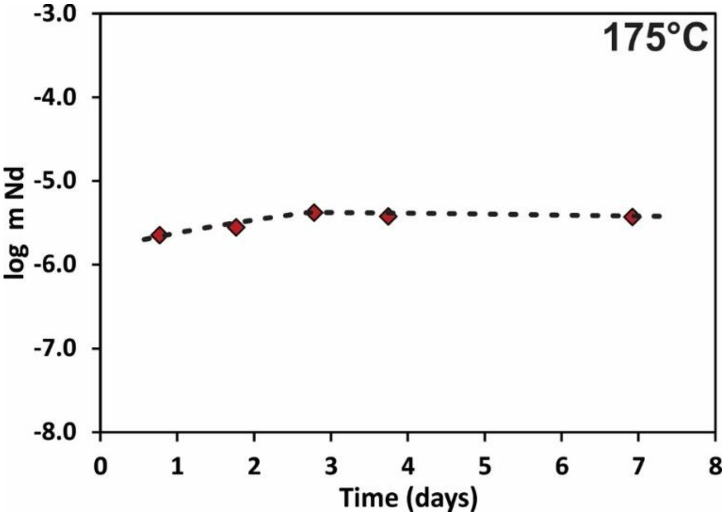

Figure 5.3 An example of the time series experiments. Each autoclave contained 0.2 m $NaHCO_3$ and 1 m NaCl. As shown in the figure, a steady-state concentration of Nd was achieved in less than 3 days.

The results and values of the parameters for the solubility experiments conducted under alkaline conditions (pH_T 7.8–9.8) are reported in Table 5.2 and include the concentration of dissolved Nd measured in the experimental solutions, the amount of $NaHCO_3$ or Na_2CO_3 added to the solutions, the calculated pH_T, and the calculated activity of HCO_3^-. The activity of HCO_3^- was determined for each experiment using the model described above. Preliminary calculations demonstrate that less than 0.1% of CO_2 is partitioned into the gas phase at these conditions, so $CO_{2(gas)}$ was excluded from these calculations.

5.3.1 Determination of predominant Nd aqueous species in acidic, carbonate-bearing solutions

Multiple Nd aqueous species were considered when analyzing the experimental data collected under acidic conditions. These comprise Nd^{3+}, $NdCl^{2+}$, $NdCl_2^+$, $NdCO_3^+$, and $Nd(CO_3)_2^-$. Polynuclear species were not considered as it can be assumed that these species become unstable at high temperatures due to the decrease in the dielectric constant of water and the associated increase in electrostatic repulsion at elevated temperatures (Brugger et al., 2014; Seward et al., 2014). As shown in Figure 5.4, all experimental data points fall within the predominance field of $CO_{2(aq)}$. Thus, to determine the dominant aqueous complex, the logarithm of the concentration of Nd was plotted as a function of the pH_T, and the logarithm of the activity of $CO_{2(aq)}$, normalized to a pH of 0 and activity of $CO_{2(aq)}$ of 1 in accordance with the stoichiometry of the considered reaction. For example, the reaction for the formation of $Nd(CO_3)_2^-$ is:

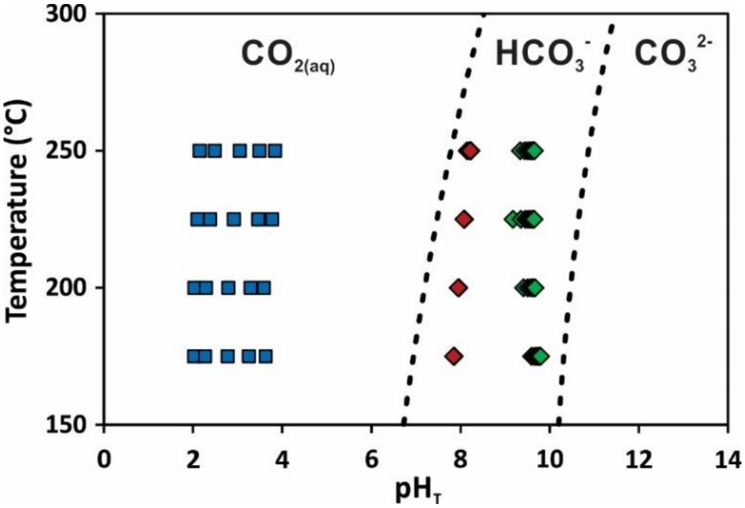

Figure 5.4 A predominance diagram for dissolved carbonate species as a function of pH_T and temperature. The experimental data points are plotted on the figure to show which carbonate species predominates at the experimental conditions. The blue squares correspond to the acidic experiments, the red diamonds to the experiments with $NaHCO_3$, and the green diamonds to the experiments with Na_2CO_3.

$$NdCO_3OH + CO_{2(aq)} \leftrightarrow Nd(CO_3)_2^- + H^+ \tag{2}$$

When plotted as a function of the logarithm of the activity of $CO_{2(aq)}$, the logarithm of the measured concentration of Nd, normalized to a pH_T of 0, should increase linearly with a slope of +1. In addition, when plotted as a function of increasing pH_T, the logarithm of the concentration of Nd, normalized to a $CO_{2(aq)}$ activity of 1 should increase with a slope of +1. The experimental data did not follow the predicted trends for the predominance of $Nd(CO_3)_2^-$ and thus this complex was deemed unlikely to be present in significant quantities. Similar exercises were carried out for the other Nd complexes considered.

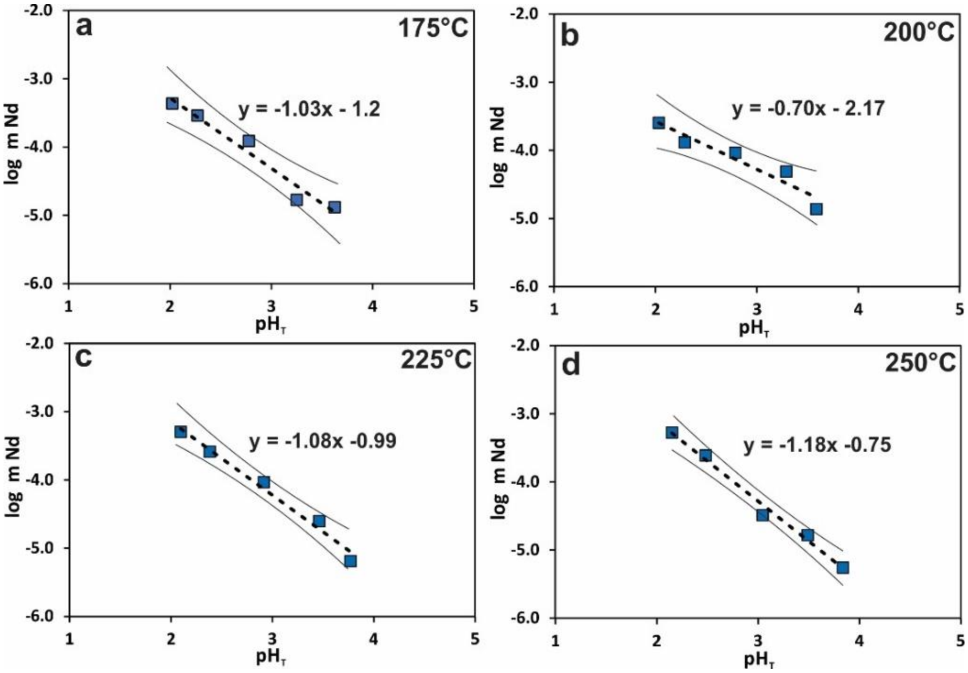

Figure 5.5a-d The concentrations of Nd for the experiments conducted under acidic solutions, plotted as a function of pH$_T$ at a) 175 °C, b) 200 °C, c) 225 °C, and d) 250 °C. The trend lines represent the linear least-squares fit of the data and are accompanied by an error envelope of 95% confidence.

Our data indicate that the dominant aqueous complex at the experimental conditions is $NdCO_3^+$, formed by the reaction:

$$NdCO_3OH + H^+ \leftrightarrow NdCO_3^+ + H_2O \quad (3)$$

The expected trends for the predominance of $NdCO_3^+$ are: 1) If plotted as a function of pH$_T$, the logarithm of the concentration of Nd should decrease with a slope of -1; and 2) If plotted as a function of the logarithm of the activity of $CO_{2(aq)}$, the logarithm of the concentration of Nd, normalized by adding pH$_T$, should have a slope of 0, owing to the absence of $CO_{2(aq)}$ in the above reaction. As shown in Figures 5.5 and 5.6, the observed trends are consistent with those predicted for $NdCO_3^+$. No detectable dependence on $CO_{2(aq)}$ was observed (Fig. 5.6).

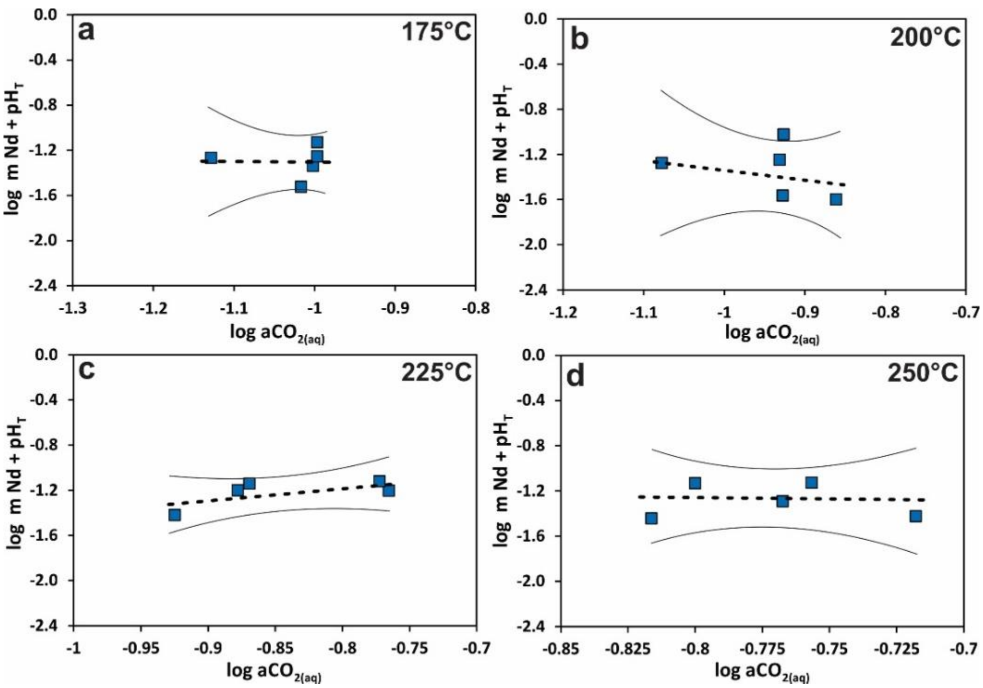

Figure 5.6a-d The concentrations of Nd for the experiments conducted under acidic solutions, plotted as a function of the logarithm of the activity of $CO_{2(aq)}$, normalized to the stoichiometry of $NdCO_3^+$ at a) 175 °C, b) 200 °C, c) 225 °C, and d) 250 °C. The trend lines represent the linear least-squares fit of the data and are accompanied by an error envelope of 95% confidence. The p(slope) values were 0.999, 0.566, 0.229, and 0.865 for 175, 200, 225, and 250 °C respectively, signifying that the slope is not significantly different from 0, and thus no dependence of Nd concentration on the activity of $CO_{2(aq)}$ was detected.

5.3.2 Determination of predominant Nd aqueous species in alkaline, carbonate-bearing solutions

Irrespective of whether $NaHCO_3$ or Na_2CO_3 was added to the solutions, the conditions of the experiments corresponded to those of the predominance field of HCO_3^- (Fig. 5.4). Therefore, to evaluate whether Nd-carbonate species predominate in solution, the logarithm of the concentration of Nd was plotted as a function of the activity of HCO_3^- for both sets of experiments (Fig. 5.7 and 5.8). As shown in Figures 5.7 and 5.8, the concentration of Nd is independent of the activity of HCO_3^- over the entire temperature range, for all experiments. To analyze the pH dependency of the saturation concentration of Nd in our experimental solutions, the two sets of experimental data, each of which had a specific pH controlled by the molality of $NaHCO_3$ or Na_2CO_3 added to the starting solution, were plotted as a function of their calculated pH_T for each experimental temperature. As shown in Figure 5.9, the concentration of Nd was also independent of the pH_T at all temperatures investigated. Thus, our experimental results suggest that the predominant Nd aqueous complex at all temperatures investigated is $NdCO_3OH^0$, formed via the congruent dissolution of Nd-hydroxylbastnäsite:

$$NdCO_3OH_{solid} \leftrightarrow NdCO_3OH_{aqueous} \tag{4}$$

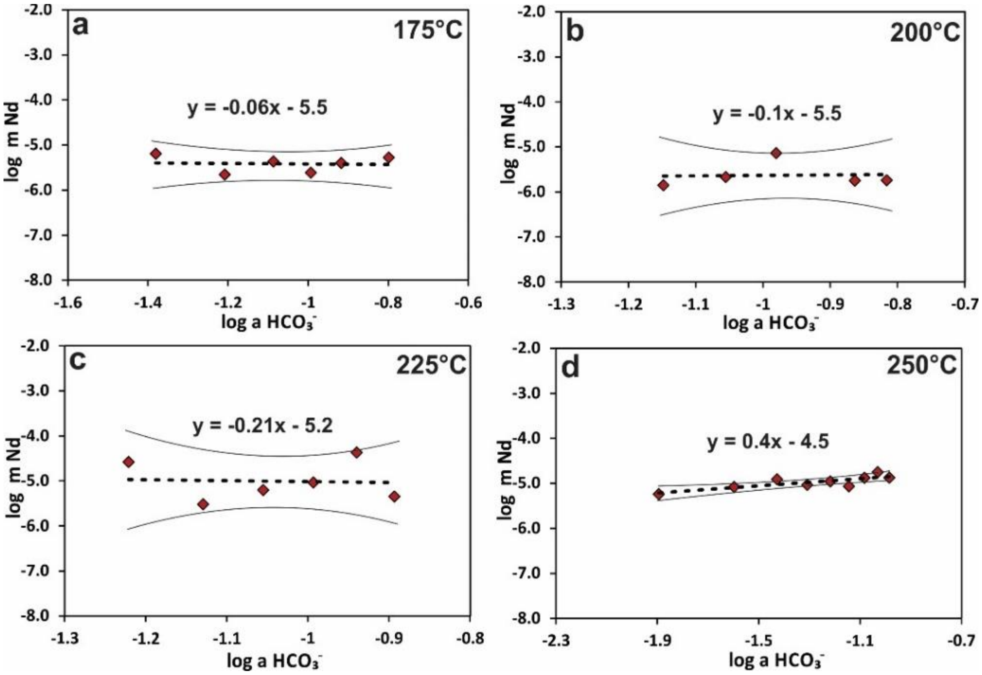

Figure 5.7a-d The concentration of Nd determined from the $NaHCO_3$ experiments. The logarithm of the concentration of Nd is plotted as a function of the logarithm of the activity of HCO_3^- at a) 175 °C, b) 200 °C, c) 225 °C, and d) 250 °C. The trend lines represent the linear least-squares fit of the data and are accompanied by an error envelope of 95% confidence. The p(slope) values were 0.903, 0.938, 0.911, and 0.007 for 175, 200, 225, and 250 °C respectively, signifying that the slope is not significantly different from 0 and thus no dependence of Nd concentration on the activity of HCO_3^- was detected.

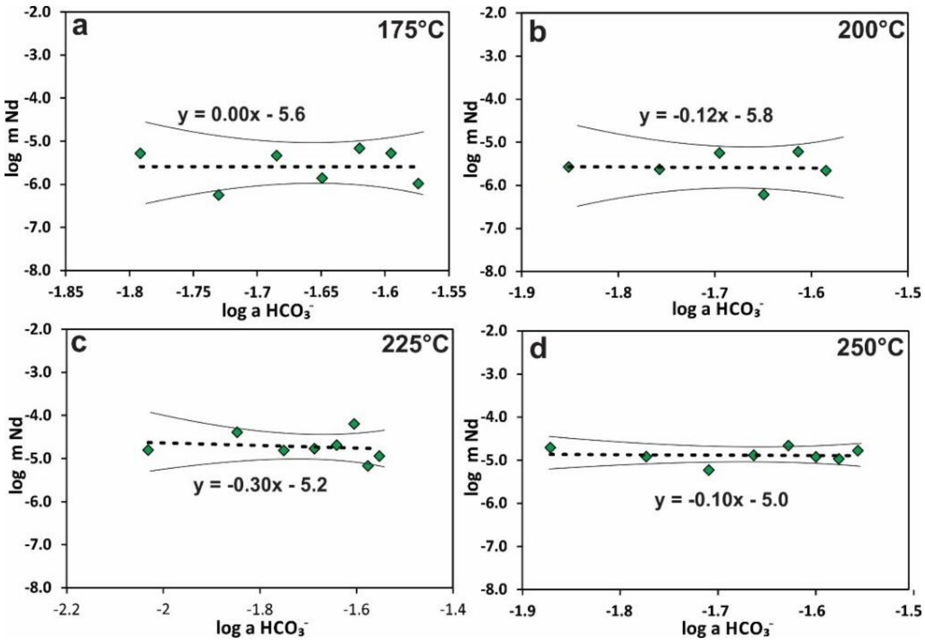

Figure 5.8a-d The concentration of Nd determined from the Na_2CO_3 experiments. The logarithm of the concentration of Nd is plotted as a function of the logarithm of the activity of HCO_3^- at a) 175 °C, b) 200 °C, c) 225 °C, and d) 250 °C. The trend lines represent the linear least-squares fit of the data and are accompanied by an error envelope of 95% confidence. The p(slope) values were 0.996, 0.946, 0.708, and 0.892 for 175, 200, 225, and 250 °C respectively, signifying that the slope is not significantly different from 0 and thus no dependence of Nd concentration on the activity of HCO_3^- was detected.

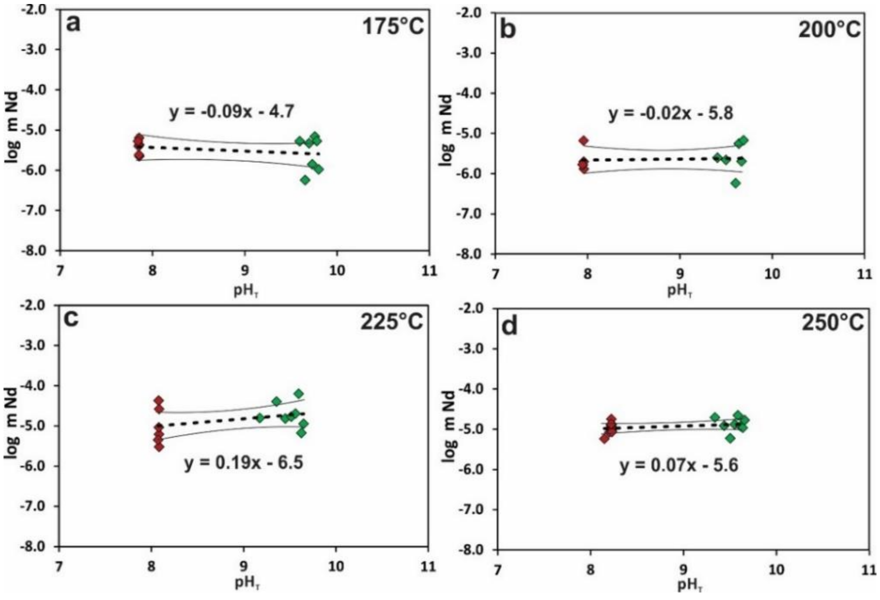

Figure 5.9a-d The concentration of Nd obtained from the $NaHCO_3$ (red diamonds) and Na_2CO_3 (green diamonds) experiments plotted as a function of pH_T at a) 175 °C, b) 200 °C, c) 225 °C, and d) 250 °C. The trend lines represent the linear least-squares fit of the data and are accompanied by an error envelope of 95% confidence. The p(slope) values were 0.385, 0.841, 0.208, and 0.241 for 175, 200, 225, and 250 °C respectively, signifying that the slope is not significantly different from 0 and thus no dependence of Nd concentration on pH_T was detected.

5.3.3 Derivation of thermodynamic data

The data collected in this study were used to calculate the solubility constants (*log K*) for $NdCO_3^+$ and $NdCO_3OH^0$ at each experimental temperature via the following reactions:

$$NdCO_3OH_{(s)} + H^+ \leftrightarrow NdCO_3^+ + H_2O \tag{5}$$

$$log\ K = \log a\ NdCO_3^+ + \log a\, H_2O - \log a\, NdCO_3OH_{(s)} + pH \tag{6}$$

$$NdCO_3OH_{(s)} \leftrightarrow NdCO_3OH^0{}_{(aq)} \tag{7}$$

$$log\ K = \log a\ NdCO_3OH^0{}_{(aq)} - \log a\, NdCO_3OH_{(s)} \tag{8}$$

We were unable to measure the solubility of Nd-hydroxylbastnäsite at conditions corresponding to the predominance of non-carbonate Nd complexes. Because of this, and considering that a complete thermodynamic dataset for Nd-hydroxylbastnäsite does not exist, derivation of the thermodynamic formation constants (log β) was not possible. Therefore, we report only the solubility constants (log *K*) for the formation of the Nd-carbonate complexes with respect to Nd-hydroxylbastnäsite (Table 5.3). Further studies focused on the thermodynamic characterization of hydroxylbastnäsite at elevated temperatures or Nd complexation in solutions containing detectable non-carbonate aqueous complexes (e.g., through UV-Vis spectroscopy) are required to determine the formation constants for $NdCO_3^+$ and $NdCO_3OH^0$.

Table 5.3 Calculated log Ks for $NdCO_3^+$ (Reaction 6) and $NdCO_3OH^0$ (Reaction 8) based on the experimental data.

T (°C)	log K	
	$NdCO_3^+$	$NdCO_3OH^0$
175	-1.303	-5.511
200	-1.339	-5.608
225	-1.217	-4.845
250	-2.281	-4.931

5.4 Discussion

The experimental data collected in this study demonstrate that Nd forms stable complexes with CO_3^{2-} over a wide range of pH at temperatures relevant to hydrothermal fluids. As shown in Figure 5.10, $NdCO_3^+$ predominates in acidic solutions (pH_T 2−4), and promotes the significant dissolution of Nd-hydroxylbastnäsite, with concentrations of Nd reaching 58 ppm in the experimental solutions. For reference, the reconstructed concentration of Nd in fluid inclusions collected from the REE-bearing Capitan Pluton in New Mexico ranged from 19−190 ppm (Banks et al., 1994). However, it should be mentioned these values did not correspond to the dissolution of hydroxylbastnäsite. As pH increases, the concentration of Nd decreases by 1 logarithmic unit per unit of pH until it reaches a solubility minimum (~1 ppm Nd) at a pH_T of ~4. The concentration of Nd remains constant as pH is raised further owing to the formation and predominance of the $NdCO_3OH^0$ species, the dissolution reaction of which is independent of pH (Fig. 5.10).

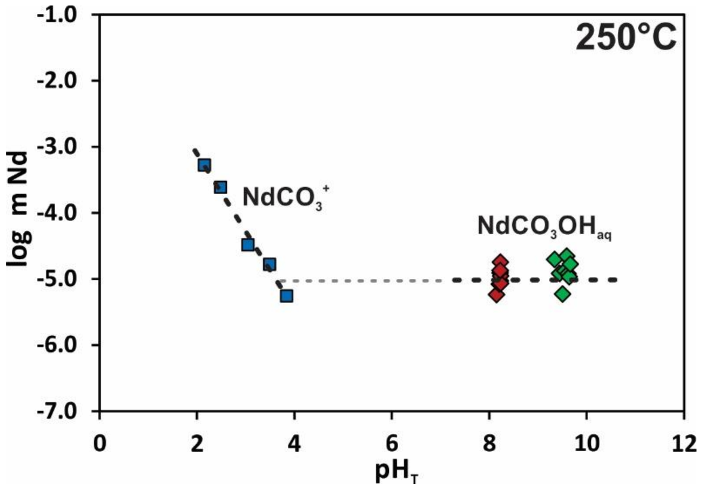

Figure 5.10 An example of the experimentally determined concentration of Nd plotted together as a function of pH_T at 250 °C. The grey dashed line is the predicted trend.

Our experiments demonstrate that there is potential for significant dissolution of Nd in carbonate-bearing hydrothermal solutions. However, it is clear that our autoclave experiments are highly simplified, and are not entirely representative of natural hydrothermal systems. For example, REE minerals invariably occur as solid solutions in nature, which we did not account for in our experiments. Furthermore, hydroxylbastnäsite is uncommon, whereas naturally occurring bastnäsite is compositionally closer to its fluorobastnäsite end-member ($NdCO_3F$), which is also more stable (Voigt et al., 2016). If we were to consider the solubility of $NdCO_3F_{(s)}$ in our experiments, assuming that the same aqueous species predominate in solution, the predicted solubility of Nd as a function of pH would change substantially; the concentration of Nd would be independent of pH under acidic conditions where $NdCO_3^+$ predominates, and increase by 1 logarithmic unit per unit of pH under alkaline conditions with the formation of $NdCO_3OH^0$. Although this assessment is qualitative, it suggests that the concentration of dissolved Nd could be significant at elevated pH, and thus, the formation of Nd-hydroxyl-carbonate complexes could be an efficient mechanism for the transport of Nd under near-neutral and alkaline conditions. The identification of these complexes also removes the need for alkali-dominated (Na and K) REE complexes to promote REE mobilization in hydrothermal systems, as has been proposed by Anenburg et al. (2020). Moreover, although previous studies have largely attributed REE mobilization at ore-grade concentrations to the formation of REE-chloride and sulfate complexes in acidic fluids (Migdisov et al., 2016), our findings suggest that alkaline solutions and the formation of REE hydroxyl-carbonate complexes should also be considered as potentially important means of REE transport. Indeed, Nd-carbonate complexes predominated over Nd-chloride complexes in our experiments.

Although there have been few experimental studies of the speciation of the REE in alkaline solutions at elevated temperatures, recent experimental results reported by Louvel et al. (2022), based on in-situ X-ray Absorption Spectroscopy (XAS), corroborate our findings by identifying hydroxyl-carbonate complexes in alkaline solutions at temperatures up to 500 °C (these complexes are interpreted to be polynuclear species). These authors further demonstrated an apparent fractionation of the REE with temperature, in which hydroxyl-carbonate complexation led to the preferential mobilization of the LREE and HREE at T > 300 °C and T < 300 °C, respectively (Louvel et al., 2022).

Determining the exact composition of a hydrothermal ore-forming fluid is challenging and, consequently, the pH of these fluids are generally unknown. However, recent direct measurements of the compositions of fluid inclusions in the Strange Lake REE deposit in Canada, coupled with estimates of temperature and pH showed that the ore fluids evolved from being extremely alkaline (up to pH 10 at 425 °C) to quite acidic (pH of 3 at 300 °C). Importantly from the perspective of this study, the early fluids transported relatively high concentrations of the REE, and were relatively enriched in carbonate (Vasyukova and Williams-Jones, 2018). Although these authors were unable to make direct measurements of carbonate anions, they predicted through charge balance, a high proportion of aqueous-carbonic inclusions, and the presence of nahcolite, that HCO_3^- is an important ligand in the alkaline solutions. The authors proposed that the transport of the REE in these fluids could have been facilitated by the formation of hydroxyl-fluoride complexes, based on thermodynamic data collected at low T. However, given the experimental results of this study, hydroxyl-carbonate complexes may also have been important for REE mobilization in these fluids. Unfortunately, a comprehensive evaluation of this and other hydrothermal systems, as well as the relative stability of Nd-carbonate versus fluoride, chloride, and sulfate complexes is not possible at this time, due to the lack of thermodynamic data for Nd-hydroxylbastnäsite. The addition of these data would permit the derivation of thermodynamic formation constants for the aqueous species identified in this study, and their incorporation into thermodynamic models to assess the role of these complexes and alkaline solutions on the formation of hydrothermal REE deposits. As a path forward, we foresee future experimental studies focused on deriving the thermodynamic stability of bastnäsite ($NdCO_3(OH,F)$), as well as thermodynamic formation constants (*log β*) for Nd-carbonate complexes via spectroscopic techniques (e.g. UV-Vis and Raman).

5.5 Conclusions

The experimental data presented in this study demonstrate that Nd forms stable complexes with carbonate ions at elevated temperatures (175−250 °C). Our results indicate that in acidic solutions ($pH < 4$), the dominant aqueous complex is $NdCO_3^+$, whereas in neutral to alkaline solutions, the $NdCO_3OH^0$ complex predominates. Solubility constants were derived for each species at the experimental temperatures with respect to Nd-hydroxylbastnäsite. A complete thermodynamic characterization of Nd-hydroxylbastnäsite is required for further analysis of the stability of these complexes. Our results suggest that Nd-carbonate complexes could lead to the significant dissolution and, thus, transport of Nd in hydrothermal fluids. The potential for alkaline solutions to transport the REE should therefore be re-assessed.

5.6 Acknowledgments

We thank Oana Marina and Chelsea Neil for their assistance with the ICP-MS analyses, and Marley Rock and Kirsten Sauer for their help with XRD analyses. Research presented in this article was supported by the Office of Science, U.S. Department of Energy, Grant No. DE-SC002226, and by Los Alamos National Laboratory's (LANL) Center for Space and Earth Sciences (CSES). CSES is funded by LANL’s Laboratory Directed Research and Development (LDRD) program under project number 20180475DR.

5.7 References

Andersen A. K., Clark J. G., Larson P. B. and Donovan J. J. (2017) REE fractionation, mineral speciation, and supergene enrichment of the Bear Lodge carbonatites, Wyoming, USA. Ore Geol. Rev. 89, 780–807.

Anenburg M., Mavrogenes J. A., Frigo C. and Wall F. (2020) Rare earth element mobility in and around carbonatites controlled by sodium, potassium, and silica. Sci. Adv. 6.

Appelo C. A. J., Parkhurst D. L. and Post V. E. A. (2014) Equations for calculating hydrogeochemical reactions of minerals and gases such as CO_2 at high pressures and temperatures. Geochim. Cosmochim. Acta 125, 49–67.

Banks D. A., Yardley B. W. D., Campbell A. R. and Jarvis K. E. (1994) REE composition of an aqueous magmatic fluid: A fluid inclusion study from the Capitan Pluton, New Mexico, U.S.A. Chem. Geol. 113, 259–272.

Beland C. M. J. and Williams-Jones A. E. (2021) The genesis of the Ashram REE deposit, Quebec: Insights from bulk-rock geochemistry, apatite-monazite-bastnäsite replacement reactions and mineral chemistry. Chem. Geol. 578, 120298.

Brugger J., Tooth B., Etschmann B., Liu W., Testemale D., Hazemann J.-L. and Grundler P. V. (2014) Structure and Thermal Stability of Bi(III) Oxy-Clusters in Aqueous Solutions. J. Solut. Chem. 43, 314–325.

Cantrell K. J. and Byrne R. H. (1986) Rare earth element complexation by carbonate and oxalate ions. Geochim. Cosmochim. Acta 51, 597–605.

Castor S. B. (2008) The Mountain Pass rare-earth carbonatite and associated ultrapotassic rocks, California. Can. Mineral. 46, 779–806.

Christensen A. N. (1973) Hydrothermal preparation of rare earth hydroxy-carbonates. The crystal structure of $NdOHCO_3$. Acta Chem. Scand. 27, 2973–2982.

Cook N. J., Ciobanu C. L., O'Rielly D., Wilson R., Das K. and Wade B. (2013) Mineral chemistry of Rare Earth Element (REE) mineralization, Browns Ranges, Western Australia. Lithos 172–173, 192–213.

Gysi A. P. and Williams-Jones A. E. (2015) The thermodynamic properties of bastnäsite-(Ce) and parisite-(Ce). Chem. Geol. 392, 87–101.

Haas J. R., Shock E. L. and Sassani D. C. (1995) Rare earth elements in hydrothermal systems: Estimates of standard partial molal thermodynamic properties of aqueous complexes of the rare earth elements at high pressures and temperatures. Geochim. Cosmochim. Acta 59, 4329–4350.

Helgeson H. C., Kirkham D. H. and Flowers G. C. (1981) Theoretical prediction of the thermodynamic behavior of aqueous electrolytes at high pressures and temperatures: IV. Calculation of activity coefficients, osmotic coefficients, and apparent molal and standard and relative partial molal properties to 600°C. Am. J. Sci. 281, 1249–1516.

Holland T. J. B. and Powell R. (1998) An internally consistent thermodynamic data set for phases of petrological interest. J. Metamorph. Geol. 16, 309–343.

Johannesson K. H. and Stetzenbach K. J. (1995) Speciation of the rare earth element neodymium in groundwaters of the Nevada Test Site and Yucca Mountain and implications for actinide solubility. Appl. Geochem. 10, 565–572.

Johnson J. W., Oelkers E. H. and Helgeson H. C. (1992) SUPCRT92: a software package for calculating the standard molal thermodynamic properties of minerals, gases, aqueous species, and reactions from 1 to 5000 bar and 0 to 1000 °C. Comput. Geosci. 18, 899–947.

Kestin J., Sengers J. V., Kamgar-Parsi B. and Levelt Sengers J. M. H. (1984) Thermophysical properties of fluid H_2O. J. Phys. Chem. Ref. Data 13, 601–609.

Louvel M., Etschmann B., Guan Q., Testemale D. and Brugger J. (2022) Carbonate complexation enhances hydrothermal transport of rare earth elements in alkaline fluids. Nat. Commun. 13, 1456.

Luo Y.-R. and Byrne R. H. (2004) Carbonate complexation of yttrium and the rare earth elements in natural waters. Geochim. Cosmochim. Acta 68, 691–699.

Marshall W. L. and Franck E. U. (1981) Ion product of water substance, 0-1000 °C, 1-10,000 bars new International Formulation and its background. J. Phys. Chem. Ref. Data 10, 295–304.

Migdisov A. (2009) An experimental study of the solubility and speciation of the Rare Earth Elements (III) in fluoride- and chloride-bearing aqueous solutions at temperatures up to 300 °C. Geochim. Cosmochim. Acta 73, 7087–7109.

Migdisov A. A. and Williams-Jones A. E. (2002) A spectrophotometric study of neodymium(III) complexation in chloride solutions. Geochim. Cosmochim. Acta 66, 4311–4323.

Migdisov A. A. and Williams-Jones A. E. (2014) Hydrothermal transport and deposition of the rare earth elements by fluorine-bearing aqueous liquids. Miner. Deposita 49, 987–997.

Migdisov A. and Williams-Jones A. E. (2008) A spectrophotometric study of Nd(III), Sm(III) and Er(III) complexation in sulfate-bearing solutions at elevated temperatures. Geochim. Cosmochim. Acta 72, 5291–5303.

Migdisov A., Williams-Jones A. E., Brugger J. and Caporuscio F. A. (2016) Hydrothermal transport, deposition, and fractionation of the REE: experimental data and thermodynamic calculations. Chem. Geol. 439, 13–42.

Migdisov Art. A., Reukov V. V. and Williams-Jones A. E. (2006) A spectrophotometric study of neodymium(III) complexation in sulfate solutions at elevated temperatures. Geochim. Cosmochim. Acta 70, 983–992.

Migdisov Art. A. and Williams-Jones A. E. (2006) A spectrophotometric study of erbium (III) speciation in chloride solutions at elevated temperatures. Chem. Geol. 234, 17–27.

Migdisov Art. A., Williams-Jones A. E. and Wagner T. (2009) An experimental study of the solubility and speciation of the Rare Earth Elements (III) in fluoride- and chloride-bearing aqueous solutions at temperatures up to 300°C. Geochim. Cosmochim. Acta 73, 7087–7109.

Migdissov A. A. and Williams-Jones A. E. (2007) An experimental study of the solubility and speciation of neodymium (III) fluoride in F-bearing aqueous solutions. Geochim. Cosmochim. Acta 71, 3056–3069.

Miron G. D., Wagner T., Kulik D. A. and Lothenbach B. (2017) An internally consistent thermodynamic dataset for aqueous species in the system Ca-Mg-Na-K-Al-Si-O-H-C-Cl to 800 °C and 5 kbar. Am. J. Sci. 317, 755–806.

Oelkers E. H. and Helgeson H. C. (1991) Calculation of activity coefficients and degrees of formation of neutral ion pairs in supercritical electrolyte solutions. Geochim. Cosmochim. Acta 55, 1235–1251.

Oelkers E. H. and Helgeson H. C. (1990) Triple-ion anions and polynuclear complexing in supercritical electrolyte solutions. Geochim. Cosmochim. Acta 54, 727–738.

Ruberti E., Enrich G. E. R., Gomes C. B. and Comin-Chiaramonti P. (2008) Hydrothermal REE Fluorocarbonate Mineralization at Barra do Itapirapuã, A Multiple Stockwork Carbonatite, Souther Brazil. Can. Mineral. 46, 901–914.

Seward T. M., Williams-Jones A. E. and Migdisov A. A. (2014) The Chemistry of Metal Transport and Deposition by Ore-Forming Hydrothermal Fluids. In Treatise on Geochemistry Elsevier. pp. 29–57.

Shivaramaiah R., Anderko A., Riman R. E. and Navrotsky A. (2016) Thermodynamics of bastnaesite: A major rare earth ore mineral. Am. Mineral. 101, 1129–1134.

Shock E. L., Sassani D. C., Willis M. and Sverjensky D. A. (1997) Inorganic species in geological fluids: Correlations among standard molal thermodynamic properties of aqueous ions and hydroxide complexes. Geochim. Cosmochim. Acta 61, 907–950.

Shvarov Y. V. and Bastrakov E. (1999) HCh, A Software Package for Geochemical Equilibrium Modeling: User's Guide.

Smith M. P., Campbell L. S. and Kynicky J. (2015) A review of the genesis of the world class Bayan Obo Fe–REE–Nb deposits, Inner Mongolia, China: Multistage processes and outstanding questions. Ore Geol. Rev. 64, 459–476.

Sverjensky D. A., Shock E. L. and Helgeson H. C. (1997) Prediction of the thermodynamic properties of aqueous metal complexes to 1000 °C and 5 kb. Geochim. Cosmochim. Acta 61, 1359–1412.

Tagirov B. R., Zotov A. and Akinfiev N. (1997) Experimental study of dissociation of HCl from 350 to 500 °C and from 500 to 2500 bars: thermodynamic properties of HCl°(aq). Geochim. Cosmochim. Acta 61, 4267–4280.

Trofanenko J., Williams-Jones A. E., Simandl G. J. and Migdisov A. A. (2016) The Nature and Origin of the REE Mineralization in the Wicheeda Carbonatite, British Columbia, Canada. Econ. Geol. 111, 199–223.

Vallina B., Rodriguez-Blanco J. D., Blanco J. A. and Benning L. G. (2014) The effect of heating on the morphology of crystalline neodymium hydroxycarbonate, $NdCO_3OH$. Mineral. Mag. 78, 1391–1397.

Vallina B., Rodriguez-Blanco J. D., Brown A. P., Blanco J. A. and Benning L. G. (2015) The role of amorphous precursors in the crystallization of La and Nd carbonates. Nanoscale 7, 12166–12179.

Van Gosen B. S., Verplanck P. L., Seal II R. R., Long K. R. and Gambogi J. (2017) Critical Mineral Resources of the United States—Economic and Environmental Geology and Prospects for Future Supply.

Vasyukova O. V. and Williams-Jones A. E. (2019) Closed system fluid-mineral-mediated trace element behaviour in peralkaline rare metal pegmatites: Evidence from Strange Lake. Chem. Geol. 505, 86–99.

Vasyukova O. V. and Williams-Jones A. E. (2018) Direct measurement of metal concentrations in fluid inclusions, a tale of hydrothermal alteration and REE ore formation from Strange Lake, Canada. Chem. Geol. 483, 385–396.

Verplanck P. L. and Hitzman M. W. (2016) Rare earth and critical elements in ore deposits. Reviews in economic geology.

Voigt M., Rodriguez-Blanco J. D., Vallina B., Benning L. G. and Oelkers E. H. (2016) An experimental study of hydroxylbastnasite solubility in aqueous solutions at 25 °C. Chem. Geol. 430, 70–77.

Voncken (2016) The Ore Minerals and Major Ore Deposits of the Rare Earths. In The Rare Earth Elements Springer International Publishing, Cham. pp. 15–52.

Voncken (2016) The Rare Earth Elements., Springer Berlin Heidelberg, New York, NY.

Williams-Jones A. E. and Palmer D. A. S. (2002) The evolution of aqueous–carbonic fluids in the Amba Dongar carbonatite, India: implications for fenitisation. Chem. Geol. 185, 283–301.

Williams-Jones A. E., Samson I. M. and Olivo G. R. (2000) The Genesis of Hydrothermal Fluorite-REE Deposits in the Gallinas Mountains, New Mexico. Econ. Geol. 95, 327–342.

Wood S. A. (1990) The aqueous geochemistry of the rare-earth elements and yttrium 2. Theoretical predictions of speciation in hydrothermal solutions to 350°C at saturation water vapor pressure. Chem. Geol. 88, 99–125.

Chapter 6

Conclusions

6.1 General conclusions

The experimental results presented in this thesis detail the solubility and speciation of Th with chloride, sulfate, and carbonate ligands in hydrothermal solutions. The complexation of Nd in carbonate-bearing fluids was also investigated. The experiments were conducted using the autoclave solubility method at 175−250 °C and saturated water pressure. The predominant aqueous complexes for each system were identified and their thermodynamic data derived.

The experiments conducted on the solubility of Th in chloride-bearing acidic solutions ($pH_T < 4$) determined that Th-chloride complexes are of negligible abundance at hydrothermal conditions, unlike the REE with which Th is commonly associated in REE deposits. Instead, two Th-hydroxyl complexes, $Th(OH)_2^{2+}$ and $Th(OH)_4^0$, were identified and formation constants for each species were derived. Extrapolations of the formation constants for these species to ambient conditions yielded constants in good agreement with those determined experimentally by other researchers. The low stability of these Th-hydroxyl complexes makes it unlikely that they contribute to the significant transport of Th in natural hydrothermal systems.

Thorium complexation in sulfate-bearing hydrothermal solutions was investigated under moderately acidic conditions (pH_T 3.7–4.6) and $Th(SO_4)_2^0$ was shown to be the dominant species at all temperatures. Thermodynamic formation constants for this species were determined, and when extrapolated to ambient temperature, showed excellent agreement with values previously reported for experiments at ambient temperature. Importantly, it was discovered that the formation of this species promotes the strong dissolution of $ThO_{2(crystalline)}$. This was unexpected as previous studies have concluded that Th is insoluble in hydrothermal fluids and consequently that it is immobile in nature. Geochemical modeling simulating the hydrothermal alteration of a REE ore deposit demonstrated that repeated flushing with a hydrothermal fluid containing modest sulfate concentrations would promote the preferential mobilization of Th over the REE. This could be an effective mechanism for fractionating these elements in nature, and potentially forming a Th-depleted REE deposit. Rocks, for which there is evidence of pervasive alteration by sulfate-rich hydrothermal fluids, were identified as exploration targets for Th-depleted REE ore deposits.

The solubility and speciation of Th were also evaluated in carbonate-bearing hydrothermal fluids at alkaline conditions (pH_T 7.8–9.8). It was found that, in contrast to the behavior of Th at low temperatures, the stability of Th-carbonate complexes is insufficient for them to predominate at elevated temperatures. Instead, the hydroxyl complexes, $Th(OH)_4^0$ and $Th(OH)_5^-$ are more stable. Thermodynamic formation constants were derived for $Th(OH)_5^-$ and refined for $Th(OH)_4^0$. Predominance diagrams were constructed for all Th aqueous species for which there are currently high-temperature thermodynamic data. From these diagrams, it was concluded that Th will be transported as the $Th(SO_4)_2^0$ complex in hydrothermal systems if sulfate is present in even modest concentrations. In alkaline solutions, Th-hydroxyl complexes dominate but are unlikely to result in the significant transport of Th.

The complexation of Nd with carbonate ligands was evaluated through experiments carried out in acidic and alkaline carbonate solutions at elevated temperatures. Two species were identified: $NdCO_3^+$ in acidic solutions (pH_T 2−4) and $NdCO_3OH^0$ in alkaline solutions (pH_T 7.8−9.8). Solubility constants for the dissolution reaction with respect to Nd-hydroxylbastnäsite ($NdCO_3OH$), were calculated for each species at the experimental temperatures. Derivation of thermodynamic formation constants for these complexes was not possible owing to a lack of thermodynamic data for Nd-hydroxylbastnäsite. A preliminary analysis of the experimental results suggests that Nd-carbonate complexes could lead to the significant dissolution, and thus, transport of Nd in hydrothermal fluids.

6.2 Contributions to knowledge

The experimental work detailed in this thesis provides the first evaluation of the thermodynamic behavior of Th in hydrothermal systems at elevated temperatures and pressures. Three manuscripts published from this thesis present a comprehensive overview of the solubility and speciation of Th with chloride, hydroxide, sulfate, and carbonate; ligands that are among the most abundant in crustal settings. One of the most noteworthy contributions of the study is that it overturns the longstanding paradigm that Th is effectively insoluble, and thus, immobile in aqueous fluids at ambient and higher temperatures. Results of the solubility experiments in sulfate-bearing hydrothermal solutions identify conditions that can lead to the exceptionally high solubility of Th and provide a mechanism with which to effectively fractionate Th from the REE in ore-forming systems. This information can aid in the strategic exploration for new, economically viable REE deposits that do not need to be treated to remove Th. Equally significant is the conclusion that Th-carbonate complexes are not stable at hydrothermal conditions (175−250 °C). This is in stark contrast to previous investigations at ambient conditions, which concluded that they are among the most stable Th species in aqueous solutions. Instead, it was determined that Th-hydroxyl complexes predominate in carbonate- and chloride-bearing hydrothermal fluids. This discovery emphasizes the need to evaluate the behavior of metal complexes at elevated temperatures, and that simply extrapolating data from low to high temperatures can lead to remarkable inaccuracies and invalid conclusions.

This thesis is the first to report data on the complexation of Nd with carbonate ligands at hydrothermal conditions. Indeed, it is the first study to experimentally investigate REE-carbonate complexation above ambient temperature. Until this study, it had been assumed that carbonate ligands are unlikely to be important in mobilizing the REE. However, the experimental results obtained in this study indicate that the transport of the REE as carbonate complexes may be important, particularly in alkaline solutions, and that their role in natural hydrothermal settings needs to be re-evaluated.

The thermodynamic data derived in these studies allow for their incorporation into geochemical models and, for the first time, permits an assessment of Th mobility in REE-bearing hydrothermal fluids. These data can now be utilized in future models to assess the mobilization, concentration, and fractionation of Th and the REE in a variety of geological settings.

6.3 Recommendations for future work

The collection of thermodynamic data at elevated temperatures is fundamental to understanding the physicochemical mechanisms involved in the mobilization and concentration of metals in hydrothermal settings. In the case of Th and the REE, there remains a paucity of studies on their solubility and speciation at elevated temperatures. Future studies should evaluate Th complexation with fluorine and phosphate above ambient conditions because these two ligands occur in significant concentrations in natural systems and, according to Pearson’s rule (Pearson, 1963), are likely to form stable complexes with Th, as has been demonstrated at ambient conditions (Rand et al., 2008). A major gap that hinders our ability to model REE transport in hydrothermal systems is the lack of experimental data on REE-hydroxyl complexation at elevated temperatures. Studies of REE speciation conducted under alkaline conditions would be especially helpful given the paucity of data at these conditions and the observation that some REE ore deposits form in part because of the transport of the REE in alkaline hydrothermal fluids (Vasyukova and Williams-Jones, 2018).

As highlighted in Chapter 5, the absence of thermodynamic data for hydroxylbastnäsite precludes the derivation of formation constants for the Nd-carbonate aqueous species identified in this study and prevents incorporation of these complexes in thermodynamic models of the behavior of Nd in hydrothermal fluids. This is an important weakness of existing models because, as mentioned in this chapter, it is thought that Nd-carbonate complexes could lead to the significant dissolution of the F-end-member, bastnäsite ($REECO_3F$) under alkaline conditions. This hypothesis, however, cannot be tested because there are also no thermodynamic data for this end-member. Thus, a study dedicated to the thermodynamic characterization of bastnasite end-members would allow for a quantitative evaluation of the mobility of Nd– and other REE–carbonate complexes in hydrothermal fluids. In addition, considering the finding of Louvel et al. (2022) that the LREE can be fractionated from the HREE by the formation of aqueous REE-carbonate complexes at ambient conditions, it would be important to conduct autoclave solubility experiments under hydrothermal conditions similar to those discussed in this thesis with a variety of REE to determine whether the conclusion holds at elevated temperatures. A further important step would be to increase the complexity of the system by incorporating simple solid solution REE phases, given that the REE invariably occur as solid solutions in nature. Deriving thermodynamic data for such phases, in addition to using them as a reactant in solubility experiments, would provide a more accurate representation of the behavior of the REE in nature.

The primary goal of deriving thermodynamic data for solid and aqueous phases is to utilize these data in models to simulate real-world settings as a means of understanding the geochemical processes that are involved in concentrating the REE and Th in nature. Thus, these data should be incorporated into future models formulated to understand the transport of Th and the REE, evaluate the genesis of Th-depleted hydrothermal ore deposits, or engineer ways to selectively extract the most valuable components in post-mining processes.

6.4 References

Louvel M., Etschmann B., Guan Q., Testemale D. and Brugger J. (2022) Carbonate complexation enhances hydrothermal transport of rare earth elements in alkaline fluids. Nat. Commun. 13, 1456.

Pearson R. G. (1963) Hard and soft acids and bases. J. Am. Chem. Soc. 85, 3533–3539.

Rand M. H., Mompean F. J., Perrone J. and Illemassene M. (2008) Chemical Thermodynamics of Thorium., OECD, NEA.

Vasyukova O. V. and Williams-Jones A. E. (2018) Direct measurement of metal concentrations in fluid inclusions, a tale of hydrothermal alteration and REE ore formation from Strange Lake, Canada. Chem. Geol. 483, 385–396.